Manuscript Details

Manuscript number VOLGEO_2018_184_R2

Title Monitoring active fumaroles through time-lapse electrical resistivity tomograms: an application to the Pisciarelli fumarolic field (Campi Flegrei, Italy).

Article type Research Paper

Abstract

Volcanoes are usually monitored through observations of many physical and chemical phenomena. In the most dangerous cases, as the one of the Campi Flegrei caldera (Italy), great amount of data are collected, both in discrete or continuously, and regularly stored. However, how to transform such mass of data in a deeper understanding of the volcano dynamics is still an open question. Dissimilar information are in fact always hard to compare, but just integrating all the available knowledge hazardous events could be prevented in a reliable way. Fluids, as water and gasses mobilized in the subsoil by the heat induced by deep magmatic sources, are widely recognized as the first engine of similar occurrences and the volcanic gas emissions represent, together with the seismic activity, one of the most considered precursors. At the same time, the electrical geophysical methods are the most applied in order to detect and characterize the fluid patterns in the subsoil. So, the integration of geoelectrical and geochemical observations should represents one of the most pursued approach in volcanoes monitoring. On the contrary, standard way to compare such data have been not yet codified. The ERT tomograms capability to individuate that parts of the subsoil where gasses cumulate is well understood in literature. However, we look for indications about its proficiency in associating the electrical resistivity changes relative to these zones, once compared to the geochemical time series, to deep related contributes, distinguishing them from the seasonal ones. The electrical signature of the fluid patterns, reconstructed through a time-lapse ERT approach, could be of relevance to better characterize the volcanic phenomena and their origins. In this paper a first test of ERT and geochemical time series integration was performed to enhance the understanding of the Pisciarelli fumarolic field evolution, now the most active area in the whole Campi Flegrei caldera.

Keywords time lapse ERT tomography; Fumarolic vent; Campi Flegrei;

Corresponding Author Maria Giulia Di Giuseppe

Order of Authors Maria Giulia Di Giuseppe, Antonio Troiano

Suggested reviewers Andre Revil, Vincenzo Lapenna, Yoichi Sasai, Jacques Zlotnicki

Opposed reviewers agata siniscalchi

Submission Files Included in this PDF

File Name [File Type]

Editor.pdf [Cover Letter]

Comments from the reviewer.pdf [Response to Reviewers]

PaperIIrev_TC.pdf [Revised Manuscript with Changes Marked]

highlights.pdf [Highlights]

PaperIIrev.pdf [Manuscript File]

fig1.jpg [Figure]

fig2.jpg [Figure]

fig3.jpg [Figure]

fig4.jpg [Figure]

fig5.jpg [Figure]

fig6.jpg [Figure]

fig7.jpg [Figure]

fig8a.jpg [Figure]

fig8b.jpg [Figure]

fig8c.jpg [Figure]

fig8d.jpg [Figure]

fig8e.jpg [Figure]

fig9.jpg [Figure]

To view all the submission files, including those not included in the PDF, click on the manuscript title on your EVISE Homepage, then click 'Download zip file'.

Research Data Related to this Submission

There are no linked research data sets for this submission. The following reason is given:
Data will be made available on request

Dear Editor,

we are now sending a revised version of the manuscript “Monitoring active fumaroles through time-lapse electrical resistivity 1 tomograms: an application to the Pisciarelli fumarolic field (Campi Flegrei, Italy).” By M. G. Di Giuseppe and A. Troiano.

We considered your invite to take into account the observations of reviewer nr.2 and we added some sentences to the text. However, we cannot avoid pointing out the differences between our approach and that of the reviewer. On one side, we understand that in previous versions of the text there was no mention of the main mechanisms contributing to electrical conduction in rocks and the factors that influence the same. On the other hand, we believe that the core of our paper is the presentation of a specific application, considering a more detailed discussion about that to be out of focus. Also with regard to the position of the reviewer with respect to the autonomous value of electrical tomography, we disagree on both issues raised. On the one hand, direct petrophysical information would certainly be useful to support the interpretation of the sections, but for us it cannot be considered a necessary condition. The subsoil model obtained through time-lapse ERT, although essential because based just on the electrical picture of the subsoil (let’s say univariate), is self-standing, at least in our opinion. On the other hand, although more surveys certainly mean more knowledge, we believe that a method such as ERT has shown, in decades of applications, its validity independently of IP surveys, even in volcanic environments.

We really hope that you could consider favourably this version of the manuscript and we wish to thank you for your attention.

Best regards

The authors.

-Reviewer 2

-

Review of “Monitoring active fumaroles through time-lapse electrical resistivity 1 tomograms: an application to the Pisciarelli fumarolic field (Campi Flegrei, Italy).” By M. G. Di Giuseppe and A. Troiano. I will let the editor decide if he wants this manuscript to be published but I do not see new research in this work. The time lapse inversion approach is very crude, there is not discussion of the underlying petrophysics (with the fact that ERT cannot be independently interpreted) and there is a lack of coupling the geophysics with the process at play (a currently hot subject of research in hydrogeophysics). However this paper has been significantly improved with respect to the first version. I think this paper could be saved if it would contain a strong discussion between the time lapse ERT observations and the final plot corresponding to Figure 9. This implies a discussion on how the differential environmental variables (saturation, temperature, salinity) affect the resistivity.

1. Many statements are too strong Example: “just integrating all the available knowledge hazardous events could be prevented in a reliable way.”. This is not demonstrated in the paper. This is only a wish from the authors.

2. The summary is not a summary with the exception of the last sentence. It just providesvague statements about volcanological crisis forecasting. Please rewrite the summary so that it reflects and summarize the content of the manuscript.

3. Intro: replace “Di Giuseppe et al., 2015;), » by « Di Giuseppe et al., 2015) » . Change « complicat ed.” By “complicated.” All these errors show that the manuscript has not been polished enough.

4. The following sentence is not substantiated enough “A mapping of the electrical resistivity changes through ERT should be indicative of potentially hazardous dynamics in the area”.

5. Regarding the sentence “The geophysical surveys based upon the electrical resistivity estimations are very effective tools for imaging tectonic and volcanic structures, and several contribution regarded the Campanian district (Di Maio et al., 1998; Bruno et al., 2007;Troiano et al., 2008, 2009; Byrdina et al., 2014; Di Giuseppe et al., 2015, 2017; Gresse et al., 2017).” Actually in a recent series of papers in JVGR (Soueid Ahmed et al., 2018, Ghorbani et al., 2018; Revil et al., 2018a, b), it was advocated that ERT is not a stand alone technique because surface conductivity cannot be separated from the bulk conductivity and that surface conductivity usually is dominant in most volcanic setting. ERT requires IP (induced polarization) to be properly interpretated. I think this point should be discussed in details since the paper, in its actuall form, completely oversell what ERT can accomplish especially without a description of the underlying petrophysics.

6. Line 200-205: it is shown in MANY papers that time lapse ERT required imperatively the use of dedicated inversion algorithm like sequential inversion or 4D inversion (including a regularization in time). Examples include: Karaoulis M., A. Revil, D.D. Werkema, B. Minsley, W.F. Woodruff, and A. Kemna, Time-lapse 3D inversion of complex conductivity data using an active time constrained (ATC) approach, Geophysical Journal International,

187, 237–251, doi: 10.1111/j.1365-246X.2011.05156.x, 2011. Karaoulis, A. Revil, J. Zhang, and D.D. Werkema, Time-lapse joint inversion of cross-well DC resistivity and seismic data: A numerical investigation, Geophysics, 77(4), D141–D157 doi: 10.1190/GEO2012-0011.1, 2012. Meyerhoff, S.B., M. Karaoulis, F. Fiebig, R.M. Maxwell, A. Revil, J.B. Martin, W. D. D. Graham, Visualization of conduit-matrix conductivity differences in a karst aquifer using time-lapse electrical resistivity, Geophys. Res. Lett., 39, L24401, doi:10.1029/2012GL053933, 2012. Karaoulis M., A. Revil, D.D., Werkema, P. Tsourlos, and B.J. Minsley, IP4DI: A software for time-lapse 2D/3D DC-resistivity and induced polarization tomography, Computers & Geosciences, 54, 164-170, 2013. This is just to cite few examples in my realm. It is well known and dmeoinstrated in many papers that inverting the snapshots independently and looking at the difference does not work because of the noise level in the data and inversion artefacts. This point should be discussed because agaion it gives the bad feeling that the authors oversell what they do and the implications of their work. Consequently I totally disagree with the statements in lines 224-229. Lines 228-229: this is not a good way to proceed. A better way is the sequential inversion is to take the result of the inversion of the previous snapshots as a strating model for the inversion of the next one. However it is demonstrated in the papers above that even this approach can propagatre artefacts in the sequence of inverted snapshots. It is also behing the 2.5+ time or 4D inversion proposed in the papers above or time lapse regularization on the Kalman filter approach. The sentence “As a final, and likely more corrected, option, the dataset could be inverted jointly, adopting a minimizing function, which reflects a metric function of both space and time (Johnson et al., 2010).” is grossly wrong since this paper does not deal with this issue indicating that the authors never read the paper they cite.

A few sentences have been added to the text, in order to mention of the main mechanisms contributing to electrical conduction in rocks and the factors that influence the same. We understand that in previous versions of the text there was no references to such issues. However, we consider a more detailed discussion about that to be out of focus, believing that the core of our paper is the presentation of a specific application.

Although direct petrophysical information would certainly be useful to support the interpretation of the sections, in our opinion it cannot be considered a necessary condition. The same for IP. We consider the model of Fig.9 a self-standing result, even if based just on the electric tomography of the subsoil.

For what concerns the inversion procedure, we changed the citation of Johnson et al., 2010 and slightly modified the related sentence.

Monitoring active fumaroles through time-lapse electrical resistivity tomograms: an application to the Pisciarelli fumarolic field (Campi Flegrei, Italy).

M. G. Di Giuseppe and A. Troiano

Istituto Nazionale di Geofisica e Vulcanologia, Sezione di Napoli 'Osservatorio Vesuviano'

Abstract

Volcanoes are usually monitored through observations of many physical and chemical phenomena. In the most dangerous cases, as the one of the Campi Flegrei caldera (Italy), great amount of data are collected, both in discrete or continuously, and regularly stored. However, how to transform such mass of data in a deeper understanding of the volcano dynamics is still an open question. Dissimilar information are in fact always hard to compare, but just integrating all the available knowledge hazardous events could be prevented in a reliable way. Fluids, as water and gasses mobilized in the subsoil by the heat induced by deep magmatic sources, are widely recognized as the first engine of similar occurrences and the volcanic gas emissions represent, together with the seismic activity, one of the most considered precursors. At the same time, the electrical geophysical methods are the most applied in order to detect and characterize the fluid patterns in the subsoil. So, the integration of geoelectrical and geochemical observations should represents one of the most pursued approach in volcanoes monitoring. On the contrary, standard way to compare such data have been not yet codified. The ERT tomograms capability to individuate that parts of the subsoil where gasses cumulate is well understood in literature. However, we look for indications about its proficiency in associating the electrical resistivity changes relative to these zones, once compared to the geochemical time series, to deep related contributes, distinguishing them from the seasonal ones. The electrical signature of the fluid patterns, reconstructed through a time-lapse ERT approach, could be of relevance to better characterize the volcanic phenomena and their origins. In this paper a first test of ERT and geochemical time series integration was performed to enhance the understanding of the Pisciarelli fumarolic field evolution, now the most active area in the whole Campi Flegrei caldera.

Introduction

Electrical resistivity tomography (ERT) represents a well-established technique, widely employed to investigate fluid-induced variations in volcanological settings (Revil et al. 2008; Byrdina et al. 2009; Finizola et al. 2009; Finizola et al. 2010; Revil et al., 2011; Di Giuseppe et al. 2015). Many literature publications describe electrical investigations devoted to the definition of the structural setting of volcanoes (Finizola et al., 2006; Revil et al., 2008; Aizawa et al., 2009; Fikos et al., 2012; Barde-Cabusson et al., 2013; DiGiuseppe et al., 2017). When applied in time-lapse mode, e.g. performing tomograms reiteratively overtime, ERT maps the temporal changes in electrical resistivity, which could be related to the changes in the fluid patterns in the subsoil (Singha et al., 2015; Slater, 2007). Because fluids are often involved in relevant volcanic phenomena, time-lapse ERT should be considered in the monitoring of active areas in order to investigate highly hazardous but ambiguous phenomena. This particularly concern for silicic volcanoes, which commonly develop pervasive hydrothermal systems during their long repose periods. The resulting magma-hydrothermal interactions are still poorly understood (Chiodini et al. 2016). In active calderas, widely investigated through electrical methods (Pribnow et al., 2003; Bruno et al., 2007; Di Giuseppe et al., 2015), the hydrothermal circulation is extremely intense, indeed, due to the major structural control, which makes the characterization of unrest phases even more complicated. In addition, the liquid and the gas interactions between mixtures of different chemical species, the most relevant among them being water and carbon dioxide, happen in the very shallowest part of the geothermal system, often creating active fumaroles. Once injected into the shallower formations from deeper magmatic sources, the CO_2 will tend to rise upward because of its low density until it is trapped by low-permeability structures or by dissolution into the groundwater (Bachu et al., 1994). The electrical resistivity of the mixture of grains and pores, which contain the fluids, changes over time, mainly due to fluid filling the pores driven by the fumarole dynamics, and the literature points out that fluids in volcanic environments affect electrical resistivity, generating detectable variations in the recordable signals (Rinaldi et al., 2011). In effects, one of the most sensible parameters to detect the approach of a new eruptive phase is to examine the variations in the composition of discharged fluids. The isotopic signature, however, is often difficult to interpret in terms of system evolution, because several mechanisms may be responsible for differences in the proportion of magmatic gases and shallower fluid components. Indeed, such proportions can be altered before the fluids reach the surface, due to the mixing between fluids of different origin, or due to reactions that modify the original isotope composition. Time-lapsed ERT can reconstruct these changes (Giese et al. 2009; Kiessling et al. 2010; Würdemann et al. 2010; Schmidt-Hattenberger et al. 2011; Zhou et al. 2012), and help to characterize the fumarole dynamics. The dissolution of CO_2 in groundwater and soil moisture indeed generates an enlargement of the low resistivity area after CO_2 injection into the vent. An opposite relationship between CO_2 concentration and electrical resistivity is observed when CO_2, rather than dissolving in water, replaces the brine in the rock matrix, causing the apparent resistivity to increase (Le Roux et al., 2013). The integration between time-lapse ERT and geochemical observations could help to characterize the phenomena related to the mixing of different chemical species, and to reconstruct interaction between fluids of magmatic origin and meteoric waters. The relationship between the contributions of deeper magmatic sources and sources linked to seasonal fluctuations could be also investigated in that manner. Here a similar application is presented, carried out in the Pisciarelli area, which represents a part of the Campi Flegrei caldera (Italy) where vigorous gaseous emissions are present. Repeated tomograms, performed bimonthly, furnished an image of the dynamics of fluids contributing to the fumarolic vent. An approach to the comparison of the gaseous emission rates, temperature and rainfall rates is suggested, to which end a characterization of the detected anomalies is provided.

The Campi Flegrei caldera.

The Campi Felgrei caldera (CFc) is one of the most hazardous volcanoes in Europe (Orsi et al., 2004) and it is inhabited by more than 300,000 people (Bevilacqua et al., 2015), including entire quarters of Naples (Fig.1a). Vertical ground movements with rates ranging from centimetres to metres per year are typical even during quiescent periods (Dvorak and Mastrolorenzo, 1991). Since 1950 the area has been in a new phase of uplift after several centuries of subsidence dating back to 1538 A.D., when the last eruption occurred in the area (Di Vito et al., 1987). The most recent episodes of intense ground uplift were during 1970-72 and 1982-84, which caused a cumulative maximum uplift of over 3.5 m, accompanied by intense seismicity. Apart from the ground uplift, the CFc unrest is characterized primarily by shallow hydrothermal manifestations (such as the vigorous gas emissions), which are most evident in the Solfatara crater and the nearby Pisciarelli areas (Fig.1b), with an involvement of the seismic activity. In effect, the recent literature on the interpretation of the unrest of the whole CFc points out the driving role played by processes involving these two areas (De Natale et al., 1991; Chiodini et al., 2003; Troiano et al., 2011; Piochi et al., 2015a), which are continuously monitored and under observation for the risk strictly related to their potential expansion into a high-density urban area. Many studies involve the mechanical effect of overpressure on a shallow magma chamber (Berrino et al., 1984; Bianchi et al., 1987; Amoruso et al., 2007;) or a sill-like deformative source (D'Auria et al., 2011). Other studies suggest that the unrest periods affecting the whole caldera could likely be related to the triggering of the local hydrothermal system caused by magma degassing episodes centred below the Solfatara - Pisciarelli area (De Natale et al., 1991; Chiodini et al., 2003; Todesco et al., 2003; De Natale et al., 2006; Gottsmann et al., 2006; Lima et al., 2009; Shirzaei and Walter, 2010; Troiano et al., 2011).

Geophysical applications allowed a detailed imaging of the subsurface structure of the Solfatara crater (Letort et al., 2012; Petrosino et al., 2012; Byrdina et al., 2014; Di Giuseppe et al., 2015; Isaia et al., 2015; Gresse et al., 2017). The structure of the Pisciarelli site is less defined. Moreover, several monitoring techniques (geodetic, thermal and geochemical) are currently applied to the CFc, especially at the Solfatara and Pisciarelli areas (INGV, 2018), but a lack of knowledge persists about the distribution and dynamics of the geothermal fluids present in the area. Specifically, the Pisciarelli area has been the subject of a severe reactivation in the last few years, concomitant with an increase of ground uplift. The main manifestations are as follows: an enlargement of the fumarolized area, the opening of a new vent (which occurred in March 2008), the opening of a new boiling pool (which occurred in March 2009 and which was probably accompanied by a small explosion because mud sputter occurred, covering the soil slope up to 3–4 m above the emission point), a further vigorous, roaring fumarole created (which appeared on the 20^{th} of December, 2009, that represents the strongest gas emission of the entire area to date), the seismic swarm of about 190 events (recorded in the area during the 30^{th} of March, 2010) and a new vent opened (during the 15^{th} of November, 2010). Finally, in the January of 2013 the disappearance of the main fumarole that was recently opened and the appearance of a vent that emits high-pressure steam and liquid water up to 3-4 m high were observed. These manifestations make the Pisciarelli unrest quite peculiar. It is indubitably linked to the global CFc unrest, as evidenced by the geochemical species emitted (Chiodini et al., 2011). However, the local aspect of the CFc dynamic in this area has to be carefully taken into account. The Pisciarelli neighbourhood has a high degree of urban development and minor events could represent a high risk for a great number of inhabitants.

A mapping of the electrical resistivity changes through ERT should be indicative of potentially hazardous dynamics in the area. Such parameters are, in fact, sensitive to properties such as salinity, porosity and phase changes of fluids flowing into the porous space, which contribute to the characterization of the fluid circulation in the subsurface.

The state of the Solfatara – Pisciarelli area.

After the last major unrest period observed in the CFc, during 1982-1984, the ground deformation trend showed a subsidence period until 2004-2005, when a new uplift phase started. Since 2010-2011 the deformation rate shows a further increase, leading to a cumulative uplift of more than 20 cm. The ground uplift is also accompanied by widespread fumarolic activity occurring in the whole CF caldera area. However, these unrest manifestation are all focused in the centre of the CFc (Figure1a), near the Solfatara - Pisciarelli area (D'Auria et al., 2011), where the evidences of volcanic effects are particularly present now. For such a reason, the ascription of a central role in the CFc unrest dynamic for these two areas has grown, and has been the subject of the many detailed numerical studies, mentioned earlier.

The geophysics surveys contributed to defining the structural outline of the Solfatara – Pisciarelli area (SP), and represented a crucial task for understanding volcanic activity. Recent surveys highlighted the main structural asset of the area. The first magnetotelluric surveys (Troiano et al., 2014) detected a near-vertical steam/gas-saturated plume-like structure, which reaches the free surface where the main fumarole fields are active, emerging from a high temperature (>300 °C), over pressured, gas-saturated plate-like reservoir, which extends down to at least 3 km in depth. Subsequent ERT surveys clarified the shallower structure of the Solfatara volcano, outlining a complex hydrothermal system, formed by a mix of upwelling fluids, gases, and meteoric water (Byrdina et al., 2014; Di Giuseppe et al., 2015; Gresse et al., 2017). Isaia et al. (2015), when considering this structural framework, ended in the suggestion that the Solfatara volcano could be a maar-diatreme structure, characterized by a shallow crater cut in the pre-eruptive basement, and a deep diatreme (down to 2–3km).

Physical and chemical observations are now performed in the whole CFc as part of the volcanic monitoring and both the Solfatara crater and the Pisciarelli area represent the great majority of the areas surveyed. Regular thermic, seismic, gravimetric, geochemical and geodetic monitoring is carried out in the area. In particular, the geochemical data had a central role in the debate on the CFc unrest (Chiodini et al., 2012, 2016; Moretti et al., 2017). A general increase of the deep magmatic component into the emitted volatiles was observed (INGV, 2018). In particular, for what concerned the SP area, the following features were observed:

- an increasing trend in the CO_2/H_2O, generally indicating a growth in the magmatic component into the fumarolic fluids

- an increasing CO concentration, that generally characterize volcanic systems at high temperature, whereas hydrothermal contributions would be usually related to lower levels of this component
- an increase of the CO-CO_2 equilibrium temperature, representing the shallower hydrothermal system conditions
- and an increasing trend in the CO_2/CH_4 ratio

Further considerations about the fluid dynamics in the area arise also from the geophysical observations. Di Giuseppe et al. (2015) discussed a migration of the shallow fluid volume eastwards during the few past decades, and supposed that water might have invaded spaces previously saturated with steam, gas or a combination thereof below the Solfatara main vents, at the same time as fluxes steam, gas or both were invading voids opening to the east. This last observation strictly followed the recent relocation of the fumarolic activity from the Solfatara area toward the Pisciarelli area, located eastward to the outer slopes of the Solfatara (Figure1b) (Troiano et al., 2014). This relocation was marked by a temperature increasing, new vents and boiling pools opening, the occurrence of seismic activity and by the impressively fast changes in the morphology of this zone.

Unfortunately, the source of such relocation is yet largely unknown and a lack of knowledge persists about the fluid dynamics in that part of the CFc hydrothermal system. Current geophysical details of the connections between the Solfatara and Pisciarelli zones are still largely crude, and the geochemical data from Pisciarelli suffers of some criticism, as discussed in Chiodini et al. (2011), who suggested that these data could be heavily modified by seasonal cycles. They would then be not-totally conclusive for investigations into the future changes caused by deep volcanic processes.

The ERT survey in the Pisciarelli area.

Two main electrical conductivity mechanisms characterize a fluid-saturated porous medium (Rinaldi et al., 2011). The first one is caused by the fluid flow inside the pores, through electro-migration of charges into the connected pore space. A second conduction mechanism occurs at the pore water–mineral interface in the electrical double layer, that is caused by a migration of the weakly adsorbed counterions (usually cations). The DC electrical conductivity of the porous rock can be expressed as a combination of those two contribution, namely the surface electrical conductivity at the water–mineral interface and the pore fluid electrical conductivity. Changes in those two quantities are mainly due to variations into the fluid filling the pore, considering that wet rocks usually have conductivities sensibly higher that dry rocks (Rinaldi et al., 2011 and references therein). Surface and pore fluid conductivities depends linearly from temperature (Vaughan et al., 1993, Revil et al., 1998, Roberts, 2002). Moreover, a dependence from the rock matrix permeability and from salinity of the pore fluids is also observed (Jardani and Revil, 2009). Many mechanisms can be advocated when changes are observed in the bulk conductivity of the rocks. The first element to consider is the compositional nature of the fluids flowing into the system. The pore space of the rocks is indeed occupied by a mixture of multiphase fluids, as water and CO2 in liquid and vapour phase. Such mixture is altered by the interaction between meteoric waters and fluids rising from the deep because of volcanic effects, which has direct effects upon the underground resistivity. When fluid changes their distribution into the shallower part of the hydrothermal system, the diffusion of the gas phases (both water vapor and CO2) and the temperature variations alter the electrical conductivity both at the pore surface and within the porous space. Also the boiling phenomena into the fluids reinforce the observed gradient in conductivity between liquid saturated and gas saturated areas, concentrating the brine and increasing salinity in the remaining liquid part. As further effect, the fracturing induced by the fluid dynamics and thermal expansion also alter the electrical conductivity of the subsoil, modifying the rock permeability.

The geoelectrical surveys are very effective tools for unveil the dynamics of tectonic and volcanic settings, and several contribution already regarded the Campanian district (Di Maio et al., 1998;

Bruno et al., 2007;Troiano et al., 2008, 2009; Byrdina et al., 2014; Di Giuseppe et al., 2015, 2017; Gresse et al., 2017).

For the first time, ERT surveys were carried out into the Pisciarelli fumarolic field after the January 2013 event, when a vent that emitted high-pressure steam and liquid water up to 3-4 metres high was observed, in order to get an insight about the geothermal fluid circulation in the very shallow aquifer. A first survey was performed along a 70 m long survey line, aligned with the main fumarole and the permanent thermal pool in the west-east direction (Figure2), while crossing the part of the area subject to abrupt morphological changes and major emissive activity. A dipole-dipole electrode configuration was adopted, with a 2.5 m spacing, which was compact and sensitive to both lateral location and depth of bodies that are the source of anomalies (Ward, 1988). An Iris Syscal Pro instrument was used as multichannel resistivimeter. The same instrument was employed as power source, being able to output a direct current with a maximum voltage and current of 800 V and 2 A, respectively.

The selected survey arrangement took into account the morphology and harsh environment characterizing the Pisciarelli area, which represented a limitation imposed on a classical ERT application. It was only possible to arrange a short survey line, with a consequent limit in the expected depth of investigation. Despite this restriction, the use of a time-lapse approach, which consists in performing identical ERT surveys several times in the same place, makes the ERT useful to investigate the evolution of the Pisciarelli structures. The time-lapse approach was followed in several ERT applications presented in the literature. As an example, Wallin et al. (2013) imaged the inland intrusion of river water in a contaminated acquifer. Nickschick et al. (2017) observed the changes in the subsurface structure beneath heavily CO_2 degassing spots in the Hartsouv Mofete field (Czech Republic). In the volcanic Pisciarelli environment, time-lapse ERT may possibly resolve the modifications of fluid phases and/or distribution induced by the contribution of a heat component or a hot gaseous component, both likely present if a magmatic source is active in the area.

The ERT survey was regularly repeated, starting in January 2014 ending April 2015. It is worth noting that the successive repetitions of the January 2013 survey were performed along a slightly longer survey line (100 m long) with respect to the first January 2013 survey and that the bimonthly interval was chosen in order to evaluate the possible influence of seasonal effects on the hydrothermal system, as indicated by the geochemical monitoring. The ERT lines were inverted using ERTlab3D® commercial software, including topography. The inverse algorithm, described by LaBrecque et al. (1999) uses a regularized solution, looking for the optimal value of the parameter vector **P** and the stabilization parameter α for which minimizing the functional $Y(\mathbf{P})=\chi^2(\mathbf{P})+\alpha\mathbf{P}^{\mathbf{T}}\underline{\mathbf{R}}\mathbf{P}$ results in $\chi^2(\mathbf{P})=\chi^2_{prior}$. The parameters **P** are the natural logarithms of the conductivity of the mesh elements and **R**, the solution roughness, acts as the stabilizing functional. χ^2_{prior} is equal to the number of data points and χ^2 is given by $\chi^2 = (\mathbf{D} - \mathbf{F(P)})^{\mathbf{T}}\mathbf{W}\,(\mathbf{D} - \mathbf{F(P)})$, where **D** is the vector of known data values, **F(P)** is the forward solution and **W** is a data weight matrix. The diagonal elements of **W** are the reciprocals of the data variances and the off-diagonal elements are zero. This assumes non-correlated data errors. When ERT data was inverted in time-lapse mode, different approaches were contemplated. As first consideration, with every dataset collected independently of the others, each tomogram can be assumed to be a representation of a constant state of the shallower geothermal system at the collection time. With this in mind, it is possible to invert each dataset independently, isolating changes in the electrical resistivity by post inversion model differencing. A second option to consider is the inversion on the differences between the background and subsequent datasets, e.g. the resistivity obtained by the inversion of the first dataset, considered as background data, can be considered as the a priori model in the difference inversion. In this case systematic errors such as those errors due to in field configuration and discretization in the forward modelling algorithm tend to null and the result is that the difference data is likely fitted more closely than the individual potentials, resulting in fewer inversion artefacts (LaBrecque and Yang, 2001). A time-lapse regularization can also be considered (Oldenborger et al., 2007), whereby the reference model for the first inversion is an uniform model and the reference model for all subsequent experimental stages is the model obtained via inversion of the data from the previous stage. Such approaches require, at least in principle, fewer model modifications to fit the data and the objective function penalizes large perturbations from previous models as opposed to large perturbations from background. Thus, such inversion is ultimately able to build up more structure in the final models, while still satisfying the data to the same level of the previous options. As a final, and likely more corrected, option, the dataset could be inverted adopting 4D approaches (Kim et al., 2009; Karaoulis et al., 2011), which consider a four-dimensional space–time model, introducing regularizations reflecting a metric function of both space and time. In the present case, time-lapse minimization was adopted during the inversion of the dataset. The final models for each dataset, are reported in Figure 3a. Average root-mean-squares (RMS) varying from 1.1 up to 1.9 resulted, which we considered satisfactory. In order to support the reliability of the images, it is common to look at **S**, the so-called inverse problem's sensitivity matrix, which take into account the effects on the data by infinitesimal changes into the model resistivity. The sensitivity has been estimated for all the tomograms presented in Figure 3.

The ERT Dataset.

The sequence of inverted resistivity images obtained in the timelapse survey is shown in Figure 3. The tomograms showed diffuse lateral and vertical heterogeneities within a resistivity range of about three orders of magnitude.

The bimonthly-recorded resistivity sections showed four main electrical anomalies:

A. the first anomaly lying at about 20 m along the profile (corresponding to the blue vertical dashed line in the figure), located at depths varying between 60-70 m a.s.l.;
B. a second zone displaced at around 35 m along the profile (corresponding to the black dashed line in the figure), located at depths between 50-65 m a.s.l.;
C. a third zone centred at around 55 m along the profile (corresponding to the red dashed line in the figure), located between 50-65 m a.s.l.;

D. A fourth zone centred at around 70 m along the profile (corresponding to the green dashed line in the figure), located at around 60 m a.s.l.;

A further anomalous zone appears at the very end of the profile. This last feature does not lye in the vegetation-free zone and could likely be linked to some anthropic artefact. The anomalies' evolution, in shape and resistivity, is reported in Figure 4, for each of the collected datasets.

Following the approach of Wallin et al. (2013), from the ERT tomograms, the time series of electrical resistivity have been extracted for each of the electrical anomalies depicted in Figure 4, while taking into consideration the mean values of the parameter in the elementary cells that compose the related part of the tomograms. These resistivity time series are reported in Figure 5.

The anomalies observed in the subsurface underneath the Pisciarelli degassing site changed over time, as a consequence of changes in several parameters on which the resistivity depends. In particular, the high pressure of fluids (CO2 and water carried along), likely mobilized by a deeper source, is capable of altering the host rocks mechanically and/or chemically. The fluid's power is capable of moving material from lower levels or widening the pores within materials. Moreover, according to Annunziatellis et al. (2008), gases like CO_2 are capable of migrating not only vertically, but also horizontally in soil as density-driven flows or advective forces, leading to horizontal changes in the anomalies. In addition, temperature fluctuations, for instance induced by the inflow of deep-lying hot fluids or by fluids mixing of in the uppermost part of the hydrothermal system, can induce significant changes in resistivity. Considering such connections, a comparison between the changes of electrical resistivity in the anomalous zones and some superficial observations was attempted. The parameters considered here are the temperature, CO2 fluxes and rainfall rates. The CO_2 fluxes and the temperatures of the emitted gasses were recorded in the Pisciarelli main vent during 2007-2016 (INGV, 2018) in correspondence with the FLXOV3measuring station. These quantities are reported in Figure 6a and 6b, respectively, where are limited to the years 2014-2015. Also the long-term temperature trend is reported in Figure 6a, which was deduced by applying the Seasonal Trend

Decomposition (STL) algorithm on the infrared imaging recorded in proximity of the upper part of the west side of the vent (Vilardo et al., 2015; INGV, 2018). The two temperature estimates, which refer to emitted gasses and surface thermal features of the area affected by diffuse degassing, respectively, are biased. However, they show a very close relationship in pattern of variability. The monthly rainfall rates, relative to the meteorological station of Pozzuoli (furnished by the 'Protezione Civile Regione Campania') are reported in Figure 6c. All data are reported as recorded in the corresponding measuring stations, but a brute comparison between these quantities can be misleading, due to the very different nature and variability of such records. Therefore, the way to compare information so different as the ERT tomograms and the surface observations (geochemical data, temperature and rainfall rates) has to be carefully investigated and a normalization criterion has to be adopted to result in a valid comparison. In order to place all these signals on a comparable scale, the so-called z-score (Klemelä, 2009) was calculated for each record separately. The z-scores were obtained by removing the mean value from each time series and dividing by the relative standard deviation. In such way, samples having zero means and unit variances are obtained. The z-scores for all the variables mentioned above (and shown in Figure 5 and 6) are reported in Figure 7.

Discussion.

The resistivity trends of the different anomalies over time, in terms of z-scores, are shown in Figure 8a. Thus emerges a peculiar behaviour of anomaly B, that shows a resistivity oscillating more in time with respect to the other anomalies, all presenting a comparable increasing attitude. In Figure 8b, the resistivity of anomaly B is compared with the rainfall rate and temperature. The B resistivity appears to be correlated with the temperature and anti-correlated with the rainfall. This suggests that the character of the B anomaly may be influenced by seasonal effects, probably driven by the influx of cold rainwater into the system. The warmer and drier months see an increase in resistivity and vice versa. Figure 8c shows, for anomaly C, how the linear increasing trend of resistivity instead appears to be less correlated to temperature and rainfall rates.

Considering on turn the geochemical data, the main vent showed an increasing amount of CO_2 emission, varying by about one order of magnitude from 2007-2016 (INGV, 2018). Superimposed on this accumulation tendency, a clear annual cyclic oscillation was distinguishable, that has been stronger in more recent years. Chiodini et al. (2011), reporting on the CO content of the Pisciarelli fumarole, until 2011, concluded that at Pisciarelli, strong seasonal effects and the possibility of re-equilibration of the fumarolic fluids at very shallow depths concealed the deep geothermo-barometric signals. In addition, the comparison of the z-scores of CO_2 emission, IR temperature and rainfalls, reported in Figure 8d shows a strong correlation between CO_2 emission and rainfalls. The comparison between CO2 emission and resistivities, reported in Figure 8e, suggests a link between the parameters. Such correlation could be likely due to a buffering and/or cumulation of the gas flowing from the geothermal system to the atmosphere in those zones. At least in principle, the contribution of chemical effects to observed changes in resistivity, such as fracture sealing or rock alteration, cannot be excluded. However, we note that these effects should not show any periodicity. Moreover, concerning the sealing, the dynamics of Pisciarelli allows a reasonable opening rather than closing of fractures. On other hands, the dominants among the new chemical species, e.g. sulfur and alunite as indicated in Piochi et al. (2015b), should induce a decrease in the bulk rocks resistivity. In contrast, the non-cyclical anomalies retrieved through the time-lapse ERT imaging present an increasing attitude. The comparison with the surface data helps to strengthen the hypotheses on the phenomena that determine the observed variations in the electrical structures.

Recognizing the relevance and meaning of the anomalies and their evolution over time in electrical images is not, however, trivial, especially considering the interplay between rainwater and hydrothermal fluids, which can generate elaborate patterns. In the case of Pisciarelli, this interaction has a feedback in the tomographic sections. The first element is the direct link between anomaly B and the surface. The second element is the diffusion over time of a low resistivity zone along the top of anomaly C, which interacts with a vertical conductive plume apparently rising up in the boundary zone between the C and D anomalies. The B anomaly corresponds to the thermal pool and it shows a seasonal character, while the boundary between the C and D anomalies corresponds to a fault zone with surface manifestations and the maximum of fracture detected in the field (Isaia et al., 2015). In our interpretation, rainwaters stored into the thermal pool penetrate into the subsoil through the narrow channel, permeating the available space, the results of which are laterally confined by the C anomaly, in turn acting as a permeability barrier. Moreover, part of the same waters dislocate also along the top of the C anomaly, which again acts as a permeability barrier, ending to interact with other fluids, of deeper origin, rising along the pre-existing fractures. This interpretative framework is summarized in Figure 9, where a sketch map is superimposed over the tomographies.

Conclusion

In this paper the results of a time lapse ERT monitoring in the volcanically active Pisciarelli site are shown. Being that pre-eruptive changes are frequently extremely rapid, and the Pisciarelli area is extremely urbanized, this site represents one of the strong sources of volcanic risk in the whole CFc and looking for pre-eruptive indicators could be relevant to prevent potentially highly destructive consequences. This is particularly true due to the non-totally conclusive findings of the routine monitoring performed in the area.

Even though the imaging we have performed brings only a small amount of large-scale information about the feeding system, due to the limited resolution at depths, the ERT imaging highlighted several anomalous zones. The interpretation of such patterns is quite difficult, being related to complex phenomena such as the interaction between the fluid components of different origins present in the vent. However, the comparison with other monitoring data (temperature, geochemical data and rainfall rates) permitted us to discern the areas dominated by seasonal effects from the ones more influenced by other, most significant contributions, linked to gas injected into the system from deep locations which cumulates in the subsoil. Moreover, such comparison can be a guideline toward a more confident interpretation of the patterns shown by fluids during such times, helping to understand what features are more related to the apport of meteoric waters into the subsoil and what could be more correlated to the inflow of fluids of deeper origins. The boundary surfaces along which the fluids displace and the fractures where fluids rise are also revealed. The reconstruction of such features, obtained through the imaging of the underground electrical resistivity changes reveal the complex interactions between the environment and the deeper volcanic sources. In this sense, the presented results point out some general aspects. The indirect information obtained through geophysical imaging proves an vehicle to underline the underground phenomena, explaining the dynamics of large volumes of subsoil without any arbitrary extrapolations, typical of techniques based on surface observations. A further methodological aspect has to be underlined. No geophysical method is self-consistent, in the sense that just the integration of information about all the physical characteristics of rocks allows the understanding of the phenomena occurring and the creation of unique lithological models. In spite of this, however, our results show how the single electrical technique has a relevant proficiency. The model presented in Fig.9 evidence the self-standing ERT capability to define and detail the phenomena at least in their essential lines. The results presented here can be considered the first test about the aptitude of time-lapse ERT to understand the evolution of an active fumarole, thanks to a significant contribution to the characterization of subsoil structures and the understanding of their evolution during time. In any case, even if the tomograms indicate that this promising approach of time-lapse ERT monitoring to sheds light on the potentially dangerous evolution of the investigated system, because the phenomena involved are extremely complex, the evaluation of such aspects deserves more effort and rigorous modelling. As further development, the establishment of permanent and longer surveying lines could substantiate the results. In particular, a continuous acquisition of the tomograms could end in longer time series of electrical resistivity changes, which could be compared to the geochemical ones following combined statistical approaches, such as wavelet coherence analysis.

Figure captions.

Fig.1. a) Map of the Campi Flegrei caldera (Italy). b) Map of the Solfatara-Pisciarelli complex, framed with the black box in panel a). The ERT survey area is enclosed in the black box and the survey profile is evidenced with the red line. The geodetic reference system is UTM-WGS84.

Fig.2. Aerial view of the Pisciarelli area, where the time-lapse ERT surveys were realized (red dashed line). Locations of the main anomalies retrieved by ERT are indicated, with the colored capital letters. The geodetic reference system is UTM-WGS84.

Fig.3. ERT resistivity sectionsrelative to the profile sketched in Fig.2. For every section, the relative date is indicated. A common logarithmic scale is used for all the resistivity sections. The main features discussed into the text (already shown in figure 2) are also indicated with the coloured dotted lines;

Fig.4. Detail of the four main electrical anomalies retrieved through time-lapse ERT. For every section, the relative date is indicated. A common logarithmic scale is used for all the resistivity sections. The main features discussed into the text are also labelled with coloured capital letters.

Fig. 5. Comparison between the electrical resistivity time series (in Ωm) as function of time, which were obtained extracting the mean value of the parameter in correspondence of the four areas shown in figure 4.

Fig. 6. a) temperature of the gas emitted at the Pisciarelli main vent (left axes, ° C) and temperature extracted from infrared thermal images through the application of the STL algorithm (right axis, ° C) during 2014-2015. (b) CO2 fluxes emitted at the Pisciarelli main vent (in $gm^{-2}d^{-1}$) during 2014-2015. (c) Monthly rainfall rates (in mm $month^{-1}$) recorded at the Pozzuoli meteorological station of the ‘Protezione Civile Regionale’ agency.

Fig.7. The z-scores extracted by the variables mentioned in Figure 5 (electrical resistivity time series) and Figure 6 (temperature, CO_2 fluxes and rainfall rates). Z-scores were obtained by removing the mean value from each time series and dividing by the relative standard deviation.

Fig. 8. Z-scores extracted by the observed variables, compared as follow: (a) electrical resistivity time series relative to the four anomalous zones shown in Figure 2. (b) electrical resistivity time series relative to the B electrical anomaly, surface IR temperature and rainfall rates. (c) electrical resistivity time series relative to the C electrical anomaly, surface IR temperature and rainfall rates. (d) CO_2 fluxes, surface IR temperature and rainfall rates. (e) electrical resistivity time series relative to the four anomalous zones, CO_2 fluxes.

Fig.9. Conceptual model of the Pisciarelli fumarolic zone. This W-E model crosses the main vent and the thermal permanent pool. The interpretative elements are reported in the legend. Electrical resistivity isolines, relative to the April 2015 tomogram are superimposed, maintaining the same common logarithm scale of Figure 3.

References

Aizawa, K., Ogawa, Y., Ishido, T., 2009. Groundwater flow and hydrothermal systems within volcanic edifices: Delineation by electric self-potential and magnetotellurics. J. Geophys. Res. 114, B01208. doi:10.1029/2008JB005910

Amoruso, A., Crescentini, L., Linde, A.T., Sacks, I.S., Scarpa, R., Romano, P., 2007. A horizontal crack in a layered structure satisfies deformation for the 2004–2006 uplift of Campi Flegrei. Geophys. Res. Lett.

34, L22313. doi:10.1029/2007GL031644

Annunziatellis, A., Beaubien, S.E., Bigi, S., Ciotoli, G., Coltella, M., Lombardi, S., 2008. Gas migration along fault systems and through the vadose zone in the Latera caldera (central Italy): Implications for CO2geological storage. Int. J. Greenh. Gas Control 2, 353–372. doi:10.1016/j.ijggc.2008.02.003

Bachu, S., Gunter, W.D., Perkins, E.H., 1994. Aquifer disposal of CO2: Hydrodynamic and mineral trapping. Energy Convers. Manag. 35, 269–279. doi:10.1016/0196-8904(94)90060-4

Barde-Cabusson, S., Bolós, X., Pedrazzi, D., Lovera, R., Serra, G., Martí, J., Casas, A., 2013. Electrical resistivity tomography revealing the internal structure of monogenetic volcanoes. Geophys. Res. Lett. 40, 2544–2549. doi:10.1002/grl.50538

Berrino, G., Corrado, G., Luongo, G., Toro, B., 1984. Ground deformation and gravity changes accompanying the 1982 Pozzuoli uplift. Bull. Volcanol. 47, 187–200. doi:10.1007/BF01961548

Bevilacqua, A., Isaia, R., Neri, A., Vitale, S., Aspinall, W.P., Bisson, M., Flandoli, F., Baxter, P.J., Bertagnini, A., Esposti Ongaro, T., Iannuzzi, E., Pistolesi, M., Rosi, M., 2015. Quantifying volcanic hazard at Campi Flegrei caldera (Italy) with uncertainty assessment: 1. Vent opening maps. J. Geophys. Res. Solid Earth 120, 2309–2329. doi:10.1002/2014JB011775

Bianchi, R., Coradini, A., Federico, C., Giberti, G., Lanciano, P., Pozzi, J.P., Sartoris, G., Scandone, R., 1987. Modeling of surface deformation in volcanic areas: The 1970-1972 and 1982-1984 crises of Campi Flegrei, Italy. J. Geophys. Res. Solid Earth 92, 14139–14150. doi:10.1029/JB092iB13p14139

Bruno, P.P.G., Ricciardi, G.P., Petrillo, Z., Di Fiore, V., Troiano, A., Chiodini, G., 2007. Geophysical and hydrogeological experiments from a shallow hydrothermal system at Solfatara Volcano, Campi Flegrei, Italy: Response to caldera unrest. J. Geophys. Res. Solid Earth 112. doi:10.1029/2006JB004383

Byrdina, S., Revil, A., Pant, S.R., Koirala, B.P., Shrestha, P.L., Tiwari, D.R., Gautam, U.P., Shrestha, K., Sapkota, S.N., Contraires, S., Perrier, F., 2009. Dipolar self-potential anomaly associated with carbon dioxide and radon flux at Syabru-Bensi hot springs in central Nepal. J. Geophys. Res. 114, B10101.

doi:10.1029/2008JB006154

Byrdina, S., Vandemeulebrouck, J., Cardellini, C., Legaz, A., Camerlynck, C., Chiodini, G., Lebourg, T., Gresse, M., Bascou, P., Motos, G., Carrier, A., Caliro, S., 2014. Relations between electrical resistivity, carbon dioxide flux, and self-potential in the shallow hydrothermal system of Solfatara (Phlegrean Fields, Italy). J. Volcanol. Geotherm. Res. 283, 172–182. doi:10.1016/j.jvolgeores.2014.07.010

Chiodini, G., Avino, R., Caliro, S., Minopoli, C., 2011. Temperature and pressure gas geoindicators at the Solfatara fumaroles (Campi Flegrei). Ann. Geophys.

Chiodini, G., Caliro, S., De Martino, P., Avino, R., Gherardi, F., U., T., E., B., G.P., R., P., R., C., R., 2012. Early signals of new volcanic unrest at Campi Flegrei caldera? Insights from geochemical data and physical simulations. Geology 40, 943–946. doi:10.1130/G33251.1

Chiodini, G., Paonita, A., Aiuppa, A., Costa, A., Caliro, S., De Martino, P., Acocella, V., Vandemeulebrouck, J., 2016. Magmas near the critical degassing pressure drive volcanic unrest towards a critical state. Nat. Commun. 7, 13712.

Chiodini, G., Todesco, M., Caliro, S., Del Gaudio, C., Macedonio, G., Russo, M., 2003. Magma degassing as a trigger of bradyseismic events: The case of Phlegrean Fields (Italy). Geophys. Res. Lett. 30. doi:10.1029/2002GL016790

D'Auria, L., Giudicepietro, F., Aquino, I., Borriello, G., Del Gaudio, C., Lo Bascio, D., Martini, M., Ricciardi, G.P., Ricciolino, P., Ricco, C., 2011. Repeated fluid-transfer episodes as a mechanism for the recent dynamics of Campi Flegrei caldera (1989–2010). J. Geophys. Res. 116, B04313. doi:10.1029/2010JB007837

De Natale, G., Pingue, F., Allard, P., Zollo, A., 1991. Geophysical and geochemical modelling of the 1982–1984 unrest phenomena at Campi Flegrei caldera (southern Italy). J. Volcanol. Geotherm. Res. 48, 199–222. doi:10.1016/0377-0273(91)90043-Y

De Natale, G., Troise, C., Pingue, F., Mastrolorenzo, G., Pappalardo, L., Battaglia, M., Boschi, E., 2006. The

Campi Flegrei caldera: unrest mechanisms and hazards. Geol. Soc. London, Spec. Publ. 269.

Di Giuseppe, M.G., Troiano, A., Fedele, A., Caputo, T., Patella, D., Troise, C., De Natale, G., 2015. Electrical resistivity tomography imaging of the near-surface structure of the Solfatara crater, Campi Flegrei (Naples, Italy). Bull. Volcanol. 77. doi:10.1007/s00445-015-0910-6

Di Maio, R., Mauriello, P., Patella, D., Petrillo, Z., Piscitelli, S., Siniscalchi, A., 1998. Electric and electromagnetic outline of the Mount Somma–Vesuvius structural setting. J. Volcanol. Geotherm. Res. 82, 219–238. doi:10.1016/S0377-0273(97)00066-8

Di Vito, M., Lirer, L., Mastrolorenzo, G., Rolandi, G., 1987. The 1538 Monte Nuovo eruption (Campi Flegrei, Italy). Bull. Volcanol. 49, 608–615. doi:10.1007/BF01079966

Dvorak, J.J., Mastrolorenzo, G., 1991. The mechanisms of recent vertical crustal movements in Campi Flegrei caldera, southern Italy. pp. 1–47. doi:10.1130/SPE263-p1

Fikos, I., Vargemezis, G., Zlotnicki, J., Puertollano, J.R., Alanis, P.B., Pigtain, R.C., Villacorte, E.U., Malipot, G.A., Sasai, Y., 2012. Electrical resistivity tomography study of Taal volcano hydrothermal system, Philippines. Bull. Volcanol. 74, 1821–1831. doi:10.1007/s00445-012-0638-5

Finizola, A., Aubert, M., Revil, A., Schütze, C., Sortino, F., 2009. Importance of structural history in the summit area of Stromboli during the 2002–2003 eruptive crisis inferred from temperature, soil CO2, self-potential, and electrical resistivity tomography. J. Volcanol. Geotherm. Res. 183, 213–227. doi:10.1016/j.jvolgeores.2009.04.002

Finizola, A., Revil, A., Rizzo, E., Piscitelli, S., Ricci, T., Morin, J., Angeletti, B., Mocochain, L., Sortino, F., 2006. Hydrogeological insights at Stromboli volcano (Italy) from geoelectrical, temperature, and CO_2 soil degassing investigations. Geophys. Res. Lett. 33, L17304. doi:10.1029/2006GL026842

Finizola, A., Ricci, T., Deiana, R., Cabusson, S.B., Rossi, M., Praticelli, N., Giocoli, A., Romano, G., Delcher, E., Suski, B., Revil, A., Menny, P., Di Gangi, F., Letort, J., Peltier, A., Villasante-Marcos, V., Douillet, G., Avard, G., Lelli, M., 2010. Adventive hydrothermal circulation on Stromboli volcano

(Aeolian Islands, Italy) revealed by geophysical and geochemical approaches: Implications for general fluid flow models on volcanoes. J. Volcanol. Geotherm. Res. 196, 111–119. doi:10.1016/j.jvolgeores.2010.07.022

Giese, R., Henninges, J., Lüth, S., Morozova, D., Schmidt-Hattenberger, C., Würdemann, H., Zimmer, M., Cosma, C., Juhlin, C., 2009. Monitoring at the CO2 SINK site: A concept integrating geophysics, geochemistry and microbiology. Energy Procedia 1, 2251–2259. doi:10.1016/j.egypro.2009.01.293

Di, Giuseppe, M.G. Di, Troiano, A., Vito, M.A. Di, Somma, R., Matano, F., 2017. Definition of small-scale volcanic structures by Electrical Resistivity Tomography: the Trentaremi cone, an example from the Campi Flegrei Caldera (Italy). Ann. Geophys. 60, S0552. doi:10.4401/ag-7397

Gottsmann, J., Folch, A., Rymer, H., 2006. Unrest at Campi Flegrei: A contribution to the magmatic versus hydrothermal debate from inverse and finite element modeling. J. Geophys. Res. 111, B07203. doi:10.1029/2005JB003745

Gresse, M., Vandemeulebrouck, J., Byrdina, S., Chiodini, G., Revil, A., Johnson, T.C., Ricci, T., Vilardo, G., Mangiacapra, A., Lebourg, T., Grangeon, J., Bascou, P., Metral, L., 2017. Three-Dimensional Electrical Resistivity Tomography of the Solfatara Crater (Italy): Implication for the Multiphase Flow Structure of the Shallow Hydrothermal System. J. Geophys. Res. Solid Earth 122, 8749–8768. doi:10.1002/2017JB014389

INGV, 2018. Bollettini di sorveglianza dei vulcani campani.

Isaia, R., Vitale, S., Di Giuseppe, M.G., Iannuzzi, E., Tramparulo, F.D., Troiano, A., 2015. Stratigraphy, structure, and volcano-tectonic evolution of Solfatara maar-diatreme (Campi Flegrei, Italy). Bull. Geol. Soc. Am. 127, 1485–1504. doi:10.1130/B31183.1

Karaoulis M., A. Revil, D.D. Werkema, B. Minsley, W.F. Woodruff, and A. Kemna, Time-lapse 3D inversion of complex conductivity data using an active time constrained (ATC) approach, Geophysical Journal International, 187, 237–251, doi: 10.1111/j.1365-246X.2011.05156.x, 2011

Kiessling, D., Schmidt-Hattenberger, C., Schuett, H., Schilling, F., Krueger, K., Schoebel, B., Danckwardt, E., Kummerow, J., 2010. Geoelectrical methods for monitoring geological CO2 storage: First results from cross-hole and surface–downhole measurements from the CO2SINK test site at Ketzin (Germany). Int. J. Greenh. Gas Control 4, 816–826. doi:10.1016/j.ijggc.2010.05.001

Kim, J. H., Yi, M. J., Park, S. G., & Kim, J. G. (2009). 4-D inversion of DC resistivity monitoring data acquired over a dynamically changing earth model. Journal of Applied Geophysics, 68(4), 522-532.

Klemelä, J., 2009. Smoothing of multivariate data : density estimation and visualization. John Wiley & Sons.

LaBrecque, D.J., Morelli, G., Daily, W., Ramirez, A., Lundegard, P., 1999. 37. Occam's Inversion of 3-D Electrical Resistivity Tomography, in: Three-Dimensional Electromagnetics. Society of Exploration Geophysicists, pp. 575–590. doi:10.1190/1.9781560802154.ch37

LaBrecque, D.J., Yang, X., 2001. Difference Inversion of ERT Data: a Fast Inversion Method for 3-D In Situ Monitoring. J. Environ. Eng. Geophys. 6, 83–89. doi:10.4133/JEEG6.2.83

Le Roux, O., Cohen, G., Loisy, C., Laveuf, C., Delaplace, P., Magnier, C., Rouchon, V., Cerepi, A., Garcia, B., 2013. The CO2-Vadose project: Time-lapse geoelectrical monitoring during CO2 diffusion in the carbonate vadose zone. Int. J. Greenh. Gas Control 16, 156–166. doi:10.1016/J.IJGGC.2013.03.016

Letort, J., Roux, P., Vandemeulebrouck, J., Coutant, O., Cros, E., Wathelet, M., Cardellini, C., Avino, R., 2012. High-resolution shallow seismic tomography of a hydrothermal area: application to the Solfatara, Pozzuoli. Geophys. J. Int. 189, 1725–1733. doi:10.1111/j.1365-246X.2012.05451.x

Lima, A., De Vivo, B., Spera, F.J., Bodnar, R.J., Milia, A., Nunziata, C., Belkin, H.E., Cannatelli, C., 2009. Thermodynamic model for uplift and deflation episodes (bradyseism) associated with magmatic–hydrothermal activity at the Campi Flegrei (Italy). Earth-Science Rev. 97, 44–58. doi:10.1016/j.earscirev.2009.10.001

Moretti, R., De Natale, G., Troise, C., 2017. A geochemical and geophysical reappraisal to the significance of the recent unrest at Campi Flegrei caldera (Southern Italy). Geochemistry, Geophys. Geosystems 18, 1244–1269. doi:10.1002/2016GC006569

Nickschick, T., Flechsig, C., Meinel, C., Mrlina, J., Kämpf, H., 2017. Architecture and temporal variations of a terrestrial CO2 degassing site using electric resistivity tomography and self-potential. Int. J. Earth Sci. 1–12. doi:10.1007/s00531-017-1470-0

Oldenborger, G.A., Knoll, M.D., Routh, P.S., LaBrecque, D.J., 2007. Time-lapse ERT monitoring of an injection/withdrawal experiment in a shallow unconfined aquifer. GEOPHYSICS 72, F177–F187. doi:10.1190/1.2734365

Orsi, G., Di Vito, M.A., Isaia, R., 2004. Volcanic hazard assessment at the restless Campi Flegrei caldera. Bull. Volcanol. 66, 514–530. doi:10.1007/s00445-003-0336-4

Petrosino, S., Damiano, N., Cusano, P., Di Vito, M.A., de Vita, S., Del Pezzo, E., 2012. Subsurface structure of the Solfatara volcano (Campi Flegrei caldera, Italy) as deduced from joint seismic-noise array, volcanological and morphostructural analysis. Geochemistry, Geophys. Geosystems 13, n/a-n/a. doi:10.1029/2011GC004030

Piochi, M., Mormone, A., Balassone, G., Strauss, H., Troise, C., De Natale, G., 2015a. Native sulfur, sulfates and sulfides from the active Campi Flegrei volcano (southern Italy): Genetic environments and degassing dynamics revealed by mineralogy and isotope geochemistry. J. Volcanol. Geotherm. Res. 304, 180–193. doi:10.1016/j.jvolgeores.2015.08.017

Piochi, M., Mormone, A., Balassone, G., Strauss, H., Troise, C., De Natale, G., 2015b. Native sulfur, sulfates and sulfides from the active Campi Flegrei volcano (southern Italy): Genetic environments and degassing dynamics revealed by mineralogy and isotope geochemistry. J. Volcanol. Geotherm. Res. 304, 180–193. doi:10.1016/j.jvolgeores.2015.08.017

Pribnow, D.F.., Schütze, C., Hurter, S.J., Flechsig, C., Sass, J.H., 2003. Fluid flow in the resurgent dome of Long Valley Caldera: implications from thermal data and deep electrical sounding. J. Volcanol. Geotherm. Res. 127, 329–345. doi:10.1016/S0377-0273(03)00175-6

Revil, A., Cathles III, L.M., Losh, S., Nunn, J.A., 1998. Electrical conductivity in shaly sands with geophysical application. J. Geophys. Res., 103 (B10) (1998), pp. 23925-23936

Revil, A., Finizola, A., Piscitelli, S., Rizzo, E., Ricci, T., Crespy, A., Angeletti, B., Balasco, M., Barde Cabusson, S., Bennati, L., Bolève, A., Byrdina, S., Carzaniga, N., Di Gangi, F., Morin, J., Perrone, A., Rossi, M., Roulleau, E., Suski, B., 2008. Inner structure of La Fossa di Vulcano (Vulcano Island, southern Tyrrhenian Sea, Italy) revealed by high-resolution electric resistivity tomography coupled with self-potential, temperature, and CO_2 diffuse degassing measurements. J. Geophys. Res. 113, B07207. doi:10.1029/2007JB005394

Revil, A., Finizola, A., Ricci, T., Delcher, E., Peltier, A., Barde-Cabusson, S., Avard, G., Bailly, T., Bennati, L., Byrdina, S., Colonge, J., Di Gangi, F., Douillet, G., Lupi, M., Letort, J., Tsang Hin Sun, E., 2011. Hydrogeology of Stromboli volcano, Aeolian Islands (Italy) from the interpretation of resistivity tomograms, self-potential, soil temperature and soil CO2 concentration measurements. Geophys. J. Int. 186, 1078–1094. doi:10.1111/j.1365-246X.2011.05112.x

Roberts, J.J., 2002. Electrical properties of microporous rock as a function of saturation and temperature. J. Appl. Phys., 91 (3).

Schmidt-Hattenberger, C., Bergmann, P., Kießling, D., Krüger, K., Rücker, C., Schütt, H., Group, K., 2011. Application of a Vertical Electrical Resistivity Array (VERA) for monitoring CO2 migration at the Ketzin site: First performance evaluation. Energy Procedia 4, 3363–3370. doi:10.1016/j.egypro.2011.02.258

Shirzaei, M., Walter, T.R., 2010. Time-dependent volcano source monitoring using interferometric synthetic aperture radar time series: A combined genetic algorithm and Kalman filter approach. J. Geophys. Res. 115, B10421. doi:10.1029/2010JB007476

Singha, K., Day-Lewis, F.D., Johnson, T., Slater, L.D., 2015. Advances in interpretation of subsurface processes with time-lapse electrical imaging. Hydrol. Process. 29, 1549–1576. doi:10.1002/hyp.10280

Slater, L., 2007. Near Surface Electrical Characterization of Hydraulic Conductivity: From Petrophysical

Properties to Aquifer Geometries—A Review. Surv. Geophys. 28, 169–197. doi:10.1007/s10712-007-9022-y

Todesco, M., Chiodini, G., Macedonio, G., 2003. Monitoring and modelling hydrothermal fluid emission at La Solfatara (Phlegrean Fields, Italy). An interdisciplinary approach to the study of diffuse degassing. J. Volcanol. Geotherm. Res. 125, 57–79. doi:10.1016/S0377-0273(03)00089-1

Troiano, A., Di Giuseppe, M., Petrillo, Z., Troise, C., De Natale, G., 2011. Ground deformation at calderas driven by fluid injection: Modelling unrest episodes at Campi Flegrei (Italy). Geophys. J. Int. 187, 833–847. doi:10.1111/j.1365-246X.2011.05149.x

Troiano, A., Di Giuseppe, M.G., Patella, D., Troise, C., De Natale, G., 2014. Electromagnetic outline of the Solfatara-Pisciarelli hydrothermal system, Campi Flegrei (Southern Italy). J. Volcanol. Geotherm. Res. 277, 9–21. doi:10.1016/j.jvolgeores.2014.03.005

Troiano, A., Di Giuseppe, M.G., Petrillo, Z., Patella, D., 2009. Imaging 2D structures by the CSAMT method: Application to the Pantano di S. Gregorio Magno faulted basin (Southern Italy). J. Geophys. Eng. 6, 120–130. doi:10.1088/1742-2132/6/2/003

Troiano, A., Petrillo, Z., Di Giuseppe, M.G., Balasco, M., Diaferia, I., Di Fiore, B., Siniscalchi, A., Patella, D., 2008. About the shallow resistivity structure of Vesuvius volcano, in: Annals of Geophysics. doi:10.4401/ag-3043

Vaughan, P.J., Udell, K.S., Wilt, M.J., 1993. The effects of steam injection on the electrical conductivity of an unconsolidated sand saturated with a salt solution. J. Geophys. Res., 98 (B1) (1993), pp. 509-518

Vilardo, G., Sansivero, F., Chiodini, G., 2015. Long-term TIR imagery processing for spatiotemporal monitoring of surface thermal features in volcanic environment: A case study in the Campi Flegrei (Southern Italy). J. Geophys. Res. Solid Earth 120, 812–826. doi:10.1002/2014JB011497

Wallin, E.L., Johnson, T.C., Greenwood, W.J., Zachara, J.M., 2013. Imaging high stage river-water intrusion into a contaminated aquifer along a major river corridor using 2-D time-lapse surface electrical resistivity tomography. Water Resour. Res. 49, 1693–1708. doi:10.1002/wrcr.20119

Ward, S.H., 1988. The Resistivity and Induced Polarization Methods, in: Symposium on the Application of Geophysics to Engineering and Environmental Problems 1988. Environment and Engineering Geophysical Society, pp. 109–250. doi:10.4133/1.2921804

Würdemann, H., Möller, F., Kühn, M., Heidug, W., Christensen, N.P., Borm, G., Schilling, F.R., 2010. CO2SINK—From site characterisation and risk assessment to monitoring and verification: One year of operational experience with the field laboratory for CO2 storage at Ketzin, Germany. Int. J. Greenh. Gas Control 4, 938–951. doi:10.1016/j.ijggc.2010.08.010

Zhou, X., Lakkaraju, V.R., Apple, M., Dobeck, L.M., Gullickson, K., Shaw, J.A., Cunningham, A.B., Wielopolski, L., Spangler, L.H., 2012. Experimental observation of signature changes in bulk soil electrical conductivity in response to engineered surface CO2 leakage. Int. J. Greenh. Gas Control 7, 20–29. doi:10.1016/j.ijggc.2011.12.006

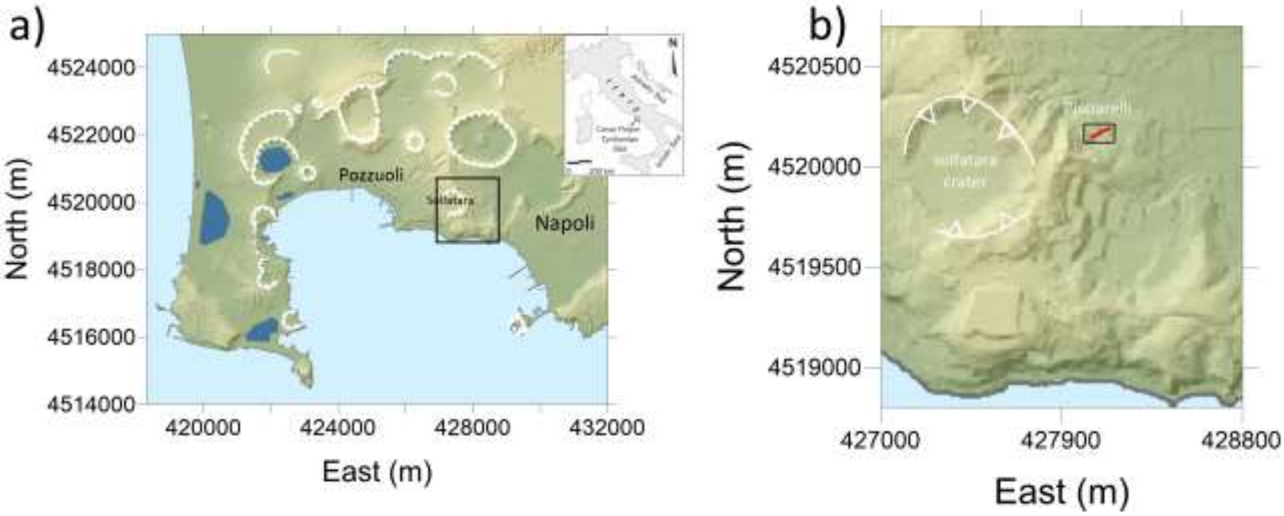
a)
4524000
4522000
4520000
4518000
4516000
4514000
North (m)
Pozzuoli
Solfatara
Napoli
420000
424000
428000
432000
East (m)
b)
4520500
4520000
4519500
4519000
North (m)
solfatara
crater
427000
427900
428800
East (m)

Figure 1.

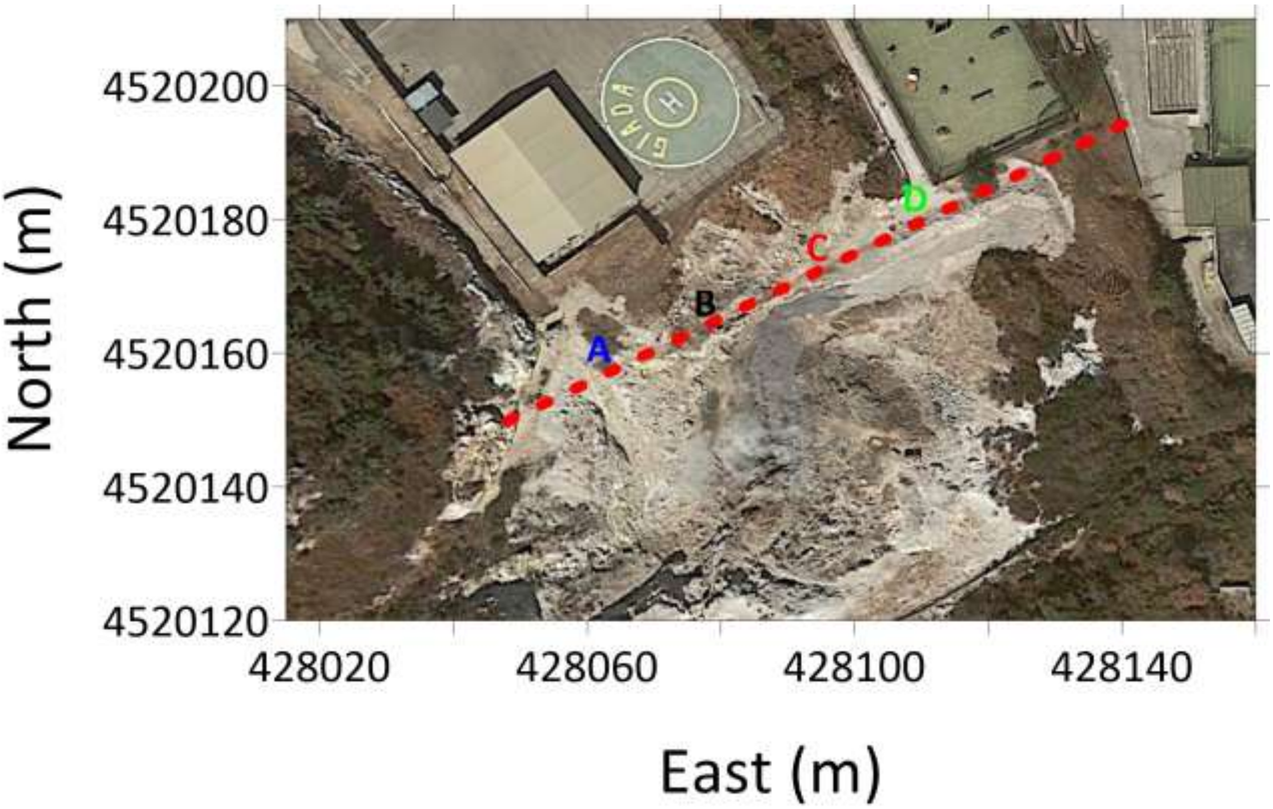
North (m)
4520200
4520180
4520160
4520140
4520120
428020
428060
428100
428140
East (m)
A
B
C
D

Figure 2.

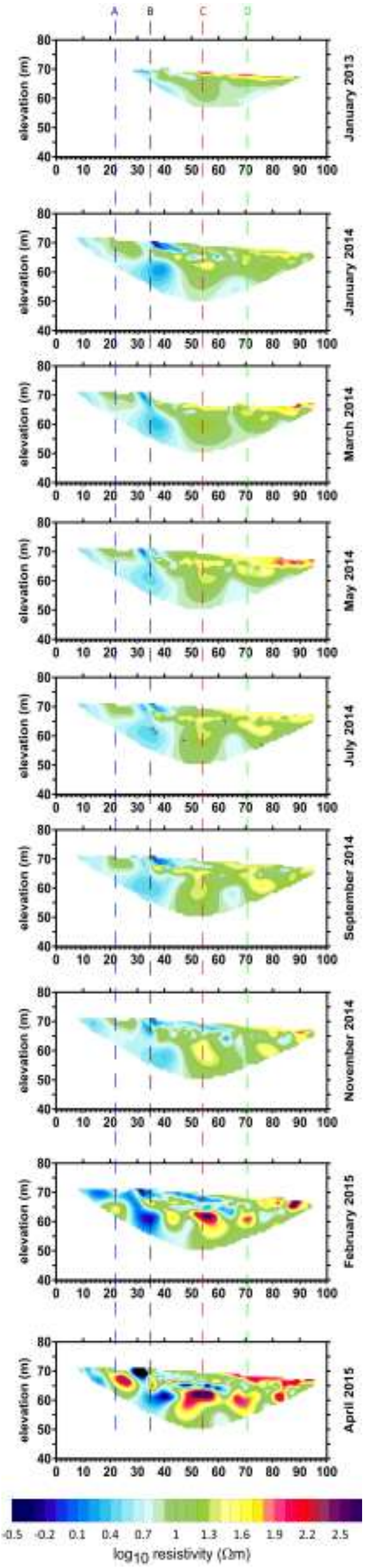
A
B
C
D
elevation (m)
January 2013
January 2014
March 2014
May 2014
July 2014
September 2014
November 2014
February 2015
April 2015
-0.5 -0.2 0.1 0.4 0.7 1 1.3 1.6 1.9 2.2 2.5
log10 resistivity (Ωm)

Figure 3

677

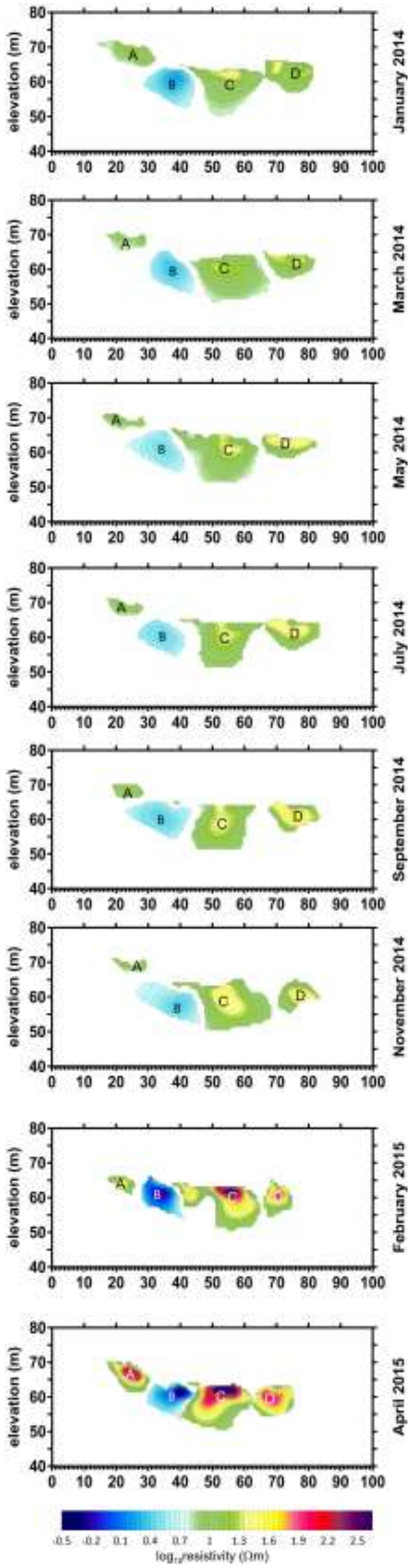

elevation (m)
January 2014
March 2014
May 2014
July 2014
September 2014
November 2014
February 2015
April 2015
A
B
C
D
0 10 20 30 40 50 60 70 80 90 100
40 50 60 70 80
-0.5 -0.2 0.1 0.4 0.7 1 1.3 1.6 1.9 2.2 2.5
log10 resistivity (Ωm)

Figure 4.

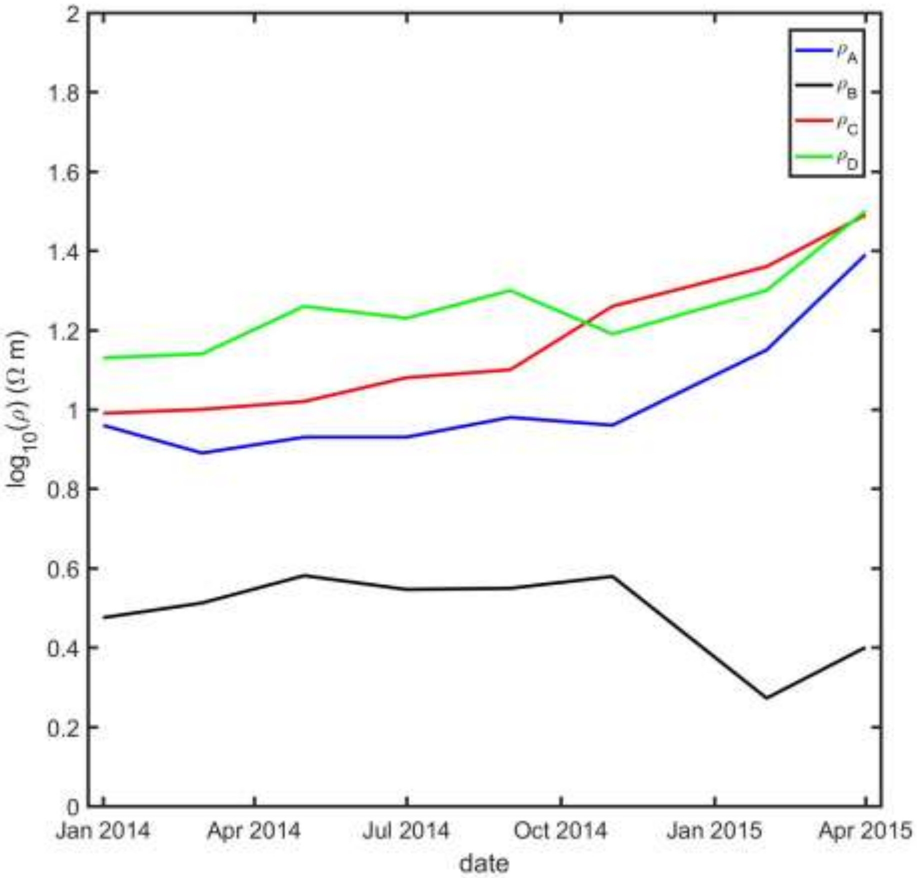

2
1.8
1.6
1.4
1.2
1
0.8
0.6
0.4
0.2
0
$\log_{10}(\rho)$ (Ω m)
ρ_A
ρ_B
ρ_C
ρ_D
Jan 2014
Apr 2014
Jul 2014
Oct 2014
Jan 2015
Apr 2015
date

Figure 5.

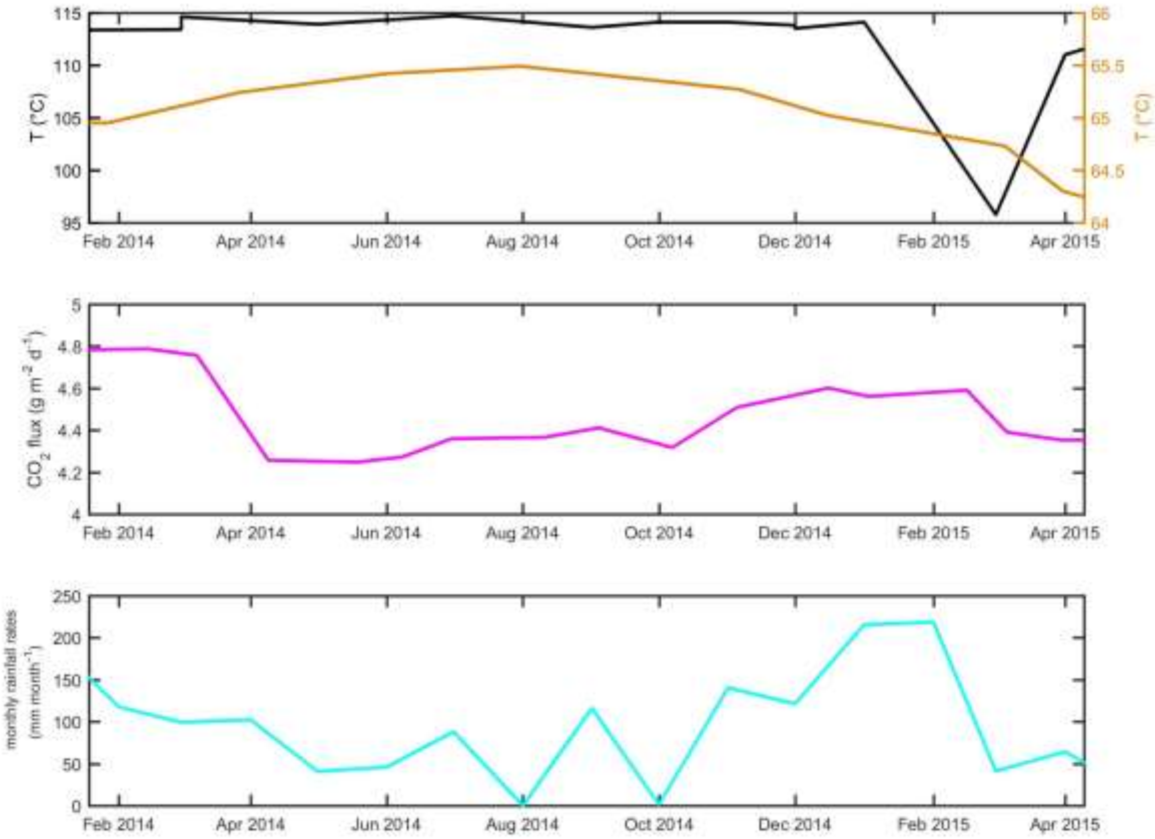

T (°C)
T (°C)
CO2 flux (g m-2 d-1)
monthly rainfall rates (mm month-1)
Feb 2014
Apr 2014
Jun 2014
Aug 2014
Oct 2014
Dec 2014
Feb 2015
Apr 2015

Figure 6.

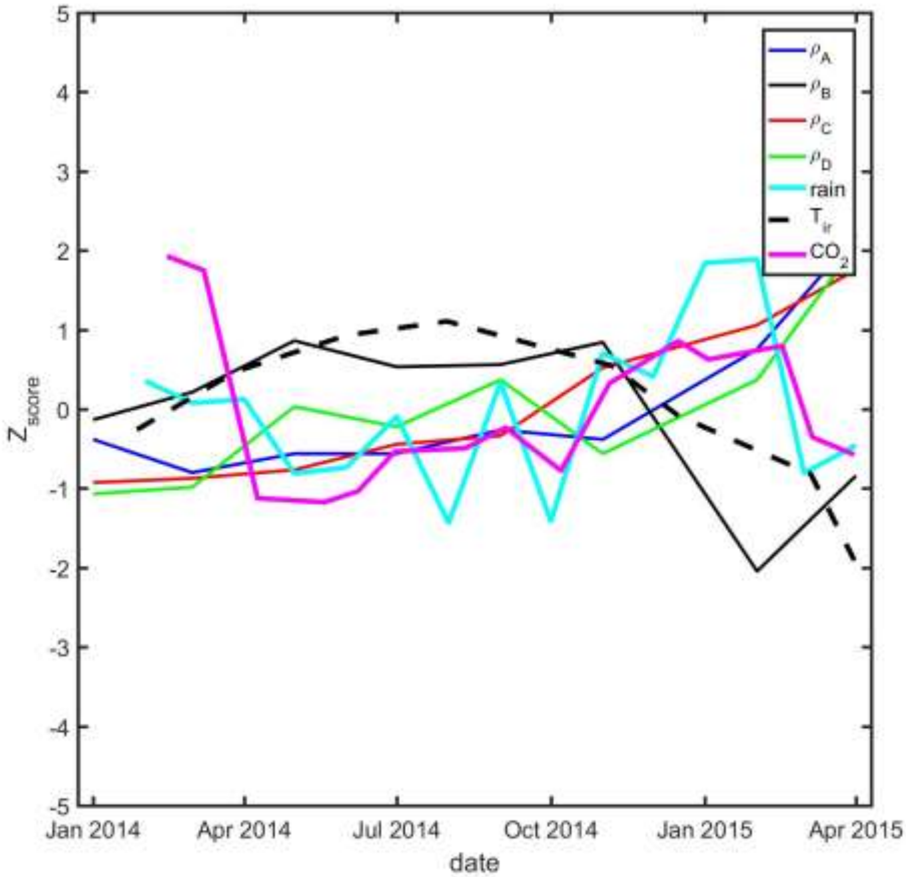
ρ_A
ρ_B
ρ_C
ρ_D
rain
T_{ir}
CO_2
5
4
3
2
1
0
-1
-2
-3
-4
-5
Z_{score}
Jan 2014
Apr 2014
Jul 2014
Oct 2014
Jan 2015
Apr 2015
date

Figure 7.

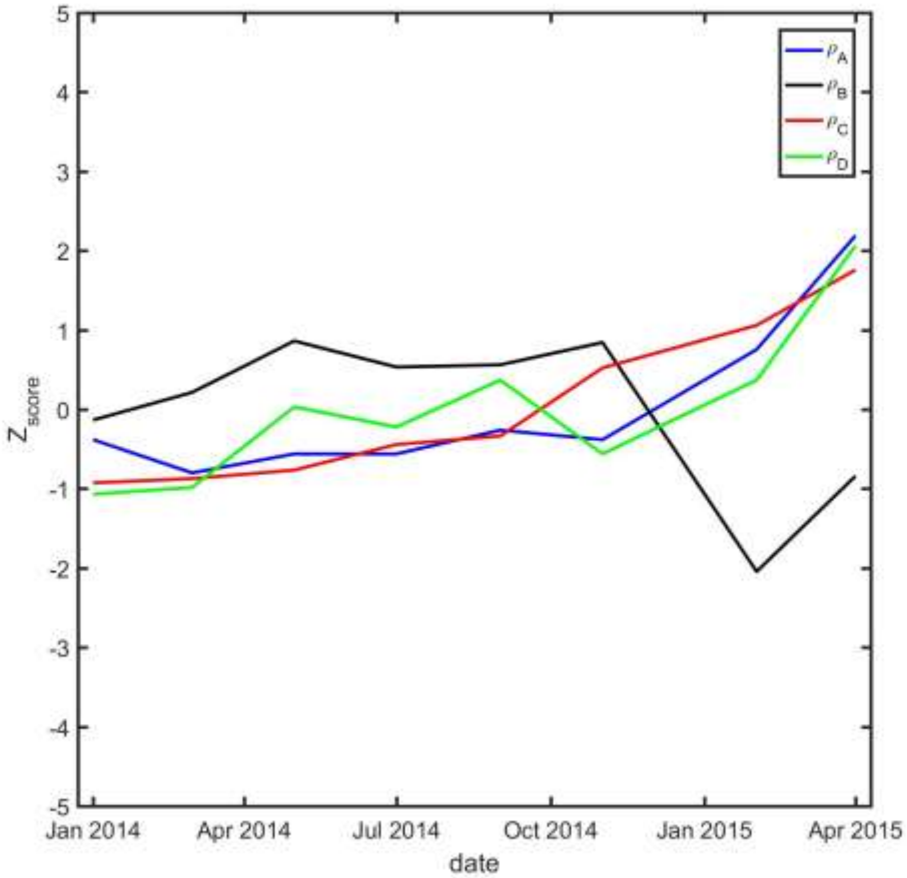

5
4
3
2
1
0
-1
-2
-3
-4
-5
Z_{score}
Jan 2014
Apr 2014
Jul 2014
Oct 2014
Jan 2015
Apr 2015
date
ρ_A
ρ_B
ρ_C
ρ_D

Figure 8a.

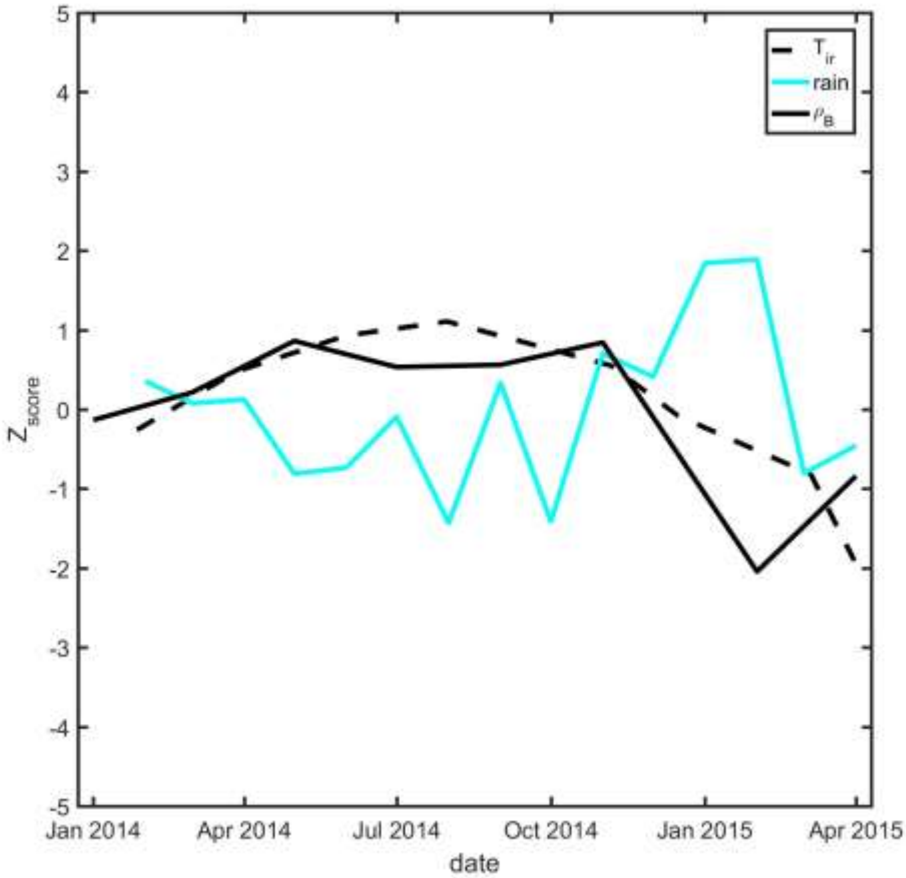
T_ir
rain
ρ_B
Z_score
5
4
3
2
1
0
-1
-2
-3
-4
-5
Jan 2014
Apr 2014
Jul 2014
Oct 2014
Jan 2015
Apr 2015
date

Figure 8b.

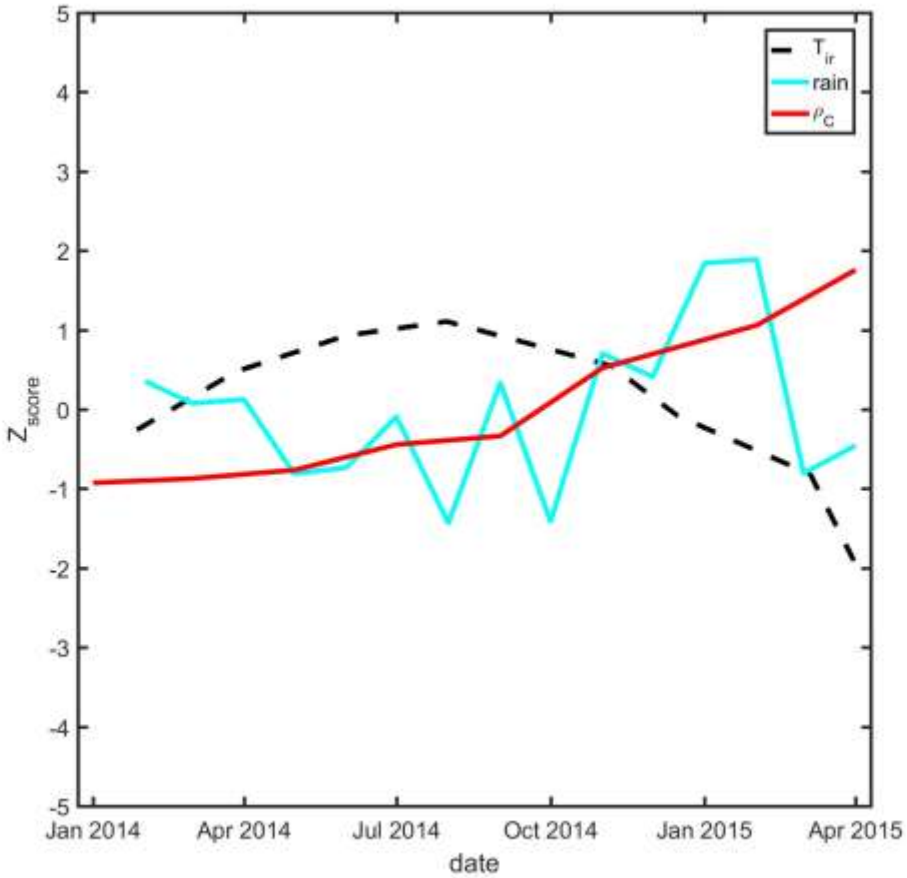
T_ir
rain
ρ_C
Z_score
date
5
4
3
2
1
0
-1
-2
-3
-4
-5
Jan 2014
Apr 2014
Jul 2014
Oct 2014
Jan 2015
Apr 2015

Figure 8c.

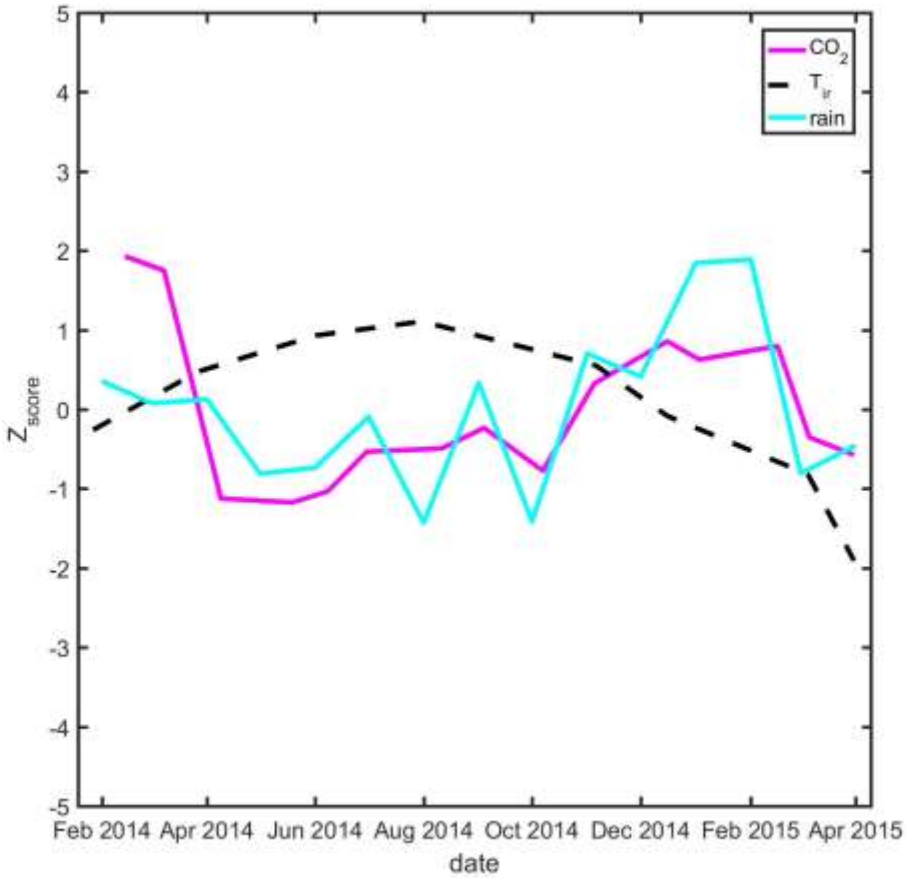
CO_2
T_{ir}
rain
5
4
3
2
1
0
-1
-2
-3
-4
-5
Z_{score}
Feb 2014
Apr 2014
Jun 2014
Aug 2014
Oct 2014
Dec 2014
Feb 2015
Apr 2015
date

Figure 8d.

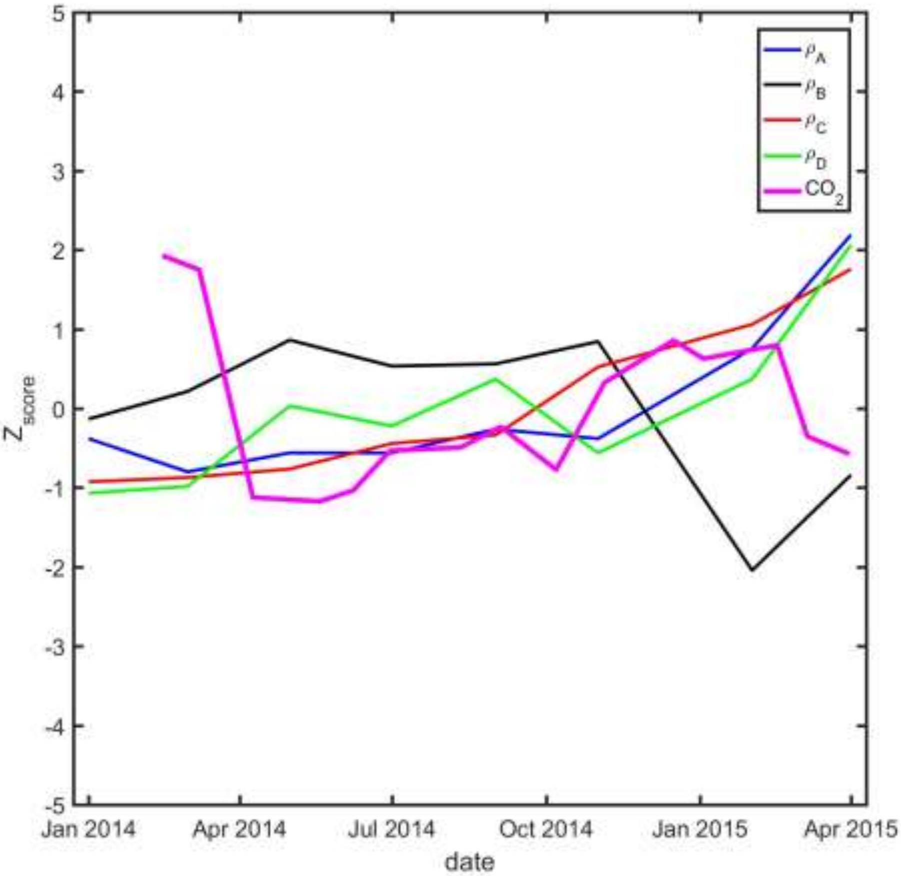
ρA
ρB
ρC
ρD
CO2
Zscore
date
Jan 2014
Apr 2014
Jul 2014
Oct 2014
Jan 2015
Apr 2015

Figure 8e.

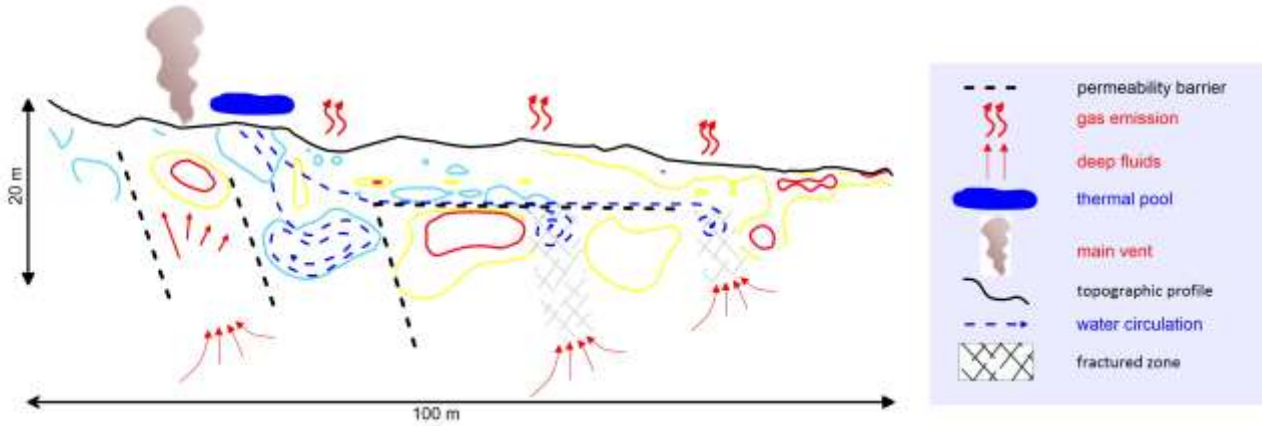
20 m
100 m
permeability barrier
gas emission
deep fluids
thermal pool
main vent
topographic profile
water circulation
fractured zone

Figure 9.

- Time lapse ERT surveys were performed in the Pisciarelli site
- ERT and superficial data integration was performed to study the site
- Mutual relationship between the parameters and their interdependence is analysed
- Seasonal anomalies and features linked to volcanic contributions are marked
- A conceptual model of the fumarolized area is presented

Monitoring active fumaroles through time-lapse electrical resistivity tomograms: an application to the Pisciarelli fumarolic field (Campi Flegrei, Italy).

M. G. Di Giuseppe and A. Troiano

Istituto Nazionale di Geofisica e Vulcanologia, Sezione di Napoli 'Osservatorio Vesuviano'

Abstract

Volcanoes are usually monitored through observations of many physical and chemical phenomena. In the most dangerous cases, as the one of the Campi Flegrei caldera (Italy), great amount of data are collected, both in discrete or continuously, and regularly stored. However, how to transform such mass of data in a deeper understanding of the volcano dynamics is still an open question. Dissimilar information are in fact always hard to compare, but just integrating all the available knowledge hazardous events could be prevented in a reliable way. Fluids, as water and gasses mobilized in the subsoil by the heat induced by deep magmatic sources, are widely recognized as the first engine of similar occurrences and the volcanic gas emissions represent, together with the seismic activity, one of the most considered precursors. At the same time, the electrical geophysical methods are the most applied in order to detect and characterize the fluid patterns in the subsoil. So, the integration of geoelectrical and geochemical observations should represents one of the most pursued approach in volcanoes monitoring. On the contrary, standard way to compare such data have been not yet codified. The ERT tomograms capability to individuate that parts of the subsoil where gasses cumulate is well understood in literature. However, we look for indications about its proficiency in associating the electrical resistivity changes relative to these zones, once compared to the geochemical time series, to deep related contributes, distinguishing them from the seasonal ones. The electrical signature of the fluid patterns, reconstructed through a time-lapse ERT approach, could be of relevance to better characterize the volcanic phenomena and their origins. In this paper a first test of ERT and geochemical time series integration was performed to enhance the understanding of the Pisciarelli fumarolic field evolution, now the most active area in the whole Campi Flegrei caldera.

Introduction

Electrical resistivity tomography (ERT) represents a well-established technique, widely employed to investigate fluid-induced variations in volcanological settings (Revil et al. 2008; Byrdina et al. 2009; Finizola et al. 2009; Finizola et al. 2010; Revil et al., 2011; Di Giuseppe et al. 2015). Many literature publications describe electrical investigations devoted to the definition of the structural setting of volcanoes (Finizola et al., 2006; Revil et al., 2008; Aizawa et al., 2009; Fikos et al., 2012; Barde-Cabusson et al., 2013; DiGiuseppe et al., 2017). When applied in time-lapse mode, e.g. performing tomograms reiteratively overtime, ERT maps the temporal changes in electrical resistivity, which could be related to the changes in the fluid patterns in the subsoil (Singha et al., 2015; Slater, 2007). Because fluids are often involved in relevant volcanic phenomena, time-lapse ERT should be considered in the monitoring of active areas in order to investigate highly hazardous but ambiguous phenomena. This particularly concern for silicic volcanoes, which commonly develop pervasive hydrothermal systems during their long repose periods. The resulting magma-hydrothermal interactions are still poorly understood (Chiodini et al. 2016). In active calderas, widely investigated through electrical methods (Pribnow et al., 2003; Bruno et al., 2007; Di Giuseppe et al., 2015), the hydrothermal circulation is extremely intense, indeed, due to the major structural control, which makes the characterization of unrest phases even more complicated. In addition, the liquid and the gas interactions between mixtures of different chemical species, the most relevant among them being water and carbon dioxide, happen in the very shallowest part of the geothermal system, often creating active fumaroles. Once injected into the shallower formations from deeper magmatic sources, the CO_2 will tend to rise upward because of its low density until it is trapped by low-permeability structures or by dissolution into the groundwater (Bachu et al., 1994). The electrical resistivity of the mixture of grains and pores, which contain the fluids, changes over time, mainly due to fluid filling the pores driven by the fumarole dynamics, and the literature points out that fluids in volcanic environments affect electrical resistivity, generating detectable variations in the recordable signals (Rinaldi et al., 2011). In effects, one of the most sensible parameters to detect the approach of a new eruptive phase is to examine the variations in the composition of discharged fluids. The isotopic signature, however, is often difficult to interpret in terms of system evolution, because several mechanisms may be responsible for differences in the proportion of magmatic gases and shallower fluid components. Indeed, such proportions can be altered before the fluids reach the surface, due to the mixing between fluids of different origin, or due to reactions that modify the original isotope composition. Time-lapsed ERT can reconstruct these changes (Giese et al. 2009; Kiessling et al. 2010; Würdemann et al. 2010; Schmidt-Hattenberger et al. 2011; Zhou et al. 2012), and help to characterize the fumarole dynamics. The dissolution of CO_2 in groundwater and soil moisture indeed generates an enlargement of the low resistivity area after CO_2 injection into the vent. An opposite relationship between CO_2 concentration and electrical resistivity is observed when CO_2, rather than dissolving in water, replaces the brine in the rock matrix, causing the apparent resistivity to increase (Le Roux et al., 2013). The integration between time-lapse ERT and geochemical observations could help to characterize the phenomena related to the mixing of different chemical species, and to reconstruct interaction between fluids of magmatic origin and meteoric waters. The relationship between the contributions of deeper magmatic sources and sources linked to seasonal fluctuations could be also investigated in that manner. Here a similar application is presented, carried out in the Pisciarelli area, which represents a part of the Campi Flegrei caldera (Italy) where vigorous gaseous emissions are present. Repeated tomograms, performed bimonthly, furnished an image of the dynamics of fluids contributing to the fumarolic vent. An approach to the comparison of the gaseous emission rates, temperature and rainfall rates is suggested, to which end a characterization of the detected anomalies is provided.

The Campi Flegrei caldera.

The Campi Felgrei caldera (CFc) is one of the most hazardous volcanoes in Europe (Orsi et al., 2004) and it is inhabited by more than 300,000 people (Bevilacqua et al., 2015), including entire quarters of Naples (Fig.1a). Vertical ground movements with rates ranging from centimetres to metres per year are typical even during quiescent periods (Dvorak and Mastrolorenzo, 1991). Since 1950 the area has been in a new phase of uplift after several centuries of subsidence dating back to 1538 A.D., when the last eruption occurred in the area (Di Vito et al., 1987). The most recent episodes of intense ground uplift were during 1970-72 and 1982-84, which caused a cumulative maximum uplift of over 3.5 m, accompanied by intense seismicity. Apart from the ground uplift, the CFc unrest is characterized primarily by shallow hydrothermal manifestations (such as the vigorous gas emissions), which are most evident in the Solfatara crater and the nearby Pisciarelli areas (Fig.1b), with an involvement of the seismic activity. In effect, the recent literature on the interpretation of the unrest of the whole CFc points out the driving role played by processes involving these two areas (De Natale et al., 1991; Chiodini et al., 2003; Troiano et al., 2011; Piochi et al., 2015a), which are continuously monitored and under observation for the risk strictly related to their potential expansion into a high-density urban area. Many studies involve the mechanical effect of overpressure on a shallow magma chamber (Berrino et al., 1984; Bianchi et al., 1987; Amoruso et al., 2007;) or a sill-like deformative source (D'Auria et al., 2011). Other studies suggest that the unrest periods affecting the whole caldera could likely be related to the triggering of the local hydrothermal system caused by magma degassing episodes centred below the Solfatara - Pisciarelli area (De Natale et al., 1991; Chiodini et al., 2003; Todesco et al., 2003; De Natale et al., 2006; Gottsmann et al., 2006; Lima et al., 2009; Shirzaei and Walter, 2010; Troiano et al., 2011).

Geophysical applications allowed a detailed imaging of the subsurface structure of the Solfatara crater (Letort et al., 2012; Petrosino et al., 2012; Byrdina et al., 2014; Di Giuseppe et al., 2015; Isaia et al., 2015; Gresse et al., 2017). The structure of the Pisciarelli site is less defined. Moreover, several monitoring techniques (geodetic, thermal and geochemical) are currently applied to the CFc, especially at the Solfatara and Pisciarelli areas (INGV, 2018), but a lack of knowledge persists about the distribution and dynamics of the geothermal fluids present in the area. Specifically, the Pisciarelli area has been the subject of a severe reactivation in the last few years, concomitant with an increase of ground uplift. The main manifestations are as follows: an enlargement of the fumarolized area, the opening of a new vent (which occurred in March 2008), the opening of a new boiling pool (which occurred in March 2009 and which was probably accompanied by a small explosion because mud sputter occurred, covering the soil slope up to 3–4 m above the emission point), a further vigorous, roaring fumarole created (which appeared on the 20th of December, 2009, that represents the strongest gas emission of the entire area to date), the seismic swarm of about 190 events (recorded in the area during the 30th of March, 2010) and a new vent opened (during the 15th of November, 2010). Finally, in the January of 2013 the disappearance of the main fumarole that was recently opened and the appearance of a vent that emits high-pressure steam and liquid water up to 3-4 m high were observed. These manifestations make the Pisciarelli unrest quite peculiar. It is indubitably linked to the global CFc unrest, as evidenced by the geochemical species emitted (Chiodini et al., 2011). However, the local aspect of the CFc dynamic in this area has to be carefully taken into account. The Pisciarelli neighbourhood has a high degree of urban development and minor events could represent a high risk for a great number of inhabitants.

A mapping of the electrical resistivity changes through ERT should be indicative of potentially hazardous dynamics in the area. Such parameters are, in fact, sensitive to properties such as salinity, porosity and phase changes of fluids flowing into the porous space, which contribute to the characterization of the fluid circulation in the subsurface.

The state of the Solfatara – Pisciarelli area.

After the last major unrest period observed in the CFc, during 1982-1984, the ground deformation trend showed a subsidence period until 2004-2005, when a new uplift phase started. Since 2010-2011 the deformation rate shows a further increase, leading to a cumulative uplift of more than 20 cm. The ground uplift is also accompanied by widespread fumarolic activity occurring in the whole CF caldera area. However, these unrest manifestation are all focused in the centre of the CFc (Figure1a), near the Solfatara - Pisciarelli area (D'Auria et al., 2011), where the evidences of volcanic effects are particularly present now. For such a reason, the ascription of a central role in the CFc unrest dynamic for these two areas has grown, and has been the subject of the many detailed numerical studies, mentioned earlier.

The geophysics surveys contributed to defining the structural outline of the Solfatara – Pisciarelli area (SP), and represented a crucial task for understanding volcanic activity. Recent surveys highlighted the main structural asset of the area. The first magnetotelluric surveys (Troiano et al., 2014) detected a near-vertical steam/gas-saturated plume-like structure, which reaches the free surface where the main fumarole fields are active, emerging from a high temperature (>300 °C), over pressured, gas-saturated plate-like reservoir, which extends down to at least 3 km in depth. Subsequent ERT surveys clarified the shallower structure of the Solfatara volcano, outlining a complex hydrothermal system, formed by a mix of upwelling fluids, gases, and meteoric water (Byrdina et al., 2014; Di Giuseppe et al., 2015; Gresse et al., 2017). Isaia et al. (2015), when considering this structural framework, ended in the suggestion that the Solfatara volcano could be a maar-diatreme structure, characterized by a shallow crater cut in the pre-eruptive basement, and a deep diatreme (down to 2–3km).

Physical and chemical observations are now performed in the whole CFc as part of the volcanic monitoring and both the Solfatara crater and the Pisciarelli area represent the great majority of the areas surveyed. Regular thermic, seismic, gravimetric, geochemical and geodetic monitoring is carried out in the area. In particular, the geochemical data had a central role in the debate on the CFc unrest (Chiodini et al., 2012, 2016; Moretti et al., 2017). A general increase of the deep magmatic component into the emitted volatiles was observed (INGV, 2018). In particular, for what concerned the SP area, the following features were observed:

- an increasing trend in the CO_2/H_2O, generally indicating a growth in the magmatic component into the fumarolic fluids

- an increasing CO concentration, that generally characterize volcanic systems at high temperature, whereas hydrothermal contributions would be usually related to lower levels of this component
- an increase of the CO-CO_2 equilibrium temperature, representing the shallower hydrothermal system conditions
- and an increasing trend in the CO_2/CH_4 ratio

Further considerations about the fluid dynamics in the area arise also from the geophysical observations. Di Giuseppe et al. (2015) discussed a migration of the shallow fluid volume eastwards during the few past decades, and supposed that water might have invaded spaces previously saturated with steam, gas or a combination thereof below the Solfatara main vents, at the same time as fluxes steam, gas or both were invading voids opening to the east. This last observation strictly followed the recent relocation of the fumarolic activity from the Solfatara area toward the Pisciarelli area, located eastward to the outer slopes of the Solfatara (Figure1b) (Troiano et al., 2014). This relocation was marked by a temperature increasing, new vents and boiling pools opening, the occurrence of seismic activity and by the impressively fast changes in the morphology of this zone.

Unfortunately, the source of such relocation is yet largely unknown and a lack of knowledge persists about the fluid dynamics in that part of the CFc hydrothermal system. Current geophysical details of the connections between the Solfatara and Pisciarelli zones are still largely crude, and the geochemical data from Pisciarelli suffers of some criticism, as discussed in Chiodini et al. (2011), who suggested that these data could be heavily modified by seasonal cycles. They would then be not-totally conclusive for investigations into the future changes caused by deep volcanic processes.

The ERT survey in the Pisciarelli area.

Two main electrical conductivity mechanisms characterize a fluid-saturated porous medium (Rinaldi et al., 2011). The first one is caused by the fluid flow inside the pores, through electro-migration of charges into the connected pore space. A second conduction mechanism occurs at the pore water–mineral interface in the electrical double layer, that is caused by a migration of the weakly adsorbed counterions (usually cations). The DC electrical conductivity of the porous rock can be expressed as a combination of those two contribution, namely the surface electrical conductivity at the water–mineral interface and the pore fluid electrical conductivity. Changes in those two quantities are mainly due to variations into the fluid filling the pore, considering that wet rocks usually have conductivities sensibly higher that dry rocks (Rinaldi et al., 2011 and references therein). Surface and pore fluid conductivities depends linearly from temperature (Vaughan et al., 1993, Revil et al., 1998, Roberts, 2002). Moreover, a dependence from the rock matrix permeability and from salinity of the pore fluids is also observed (Jardani and Revil, 2009). Many mechanisms can be advocated when changes are observed in the bulk conductivity of the rocks. The first element to consider is the compositional nature of the fluids flowing into the system. The pore space of the rocks is indeed occupied by a mixture of multiphase fluids, as water and CO2 in liquid and vapour phase. Such mixture is altered by the interaction between meteoric waters and fluids rising from the deep because of volcanic effects, which has direct effects upon the underground resistivity. When fluid changes their distribution into the shallower part of the hydrothermal system, the diffusion of the gas phases (both water vapor and CO2) and the temperature variations alter the electrical conductivity both at the pore surface and within the porous space. Also the boiling phenomena into the fluids reinforce the observed gradient in conductivity between liquid saturated and gas saturated areas, concentrating the brine and increasing salinity in the remaining liquid part. As further effect, the fracturing induced by the fluid dynamics and thermal expansion also alter the electrical conductivity of the subsoil, modifying the rock permeability.

The geoelectrical surveys are very effective tools for unveil the dynamics of tectonic and volcanic settings, and several contribution already regarded the Campanian district (Di Maio et al., 1998;

Bruno et al., 2007;Troiano et al., 2008, 2009; Byrdina et al., 2014; Di Giuseppe et al., 2015, 2017; Gresse et al., 2017).

For the first time, ERT surveys were carried out into the Pisciarelli fumarolic field after the January 2013 event, when a vent that emitted high-pressure steam and liquid water up to 3-4 metres high was observed, in order to get an insight about the geothermal fluid circulation in the very shallow aquifer. A first survey was performed along a 70 m long survey line, aligned with the main fumarole and the permanent thermal pool in the west-east direction (Figure2), while crossing the part of the area subject to abrupt morphological changes and major emissive activity. A dipole-dipole electrode configuration was adopted, with a 2.5 m spacing, which was compact and sensitive to both lateral location and depth of bodies that are the source of anomalies (Ward, 1988). An Iris Syscal Pro instrument was used as multichannel resistivimeter. The same instrument was employed as power source, being able to output a direct current with a maximum voltage and current of 800 V and 2 A, respectively.

The selected survey arrangement took into account the morphology and harsh environment characterizing the Pisciarelli area, which represented a limitation imposed on a classical ERT application. It was only possible to arrange a short survey line, with a consequent limit in the expected depth of investigation. Despite this restriction, the use of a time-lapse approach, which consists in performing identical ERT surveys several times in the same place, makes the ERT useful to investigate the evolution of the Pisciarelli structures. The time-lapse approach was followed in several ERT applications presented in the literature. As an example, Wallin et al. (2013) imaged the inland intrusion of river water in a contaminated acquifer. Nickschick et al. (2017) observed the changes in the subsurface structure beneath heavily CO_2 degassing spots in the Hartsouv Mofete field (Czech Republic). In the volcanic Pisciarelli environment, time-lapse ERT may possibly resolve the modifications of fluid phases and/or distribution induced by the contribution of a heat component or a hot gaseous component, both likely present if a magmatic source is active in the area.

The ERT survey was regularly repeated, starting in January 2014 ending April 2015. It is worth noting that the successive repetitions of the January 2013 survey were performed along a slightly longer survey line (100 m long) with respect to the first January 2013 survey and that the bimonthly interval was chosen in order to evaluate the possible influence of seasonal effects on the hydrothermal system, as indicated by the geochemical monitoring. The ERT lines were inverted using ERTlab3D® commercial software, including topography. The inverse algorithm, described by LaBrecque et al. (1999) uses a regularized solution, looking for the optimal value of the parameter vector **P** and the stabilization parameter α for which minimizing the functional $Y(\mathbf{P})=\chi^2(\mathbf{P})+\alpha\mathbf{P}^{\mathbf{T}}\underline{\mathbf{R}}\mathbf{P}$ results in $\chi^2(\mathbf{P})= \chi^2_{prior}$. The parameters **P** are the natural logarithms of the conductivity of the mesh elements and **R**, the solution roughness, acts as the stabilizing functional. χ^2_{prior} is equal to the number of data points and χ^2 is given by $\chi^2 = (\mathbf{D} - \mathbf{F}(\mathbf{P}))^{\mathbf{T}}\mathbf{W}\,(\mathbf{D} - \mathbf{F}(\mathbf{P}))$, where **D** is the vector of known data values, **F(P)** is the forward solution and **W** is a data weight matrix. The diagonal elements of **W** are the reciprocals of the data variances and the off-diagonal elements are zero. This assumes non-correlated data errors. When ERT data was inverted in time-lapse mode, different approaches were contemplated. As first consideration, with every dataset collected independently of the others, each tomogram can be assumed to be a representation of a constant state of the shallower geothermal system at the collection time. With this in mind, it is possible to invert each dataset independently, isolating changes in the electrical resistivity by post inversion model differencing. A second option to consider is the inversion on the differences between the background and subsequent datasets, e.g. the resistivity obtained by the inversion of the first dataset, considered as background data, can be considered as the a priori model in the difference inversion. In this case systematic errors such as those errors due to in field configuration and discretization in the forward modelling algorithm tend to null and the result is that the difference data is likely fitted more closely than the individual potentials, resulting in fewer inversion artefacts (LaBrecque and Yang, 2001). A time-lapse regularization can also be considered (Oldenborger et al., 2007), whereby the reference model for the first inversion is an uniform model and the reference model for all subsequent experimental stages is the model obtained via inversion of the data from the previous stage. Such approaches require, at least in principle, fewer model modifications to fit the data and the objective function penalizes large perturbations from previous models as opposed to large perturbations from background. Thus, such inversion is ultimately able to build up more structure in the final models, while still satisfying the data to the same level of the previous options. As a final, and likely more corrected, option, the dataset could be inverted adopting 4D approaches (Kim et al., 2009; Karaoulis et al., 2011), which consider a four-dimensional space–time model, introducing regularizations reflecting a metric function of both space and time. In the present case, time-lapse minimization was adopted during the inversion of the dataset. The final models for each dataset, are reported in Figure 3a. Average root-mean-squares (RMS) varying from 1.1 up to 1.9 resulted, which we considered satisfactory. In order to support the reliability of the images, it is common to look at **S**, the so-called inverse problem's sensitivity matrix, which take into account the effects on the data by infinitesimal changes into the model resistivity. The sensitivity has been estimated for all the tomograms presented in Figure 3.

The ERT Dataset.

The sequence of inverted resistivity images obtained in the timelapse survey is shown in Figure 3. The tomograms showed diffuse lateral and vertical heterogeneities within a resistivity range of about three orders of magnitude.

The bimonthly-recorded resistivity sections showed four main electrical anomalies:

A. the first anomaly lying at about 20 m along the profile (corresponding to the blue vertical dashed line in the figure), located at depths verying between 60-70 m a.s.l.;
B. a second zone displaced at around 35 m along the profile (corresponding to the black dashed line in the figure), located at depths between 50-65 m a.s.l.;
C. a third zone centred at around 55 m along the profile (corresponding to the red dashed line in the figure), located between 50-65 m a.s.l.;

D. A fourth zone centred at around 70 m along the profile (corresponding to the green dashed line in the figure), located at around 60 m a.s.l.;

A further anomalous zone appears at the very end of the profile. This last feature does not lye in the vegetation-free zone and could likely be linked to some anthropic artefact. The anomalies' evolution, in shape and resistivity, is reported in Figure 4, for each of the collected datasets.

Following the approach of Wallin et al. (2013), from the ERT tomograms, the time series of electrical resistivity have been extracted for each of the electrical anomalies depicted in Figure 4, while taking into consideration the mean values of the parameter in the elementary cells that compose the related part of the tomograms. These resistivity time series are reported in Figure 5.

The anomalies observed in the subsurface underneath the Pisciarelli degassing site changed over time, as a consequence of changes in several parameters on which the resistivity depends. In particular, the high pressure of fluids (CO2 and water carried along), likely mobilized by a deeper source, is capable of altering the host rocks mechanically and/or chemically. The fluid's power is capable of moving material from lower levels or widening the pores within materials. Moreover, according to Annunziatellis et al. (2008), gases like CO_2 are capable of migrating not only vertically, but also horizontally in soil as density-driven flows or advective forces, leading to horizontal changes in the anomalies. In addition, temperature fluctuations, for instance induced by the inflow of deep-lying hot fluids or by fluids mixing of in the uppermost part of the hydrothermal system, can induce significant changes in resistivity. Considering such connections, a comparison between the changes of electrical resistivity in the anomalous zones and some superficial observations was attempted. The parameters considered here are the temperature, CO2 fluxes and rainfall rates. The CO_2 fluxes and the temperatures of the emitted gasses were recorded in the Pisciarelli main vent during 2007-2016 (INGV, 2018) in correspondence with the FLXOV3measuring station. These quantities are reported in Figure 6a and 6b, respectively, where are limited to the years 2014-2015. Also the long-term temperature trend is reported in Figure 6a, which was deduced by applying the Seasonal Trend

Decomposition (STL) algorithm on the infrared imaging recorded in proximity of the upper part of the west side of the vent (Vilardo et al., 2015; INGV, 2018). The two temperature estimates, which refer to emitted gasses and surface thermal features of the area affected by diffuse degassing, respectively, are biased. However, they show a very close relationship in pattern of variability. The monthly rainfall rates, relative to the meteorological station of Pozzuoli (furnished by the 'Protezione Civile Regione Campania') are reported in Figure 6c. All data are reported as recorded in the corresponding measuring stations, but a brute comparison between these quantities can be misleading, due to the very different nature and variability of such records. Therefore, the way to compare information so different as the ERT tomograms and the surface observations (geochemical data, temperature and rainfall rates) has to be carefully investigated and a normalization criterion has to be adopted to result in a valid comparison. In order to place all these signals on a comparable scale, the so-called z-score (Klemelä, 2009) was calculated for each record separately. The z-scores were obtained by removing the mean value from each time series and dividing by the relative standard deviation. In such way, samples having zero means and unit variances are obtained. The z-scores for all the variables mentioned above (and shown in Figure 5 and 6) are reported in Figure 7.

Discussion.

The resistivity trends of the different anomalies over time, in terms of z-scores, are shown in Figure 8a. Thus emerges a peculiar behaviour of anomaly B, that shows a resistivity oscillating more in time with respect to the other anomalies, all presenting a comparable increasing attitude. In Figure 8b, the resistivity of anomaly B is compared with the rainfall rate and temperature. The B resistivity appears to be correlated with the temperature and anti-correlated with the rainfall. This suggests that the character of the B anomaly may be influenced by seasonal effects, probably driven by the influx of cold rainwater into the system. The warmer and drier months see an increase in resistivity and vice versa. Figure 8c shows, for anomaly C, how the linear increasing trend of resistivity instead appears to be less correlated to temperature and rainfall rates.

Considering on turn the geochemical data, the main vent showed an increasing amount of CO_2 emission, varying by about one order of magnitude from 2007-2016 (INGV, 2018). Superimposed on this accumulation tendency, a clear annual cyclic oscillation was distinguishable, that has been stronger in more recent years. Chiodini et al. (2011), reporting on the CO content of the Pisciarelli fumarole, until 2011, concluded that at Pisciarelli, strong seasonal effects and the possibility of re-equilibration of the fumarolic fluids at very shallow depths concealed the deep geothermo-barometric signals. In addition, the comparison of the z-scores of CO_2 emission, IR temperature and rainfalls, reported in Figure 8d shows a strong correlation between CO_2 emission and rainfalls. The comparison between CO2 emission and resistivities, reported in Figure 8e, suggests a link between the parameters. Such correlation could be likely due to a buffering and/or cumulation of the gas flowing from the geothermal system to the atmosphere in those zones. At least in principle, the contribution of chemical effects to observed changes in resistivity, such as fracture sealing or rock alteration, cannot be excluded. However, we note that these effects should not show any periodicity. Moreover, concerning the sealing, the dynamics of Pisciarelli allows a reasonable opening rather than closing of fractures. On other hands, the dominants among the new chemical species, e.g. sulfur and alunite as indicated in Piochi et al. (2015b), should induce a decrease in the bulk rocks resistivity. In contrast, the non-cyclical anomalies retrieved through the time-lapse ERT imaging present an increasing attitude. The comparison with the surface data helps to strengthen the hypotheses on the phenomena that determine the observed variations in the electrical structures.

Recognizing the relevance and meaning of the anomalies and their evolution over time in electrical images is not, however, trivial, especially considering the interplay between rainwater and hydrothermal fluids, which can generate elaborate patterns. In the case of Pisciarelli, this interaction has a feedback in the tomographic sections. The first element is the direct link between anomaly B and the surface. The second element is the diffusion over time of a low resistivity zone along the top of anomaly C, which interacts with a vertical conductive plume apparently rising up in the boundary zone between the C and D anomalies. The B anomaly corresponds to the thermal pool and it shows a seasonal character, while the boundary between the C and D anomalies corresponds to a fault zone with surface manifestations and the maximum of fracture detected in the field (Isaia et al., 2015). In our interpretation, rainwaters stored into the thermal pool penetrate into the subsoil through the narrow channel, permeating the available space, the results of which are laterally confined by the C anomaly, in turn acting as a permeability barrier. Moreover, part of the same waters dislocate also along the top of the C anomaly, which again acts as a permeability barrier, ending to interact with other fluids, of deeper origin, rising along the pre-existing fractures. This interpretative framework is summarized in Figure 9, where a sketch map is superimposed over the tomographies.

Conclusion

In this paper the results of a time lapse ERT monitoring in the volcanically active Pisciarelli site are shown. Being that pre-eruptive changes are frequently extremely rapid, and the Pisciarelli area is extremely urbanized, this site represents one of the strong sources of volcanic risk in the whole CFc and looking for pre-eruptive indicators could be relevant to prevent potentially highly destructive consequences. This is particularly true due to the non-totally conclusive findings of the routine monitoring performed in the area.

Even though the imaging we have performed brings only a small amount of large-scale information about the feeding system, due to the limited resolution at depths, the ERT imaging highlighted several anomalous zones. The interpretation of such patterns is quite difficult, being related to complex phenomena such as the interaction between the fluid components of different origins present in the vent. However, the comparison with other monitoring data (temperature, geochemical data and rainfall rates) permitted us to discern the areas dominated by seasonal effects from the ones more influenced by other, most significant contributions, linked to gas injected into the system from deep locations which cumulates in the subsoil. Moreover, such comparison can be a guideline toward a more confident interpretation of the patterns shown by fluids during such times, helping to understand what features are more related to the apport of meteoric waters into the subsoil and what could be more correlated to the inflow of fluids of deeper origins. The boundary surfaces along which the fluids displace and the fractures where fluids rise are also revealed. The reconstruction of such features, obtained through the imaging of the underground electrical resistivity changes reveal the complex interactions between the environment and the deeper volcanic sources. In this sense, the presented results point out some general aspects. The indirect information obtained through geophysical imaging proves an vehicle to underline the underground phenomena, explaining the dynamics of large volumes of subsoil without any arbitrary extrapolations, typical of techniques based on surface observations. A further methodological aspect has to be underlined. No geophysical method is self-consistent, in the sense that just the integration of information about all the physical characteristics of rocks allows the understanding of the phenomena occurring and the creation of unique lithological models. In spite of this, however, our results show how the single electrical technique has a relevant proficiency. The model presented in Fig.9 evidence the self-standing ERT capability to define and detail the phenomena at least in their essential lines. The results presented here can be considered the first test about the aptitude of time-lapse ERT to understand the evolution of an active fumarole, thanks to a significant contribution to the characterization of subsoil structures and the understanding of their evolution during time. In any case, even if the tomograms indicate that this promising approach of time-lapse ERT monitoring to sheds light on the potentially dangerous evolution of the investigated system, because the phenomena involved are extremely complex, the evaluation of such aspects deserves more effort and rigorous modelling. As further development, the establishment of permanent and longer surveying lines could substantiate the results. In particular, a continuous acquisition of the tomograms could end in longer time series of electrical resistivity changes, which could be compared to the geochemical ones following combined statistical approaches, such as wavelet coherence analysis.

Figure captions.

Fig.1. a) Map of the Campi Flegrei caldera (Italy). b) Map of the Solfatara‑Pisciarelli complex, framed with the black box in panel a). The ERT survey area is enclosed in the black box and the survey profile is evidenced with the red line. The geodetic reference system is UTM-WGS84.

Fig.2. Aerial view of the Pisciarelli area, where the time-lapse ERT surveys were realized (red dashed line). Locations of the main anomalies retrieved by ERT are indicated, with the colored capital letters. The geodetic reference system is UTM-WGS84.

Fig.3. ERT resistivity sectionsrelative to the profile sketched in Fig.2. For every section, the relative date is indicated. A common logarithmic scale is used for all the resistivity sections. The main features discussed into the text (already shown in figure 2) are also indicated with the coloured dotted lines;

Fig.4. Detail of the four main electrical anomalies retrieved through time-lapse ERT. For every section, the relative date is indicated. A common logarithmic scale is used for all the resistivity sections. The main features discussed into the text are also labelled with coloured capital letters.

Fig. 5. Comparison between the electrical resistivity time series (in Ωm) as function of time, which were obtained extracting the mean value of the parameter in correspondence of the four areas shown in figure 4.

Fig. 6. a) temperature of the gas emitted at the Pisciarelli main vent (left axes, ° C) and temperature extracted from infrared thermal images through the application of the STL algorithm (right axis, ° C) during 2014-2015. (b) CO2 fluxes emitted at the Pisciarelli main vent (in $gm^{-2}d^{-1}$) during 2014-2015. (c) Monthly rainfall rates (in mm $month^{-1}$) recorded at the Pozzuoli meteorological station of the ‘Protezione Civile Regionale’ agency.

Fig.7. The z-scores extracted by the variables mentioned in Figure 5 (electrical resistivity time series) and Figure 6 (temperature, CO_2 fluxes and rainfall rates). Z-scores were obtained by removing the mean value from each time series and dividing by the relative standard deviation.

Fig. 8. Z-scores extracted by the observed variables, compared as follow: (a) electrical resistivity time series relative to the four anomalous zones shown in Figure 2. (b) electrical resistivity time series relative to the B electrical anomaly, surface IR temperature and rainfall rates. (c) electrical resistivity time series relative to the C electrical anomaly, surface IR temperature and rainfall rates. (d) CO_2 fluxes, surface IR temperature and rainfall rates. (e) electrical resistivity time series relative to the four anomalous zones, CO_2 fluxes.

Fig.9. Conceptual model of the Pisciarelli fumarolic zone. This W-E model crosses the main vent and the thermal permanent pool. The interpretative elements are reported in the legend. Electrical resistivity isolines, relative to the April 2015 tomogram are superimposed, maintaining the same common logarithm scale of Figure 3.

References

Aizawa, K., Ogawa, Y., Ishido, T., 2009. Groundwater flow and hydrothermal systems within volcanic edifices: Delineation by electric self-potential and magnetotellurics. J. Geophys. Res. 114, B01208. doi:10.1029/2008JB005910

Amoruso, A., Crescentini, L., Linde, A.T., Sacks, I.S., Scarpa, R., Romano, P., 2007. A horizontal crack in a layered structure satisfies deformation for the 2004–2006 uplift of Campi Flegrei. Geophys. Res. Lett.

34, L22313. doi:10.1029/2007GL031644

Annunziatellis, A., Beaubien, S.E., Bigi, S., Ciotoli, G., Coltella, M., Lombardi, S., 2008. Gas migration along fault systems and through the vadose zone in the Latera caldera (central Italy): Implications for CO_2geological storage. Int. J. Greenh. Gas Control 2, 353–372. doi:10.1016/j.ijggc.2008.02.003

Bachu, S., Gunter, W.D., Perkins, E.H., 1994. Aquifer disposal of CO_2: Hydrodynamic and mineral trapping. Energy Convers. Manag. 35, 269–279. doi:10.1016/0196-8904(94)90060-4

Barde-Cabusson, S., Bolós, X., Pedrazzi, D., Lovera, R., Serra, G., Martí, J., Casas, A., 2013. Electrical resistivity tomography revealing the internal structure of monogenetic volcanoes. Geophys. Res. Lett. 40, 2544–2549. doi:10.1002/grl.50538

Berrino, G., Corrado, G., Luongo, G., Toro, B., 1984. Ground deformation and gravity changes accompanying the 1982 Pozzuoli uplift. Bull. Volcanol. 47, 187–200. doi:10.1007/BF01961548

Bevilacqua, A., Isaia, R., Neri, A., Vitale, S., Aspinall, W.P., Bisson, M., Flandoli, F., Baxter, P.J., Bertagnini, A., Esposti Ongaro, T., Iannuzzi, E., Pistolesi, M., Rosi, M., 2015. Quantifying volcanic hazard at Campi Flegrei caldera (Italy) with uncertainty assessment: 1. Vent opening maps. J. Geophys. Res. Solid Earth 120, 2309–2329. doi:10.1002/2014JB011775

Bianchi, R., Coradini, A., Federico, C., Giberti, G., Lanciano, P., Pozzi, J.P., Sartoris, G., Scandone, R., 1987. Modeling of surface deformation in volcanic areas: The 1970-1972 and 1982-1984 crises of Campi Flegrei, Italy. J. Geophys. Res. Solid Earth 92, 14139–14150. doi:10.1029/JB092iB13p14139

Bruno, P.P.G., Ricciardi, G.P., Petrillo, Z., Di Fiore, V., Troiano, A., Chiodini, G., 2007. Geophysical and hydrogeological experiments from a shallow hydrothermal system at Solfatara Volcano, Campi Flegrei, Italy: Response to caldera unrest. J. Geophys. Res. Solid Earth 112. doi:10.1029/2006JB004383

Byrdina, S., Revil, A., Pant, S.R., Koirala, B.P., Shrestha, P.L., Tiwari, D.R., Gautam, U.P., Shrestha, K., Sapkota, S.N., Contraires, S., Perrier, F., 2009. Dipolar self-potential anomaly associated with carbon dioxide and radon flux at Syabru-Bensi hot springs in central Nepal. J. Geophys. Res. 114, B10101.

doi:10.1029/2008JB006154

Byrdina, S., Vandemeulebrouck, J., Cardellini, C., Legaz, A., Camerlynck, C., Chiodini, G., Lebourg, T., Gresse, M., Bascou, P., Motos, G., Carrier, A., Caliro, S., 2014. Relations between electrical resistivity, carbon dioxide flux, and self-potential in the shallow hydrothermal system of Solfatara (Phlegrean Fields, Italy). J. Volcanol. Geotherm. Res. 283, 172–182. doi:10.1016/j.jvolgeores.2014.07.010

Chiodini, G., Avino, R., Caliro, S., Minopoli, C., 2011. Temperature and pressure gas geoindicators at the Solfatara fumaroles (Campi Flegrei). Ann. Geophys.

Chiodini, G., Caliro, S., De Martino, P., Avino, R., Gherardi, F., U., T., E., B., G.P., R., P., R., C., R., 2012. Early signals of new volcanic unrest at Campi Flegrei caldera? Insights from geochemical data and physical simulations. Geology 40, 943–946. doi:10.1130/G33251.1

Chiodini, G., Paonita, A., Aiuppa, A., Costa, A., Caliro, S., De Martino, P., Acocella, V., Vandemeulebrouck, J., 2016. Magmas near the critical degassing pressure drive volcanic unrest towards a critical state. Nat. Commun. 7, 13712.

Chiodini, G., Todesco, M., Caliro, S., Del Gaudio, C., Macedonio, G., Russo, M., 2003. Magma degassing as a trigger of bradyseismic events: The case of Phlegrean Fields (Italy). Geophys. Res. Lett. 30. doi:10.1029/2002GL016790

D'Auria, L., Giudicepietro, F., Aquino, I., Borriello, G., Del Gaudio, C., Lo Bascio, D., Martini, M., Ricciardi, G.P., Ricciolino, P., Ricco, C., 2011. Repeated fluid-transfer episodes as a mechanism for the recent dynamics of Campi Flegrei caldera (1989–2010). J. Geophys. Res. 116, B04313. doi:10.1029/2010JB007837

De Natale, G., Pingue, F., Allard, P., Zollo, A., 1991. Geophysical and geochemical modelling of the 1982–1984 unrest phenomena at Campi Flegrei caldera (southern Italy). J. Volcanol. Geotherm. Res. 48, 199–222. doi:10.1016/0377-0273(91)90043-Y

De Natale, G., Troise, C., Pingue, F., Mastrolorenzo, G., Pappalardo, L., Battaglia, M., Boschi, E., 2006. The

Campi Flegrei caldera: unrest mechanisms and hazards. Geol. Soc. London, Spec. Publ. 269.

Di Giuseppe, M.G., Troiano, A., Fedele, A., Caputo, T., Patella, D., Troise, C., De Natale, G., 2015. Electrical resistivity tomography imaging of the near-surface structure of the Solfatara crater, Campi Flegrei (Naples, Italy). Bull. Volcanol. 77. doi:10.1007/s00445-015-0910-6

Di Maio, R., Mauriello, P., Patella, D., Petrillo, Z., Piscitelli, S., Siniscalchi, A., 1998. Electric and electromagnetic outline of the Mount Somma–Vesuvius structural setting. J. Volcanol. Geotherm. Res. 82, 219–238. doi:10.1016/S0377-0273(97)00066-8

Di Vito, M., Lirer, L., Mastrolorenzo, G., Rolandi, G., 1987. The 1538 Monte Nuovo eruption (Campi Flegrei, Italy). Bull. Volcanol. 49, 608–615. doi:10.1007/BF01079966

Dvorak, J.J., Mastrolorenzo, G., 1991. The mechanisms of recent vertical crustal movements in Campi Flegrei caldera, southern Italy. pp. 1–47. doi:10.1130/SPE263-p1

Fikos, I., Vargemezis, G., Zlotnicki, J., Puertollano, J.R., Alanis, P.B., Pigtain, R.C., Villacorte, E.U., Malipot, G.A., Sasai, Y., 2012. Electrical resistivity tomography study of Taal volcano hydrothermal system, Philippines. Bull. Volcanol. 74, 1821–1831. doi:10.1007/s00445-012-0638-5

Finizola, A., Aubert, M., Revil, A., Schütze, C., Sortino, F., 2009. Importance of structural history in the summit area of Stromboli during the 2002–2003 eruptive crisis inferred from temperature, soil CO2, self-potential, and electrical resistivity tomography. J. Volcanol. Geotherm. Res. 183, 213–227. doi:10.1016/j.jvolgeores.2009.04.002

Finizola, A., Revil, A., Rizzo, E., Piscitelli, S., Ricci, T., Morin, J., Angeletti, B., Mocochain, L., Sortino, F., 2006. Hydrogeological insights at Stromboli volcano (Italy) from geoelectrical, temperature, and CO_2 soil degassing investigations. Geophys. Res. Lett. 33, L17304. doi:10.1029/2006GL026842

Finizola, A., Ricci, T., Deiana, R., Cabusson, S.B., Rossi, M., Praticelli, N., Giocoli, A., Romano, G., Delcher, E., Suski, B., Revil, A., Menny, P., Di Gangi, F., Letort, J., Peltier, A., Villasante-Marcos, V., Douillet, G., Avard, G., Lelli, M., 2010. Adventive hydrothermal circulation on Stromboli volcano

(Aeolian Islands, Italy) revealed by geophysical and geochemical approaches: Implications for general fluid flow models on volcanoes. J. Volcanol. Geotherm. Res. 196, 111–119. doi:10.1016/j.jvolgeores.2010.07.022

Giese, R., Henninges, J., Lüth, S., Morozova, D., Schmidt-Hattenberger, C., Würdemann, H., Zimmer, M., Cosma, C., Juhlin, C., 2009. Monitoring at the CO2 SINK site: A concept integrating geophysics, geochemistry and microbiology. Energy Procedia 1, 2251–2259. doi:10.1016/j.egypro.2009.01.293

Di, Giuseppe, M.G. Di, Troiano, A., Vito, M.A. Di, Somma, R., Matano, F., 2017. Definition of small-scale volcanic structures by Electrical Resistivity Tomography: the Trentaremi cone, an example from the Campi Flegrei Caldera (Italy). Ann. Geophys. 60, S0552. doi:10.4401/ag-7397

Gottsmann, J., Folch, A., Rymer, H., 2006. Unrest at Campi Flegrei: A contribution to the magmatic versus hydrothermal debate from inverse and finite element modeling. J. Geophys. Res. 111, B07203. doi:10.1029/2005JB003745

Gresse, M., Vandemeulebrouck, J., Byrdina, S., Chiodini, G., Revil, A., Johnson, T.C., Ricci, T., Vilardo, G., Mangiacapra, A., Lebourg, T., Grangeon, J., Bascou, P., Metral, L., 2017. Three-Dimensional Electrical Resistivity Tomography of the Solfatara Crater (Italy): Implication for the Multiphase Flow Structure of the Shallow Hydrothermal System. J. Geophys. Res. Solid Earth 122, 8749–8768. doi:10.1002/2017JB014389

INGV, 2018. Bollettini di sorveglianza dei vulcani campani.

Isaia, R., Vitale, S., Di Giuseppe, M.G., Iannuzzi, E., Tramparulo, F.D., Troiano, A., 2015. Stratigraphy, structure, and volcano-tectonic evolution of Solfatara maar-diatreme (Campi Flegrei, Italy). Bull. Geol. Soc. Am. 127, 1485–1504. doi:10.1130/B31183.1

Karaoulis M., A. Revil, D.D. Werkema, B. Minsley, W.F. Woodruff, and A. Kemna, Time-lapse 3D inversion of complex conductivity data using an active time constrained (ATC) approach, Geophysical Journal International, 187, 237–251, doi: 10.1111/j.1365-246X.2011.05156.x, 2011

Kiessling, D., Schmidt-Hattenberger, C., Schuett, H., Schilling, F., Krueger, K., Schoebel, B., Danckwardt, E., Kummerow, J., 2010. Geoelectrical methods for monitoring geological CO2 storage: First results from cross-hole and surface–downhole measurements from the CO2SINK test site at Ketzin (Germany). Int. J. Greenh. Gas Control 4, 816–826. doi:10.1016/j.ijggc.2010.05.001

Kim, J. H., Yi, M. J., Park, S. G., & Kim, J. G. (2009). 4-D inversion of DC resistivity monitoring data acquired over a dynamically changing earth model. Journal of Applied Geophysics, 68(4), 522-532.

Klemelä, J., 2009. Smoothing of multivariate data : density estimation and visualization. John Wiley & Sons.

LaBrecque, D.J., Morelli, G., Daily, W., Ramirez, A., Lundegard, P., 1999. 37. Occam's Inversion of 3-D Electrical Resistivity Tomography, in: Three-Dimensional Electromagnetics. Society of Exploration Geophysicists, pp. 575–590. doi:10.1190/1.9781560802154.ch37

LaBrecque, D.J., Yang, X., 2001. Difference Inversion of ERT Data: a Fast Inversion Method for 3-D In Situ Monitoring. J. Environ. Eng. Geophys. 6, 83–89. doi:10.4133/JEEG6.2.83

Le Roux, O., Cohen, G., Loisy, C., Laveuf, C., Delaplace, P., Magnier, C., Rouchon, V., Cerepi, A., Garcia, B., 2013. The CO2-Vadose project: Time-lapse geoelectrical monitoring during CO2 diffusion in the carbonate vadose zone. Int. J. Greenh. Gas Control 16, 156–166. doi:10.1016/J.IJGGC.2013.03.016

Letort, J., Roux, P., Vandemeulebrouck, J., Coutant, O., Cros, E., Wathelet, M., Cardellini, C., Avino, R., 2012. High-resolution shallow seismic tomography of a hydrothermal area: application to the Solfatara, Pozzuoli. Geophys. J. Int. 189, 1725–1733. doi:10.1111/j.1365-246X.2012.05451.x

Lima, A., De Vivo, B., Spera, F.J., Bodnar, R.J., Milia, A., Nunziata, C., Belkin, H.E., Cannatelli, C., 2009. Thermodynamic model for uplift and deflation episodes (bradyseism) associated with magmatic–hydrothermal activity at the Campi Flegrei (Italy). Earth-Science Rev. 97, 44–58. doi:10.1016/j.earscirev.2009.10.001

Moretti, R., De Natale, G., Troise, C., 2017. A geochemical and geophysical reappraisal to the significance of the recent unrest at Campi Flegrei caldera (Southern Italy). Geochemistry, Geophys. Geosystems 18, 1244–1269. doi:10.1002/2016GC006569

Nickschick, T., Flechsig, C., Meinel, C., Mrlina, J., Kämpf, H., 2017. Architecture and temporal variations of a terrestrial CO2 degassing site using electric resistivity tomography and self-potential. Int. J. Earth Sci. 1–12. doi:10.1007/s00531-017-1470-0

Oldenborger, G.A., Knoll, M.D., Routh, P.S., LaBrecque, D.J., 2007. Time-lapse ERT monitoring of an injection/withdrawal experiment in a shallow unconfined aquifer. GEOPHYSICS 72, F177–F187. doi:10.1190/1.2734365

Orsi, G., Di Vito, M.A., Isaia, R., 2004. Volcanic hazard assessment at the restless Campi Flegrei caldera. Bull. Volcanol. 66, 514–530. doi:10.1007/s00445-003-0336-4

Petrosino, S., Damiano, N., Cusano, P., Di Vito, M.A., de Vita, S., Del Pezzo, E., 2012. Subsurface structure of the Solfatara volcano (Campi Flegrei caldera, Italy) as deduced from joint seismic-noise array, volcanological and morphostructural analysis. Geochemistry, Geophys. Geosystems 13, n/a-n/a. doi:10.1029/2011GC004030

Piochi, M., Mormone, A., Balassone, G., Strauss, H., Troise, C., De Natale, G., 2015a. Native sulfur, sulfates and sulfides from the active Campi Flegrei volcano (southern Italy): Genetic environments and degassing dynamics revealed by mineralogy and isotope geochemistry. J. Volcanol. Geotherm. Res. 304, 180–193. doi:10.1016/j.jvolgeores.2015.08.017

Piochi, M., Mormone, A., Balassone, G., Strauss, H., Troise, C., De Natale, G., 2015b. Native sulfur, sulfates and sulfides from the active Campi Flegrei volcano (southern Italy): Genetic environments and degassing dynamics revealed by mineralogy and isotope geochemistry. J. Volcanol. Geotherm. Res. 304, 180–193. doi:10.1016/j.jvolgeores.2015.08.017

Pribnow, D.F.., Schütze, C., Hurter, S.J., Flechsig, C., Sass, J.H., 2003. Fluid flow in the resurgent dome of Long Valley Caldera: implications from thermal data and deep electrical sounding. J. Volcanol. Geotherm. Res. 127, 329–345. doi:10.1016/S0377-0273(03)00175-6

Revil, A., Cathles III, L.M., Losh, S., Nunn, J.A., 1998. Electrical conductivity in shaly sands with geophysical application. J. Geophys. Res., 103 (B10) (1998), pp. 23925-23936

Revil, A., Finizola, A., Piscitelli, S., Rizzo, E., Ricci, T., Crespy, A., Angeletti, B., Balasco, M., Barde Cabusson, S., Bennati, L., Bolève, A., Byrdina, S., Carzaniga, N., Di Gangi, F., Morin, J., Perrone, A., Rossi, M., Roulleau, E., Suski, B., 2008. Inner structure of La Fossa di Vulcano (Vulcano Island, southern Tyrrhenian Sea, Italy) revealed by high-resolution electric resistivity tomography coupled with self-potential, temperature, and CO_2 diffuse degassing measurements. J. Geophys. Res. 113, B07207. doi:10.1029/2007JB005394

Revil, A., Finizola, A., Ricci, T., Delcher, E., Peltier, A., Barde-Cabusson, S., Avard, G., Bailly, T., Bennati, L., Byrdina, S., Colonge, J., Di Gangi, F., Douillet, G., Lupi, M., Letort, J., Tsang Hin Sun, E., 2011. Hydrogeology of Stromboli volcano, Aeolian Islands (Italy) from the interpretation of resistivity tomograms, self-potential, soil temperature and soil CO2 concentration measurements. Geophys. J. Int. 186, 1078–1094. doi:10.1111/j.1365-246X.2011.05112.x

Roberts, J.J., 2002. Electrical properties of microporous rock as a function of saturation and temperature. J. Appl. Phys., 91 (3).

Schmidt-Hattenberger, C., Bergmann, P., Kießling, D., Krüger, K., Rücker, C., Schütt, H., Group, K., 2011. Application of a Vertical Electrical Resistivity Array (VERA) for monitoring CO2 migration at the Ketzin site: First performance evaluation. Energy Procedia 4, 3363–3370. doi:10.1016/j.egypro.2011.02.258

Shirzaei, M., Walter, T.R., 2010. Time-dependent volcano source monitoring using interferometric synthetic aperture radar time series: A combined genetic algorithm and Kalman filter approach. J. Geophys. Res. 115, B10421. doi:10.1029/2010JB007476

Singha, K., Day-Lewis, F.D., Johnson, T., Slater, L.D., 2015. Advances in interpretation of subsurface processes with time-lapse electrical imaging. Hydrol. Process. 29, 1549–1576. doi:10.1002/hyp.10280

Slater, L., 2007. Near Surface Electrical Characterization of Hydraulic Conductivity: From Petrophysical

Properties to Aquifer Geometries—A Review. Surv. Geophys. 28, 169–197. doi:10.1007/s10712-007-9022-y

Todesco, M., Chiodini, G., Macedonio, G., 2003. Monitoring and modelling hydrothermal fluid emission at La Solfatara (Phlegrean Fields, Italy). An interdisciplinary approach to the study of diffuse degassing. J. Volcanol. Geotherm. Res. 125, 57–79. doi:10.1016/S0377-0273(03)00089-1

Troiano, A., Di Giuseppe, M., Petrillo, Z., Troise, C., De Natale, G., 2011. Ground deformation at calderas driven by fluid injection: Modelling unrest episodes at Campi Flegrei (Italy). Geophys. J. Int. 187, 833–847. doi:10.1111/j.1365-246X.2011.05149.x

Troiano, A., Di Giuseppe, M.G., Patella, D., Troise, C., De Natale, G., 2014. Electromagnetic outline of the Solfatara-Pisciarelli hydrothermal system, Campi Flegrei (Southern Italy). J. Volcanol. Geotherm. Res. 277, 9–21. doi:10.1016/j.jvolgeores.2014.03.005

Troiano, A., Di Giuseppe, M.G., Petrillo, Z., Patella, D., 2009. Imaging 2D structures by the CSAMT method: Application to the Pantano di S. Gregorio Magno faulted basin (Southern Italy). J. Geophys. Eng. 6, 120–130. doi:10.1088/1742-2132/6/2/003

Troiano, A., Petrillo, Z., Di Giuseppe, M.G., Balasco, M., Diaferia, I., Di Fiore, B., Siniscalchi, A., Patella, D., 2008. About the shallow resistivity structure of Vesuvius volcano, in: Annals of Geophysics. doi:10.4401/ag-3043

Vaughan, P.J., Udell, K.S., Wilt, M.J., 1993. The effects of steam injection on the electrical conductivity of an unconsolidated sand saturated with a salt solution. J. Geophys. Res., 98 (B1) (1993), pp. 509-518

Vilardo, G., Sansivero, F., Chiodini, G., 2015. Long-term TIR imagery processing for spatiotemporal monitoring of surface thermal features in volcanic environment: A case study in the Campi Flegrei (Southern Italy). J. Geophys. Res. Solid Earth 120, 812–826. doi:10.1002/2014JB011497

Wallin, E.L., Johnson, T.C., Greenwood, W.J., Zachara, J.M., 2013. Imaging high stage river-water intrusion into a contaminated aquifer along a major river corridor using 2-D time-lapse surface electrical resistivity tomography. Water Resour. Res. 49, 1693–1708. doi:10.1002/wrcr.20119

Ward, S.H., 1988. The Resistivity and Induced Polarization Methods, in: Symposium on the Application of Geophysics to Engineering and Environmental Problems 1988. Environment and Engineering Geophysical Society, pp. 109–250. doi:10.4133/1.2921804

Würdemann, H., Möller, F., Kühn, M., Heidug, W., Christensen, N.P., Borm, G., Schilling, F.R., 2010. CO2SINK—From site characterisation and risk assessment to monitoring and verification: One year of operational experience with the field laboratory for CO2 storage at Ketzin, Germany. Int. J. Greenh. Gas Control 4, 938–951. doi:10.1016/j.ijggc.2010.08.010

Zhou, X., Lakkaraju, V.R., Apple, M., Dobeck, L.M., Gullickson, K., Shaw, J.A., Cunningham, A.B., Wielopolski, L., Spangler, L.H., 2012. Experimental observation of signature changes in bulk soil electrical conductivity in response to engineered surface CO2 leakage. Int. J. Greenh. Gas Control 7, 20–29. doi:10.1016/j.ijggc.2011.12.006

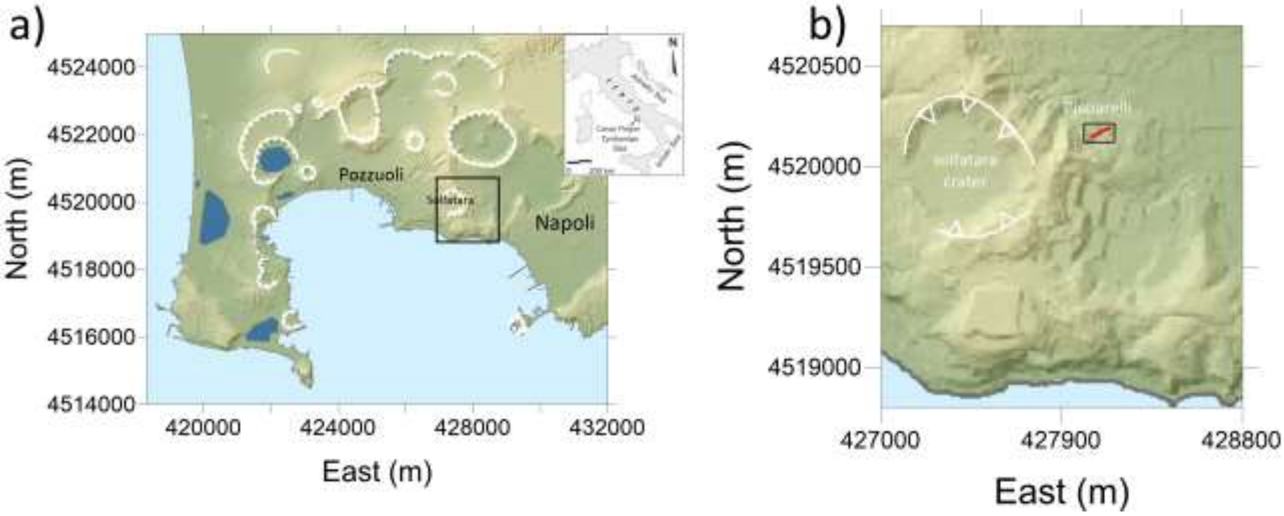
a)
4524000
4522000
4520000
4518000
4516000
4514000
North (m)
420000
424000
428000
432000
East (m)
Pozzuoli
Napoli
b)
4520500
4520000
4519500
4519000
North (m)
427000
427900
428800
East (m)

Figure 1.

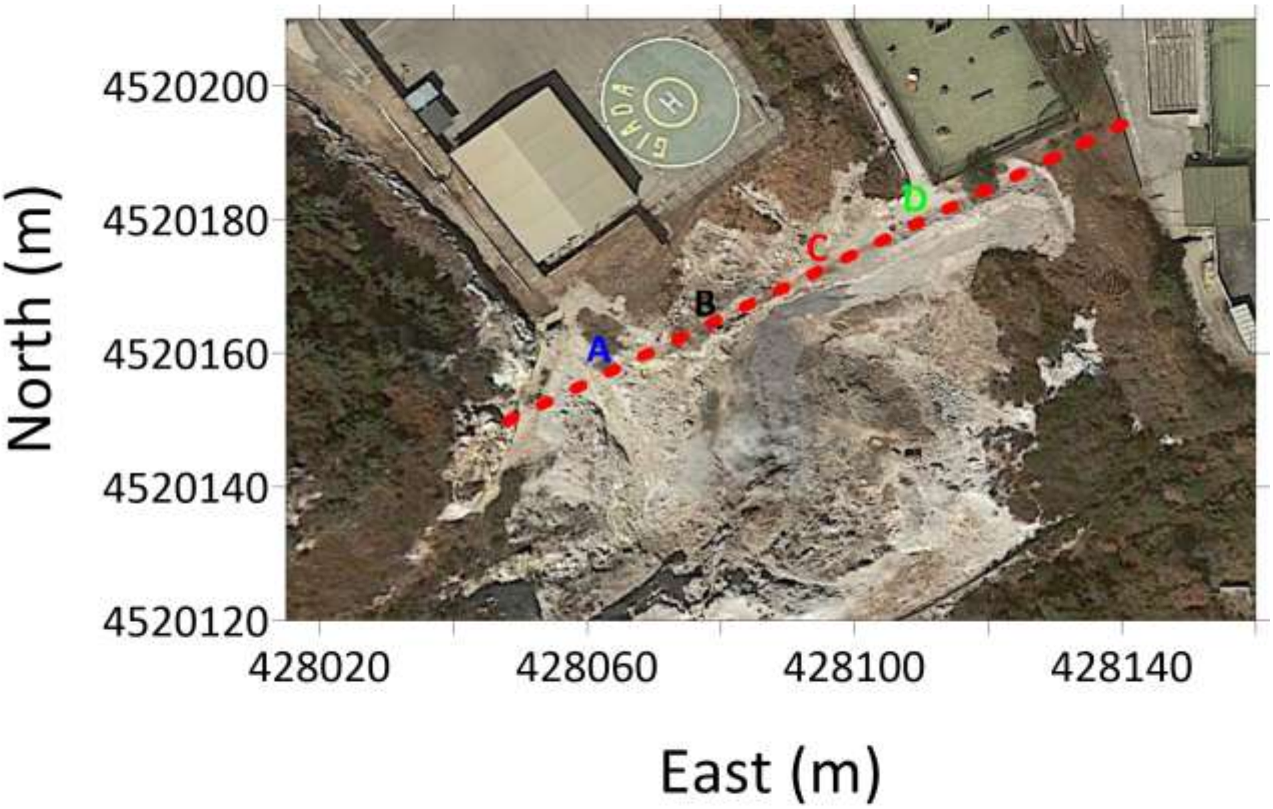
North (m)
4520200
4520180
4520160
4520140
4520120
428020
428060
428100
428140
East (m)
A
B
C
D

Figure 2.

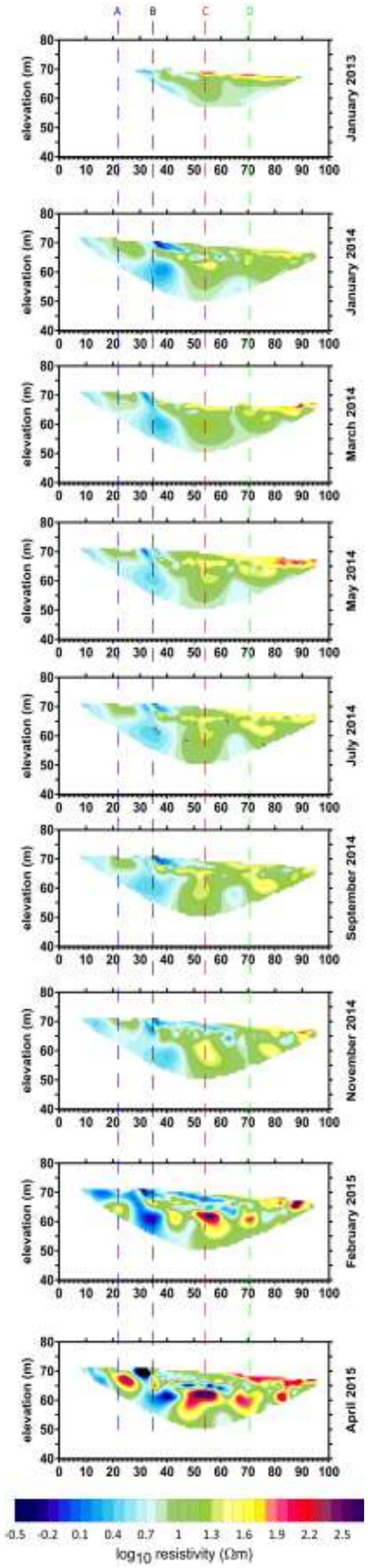
A
B
C
D
elevation (m)
January 2013
January 2014
March 2014
May 2014
July 2014
September 2014
November 2014
February 2015
April 2015
-0.5 -0.2 0.1 0.4 0.7 1 1.3 1.6 1.9 2.2 2.5
log10 resistivity (Ωm)

Figure 3

677

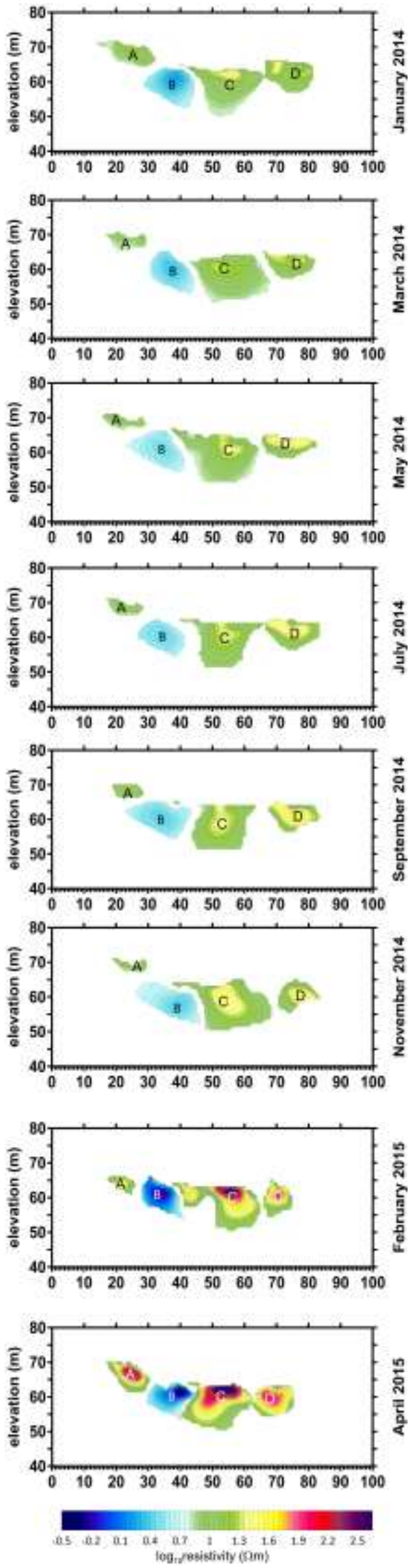
elevation (m)
January 2014
March 2014
May 2014
July 2014
September 2014
November 2014
February 2015
April 2015
A
B
C
D
log10 resistivity (Ωm)

Figure 4.

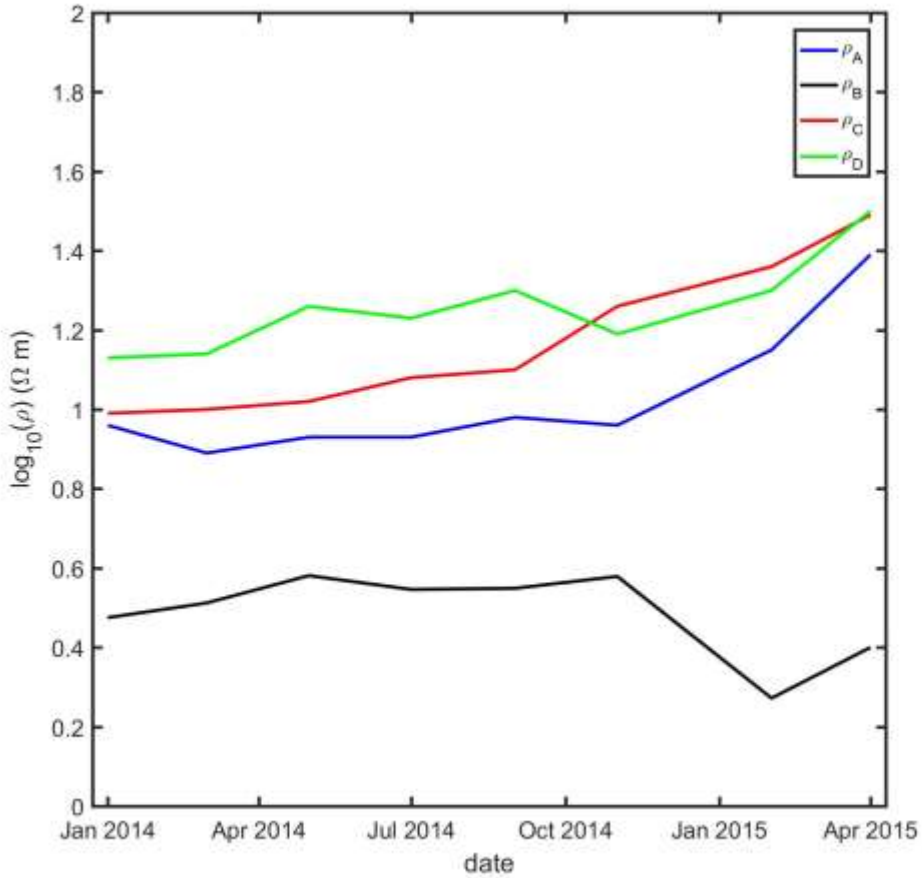
ρ_A
ρ_B
ρ_C
ρ_D
$\log_{10}(\rho)$ (Ω m)
2
1.8
1.6
1.4
1.2
1
0.8
0.6
0.4
0.2
0
Jan 2014
Apr 2014
Jul 2014
Oct 2014
Jan 2015
Apr 2015
date

Figure 5.

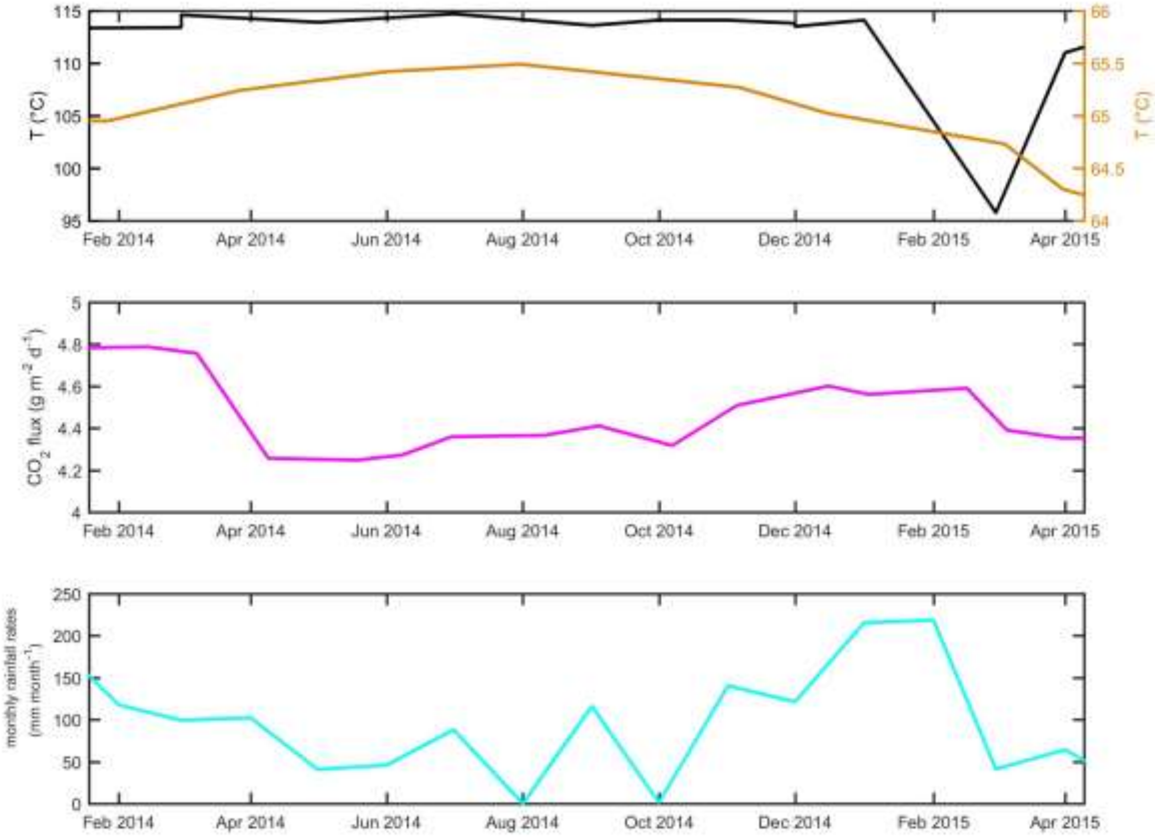

T (°C)
T (°C)
CO2 flux (g m-2 d-1)
monthly rainfall rates (mm month-1)
Feb 2014
Apr 2014
Jun 2014
Aug 2014
Oct 2014
Dec 2014
Feb 2015
Apr 2015

Figure 6.

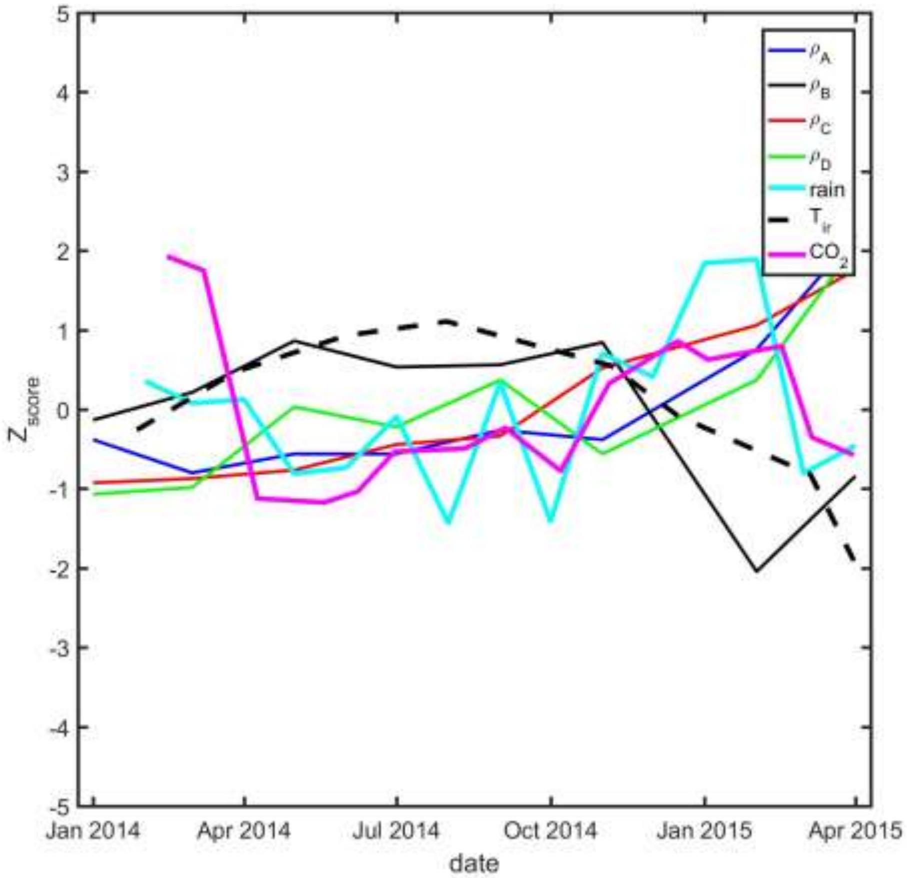

5
4
3
2
1
0
-1
-2
-3
-4
-5
Z_{score}
Jan 2014
Apr 2014
Jul 2014
Oct 2014
Jan 2015
Apr 2015
date
ρ_A
ρ_B
ρ_C
ρ_D
rain
T_{ir}
CO_2

Figure 7.

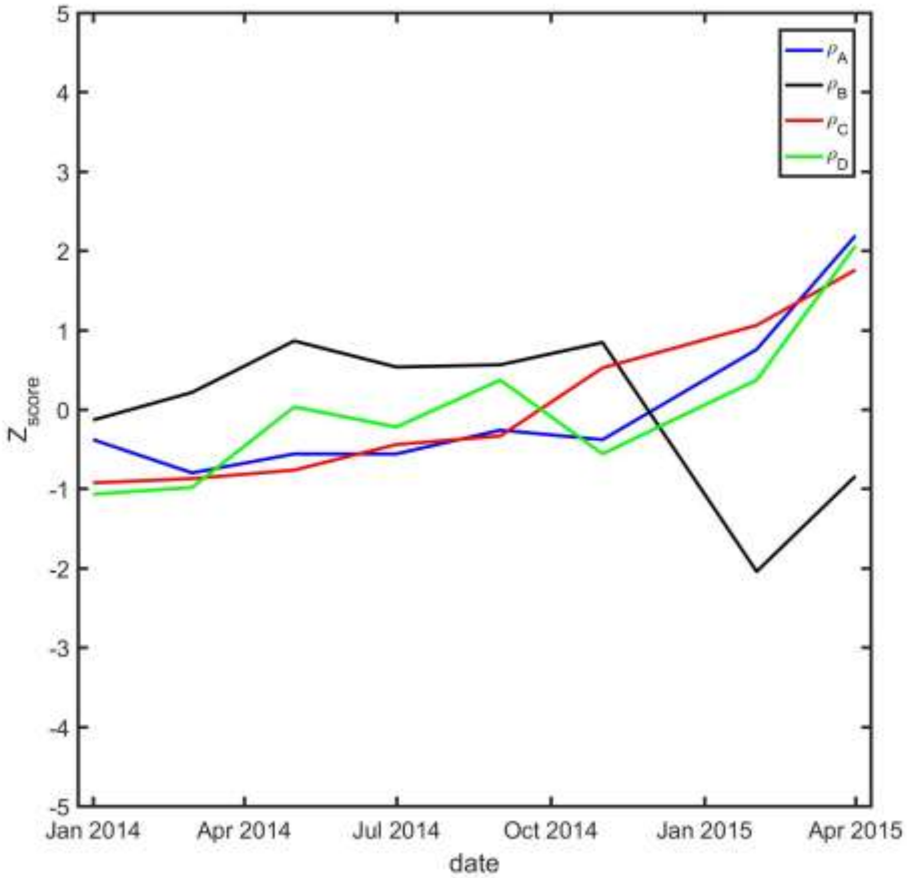

5
4
3
2
1
0
-1
-2
-3
-4
-5
Z_{score}
Jan 2014
Apr 2014
Jul 2014
Oct 2014
Jan 2015
Apr 2015
date
ρ_A
ρ_B
ρ_C
ρ_D

Figure 8a.

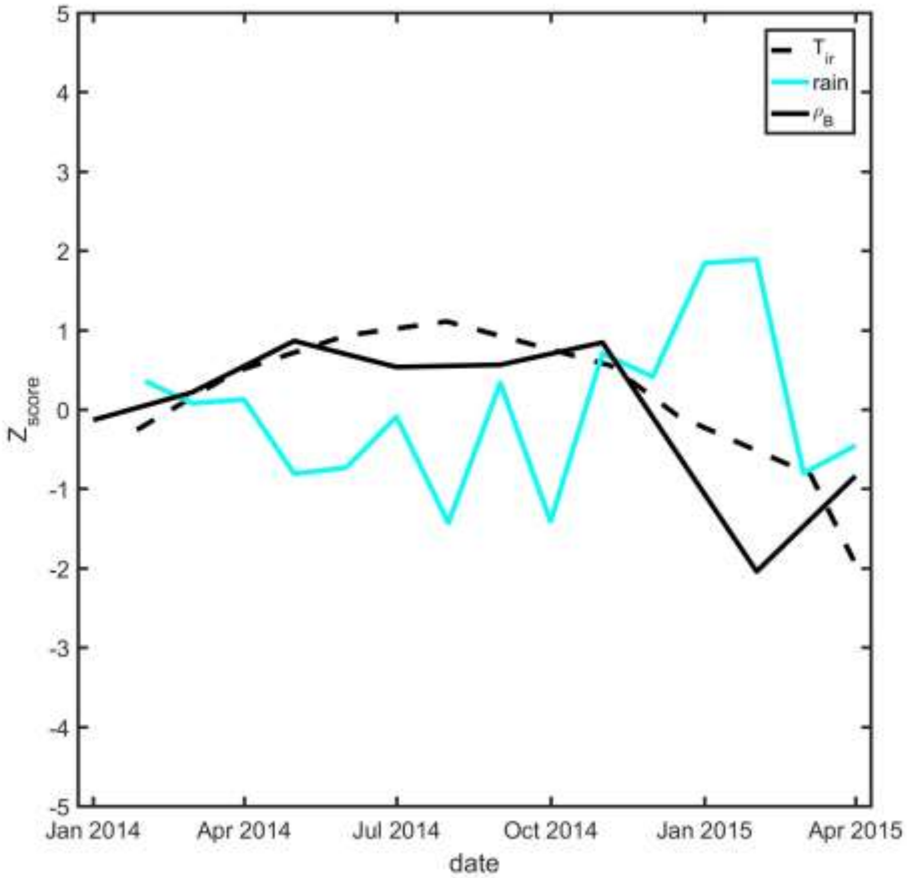

5
4
3
2
1
0
-1
-2
-3
-4
-5
Z score
Jan 2014
Apr 2014
Jul 2014
Oct 2014
Jan 2015
Apr 2015
date
T ir
rain
ρ B

Figure 8b.

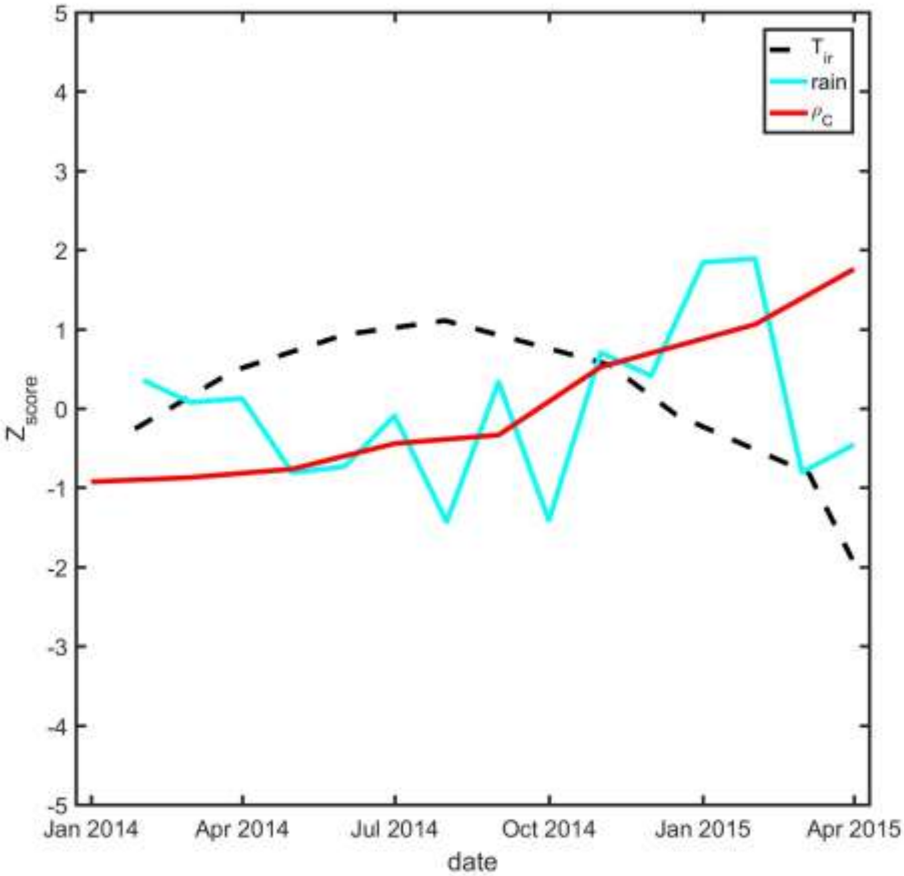
T_ir
rain
ρ_C
Z_score
5
4
3
2
1
0
-1
-2
-3
-4
-5
Jan 2014
Apr 2014
Jul 2014
Oct 2014
Jan 2015
Apr 2015
date

Figure 8c.

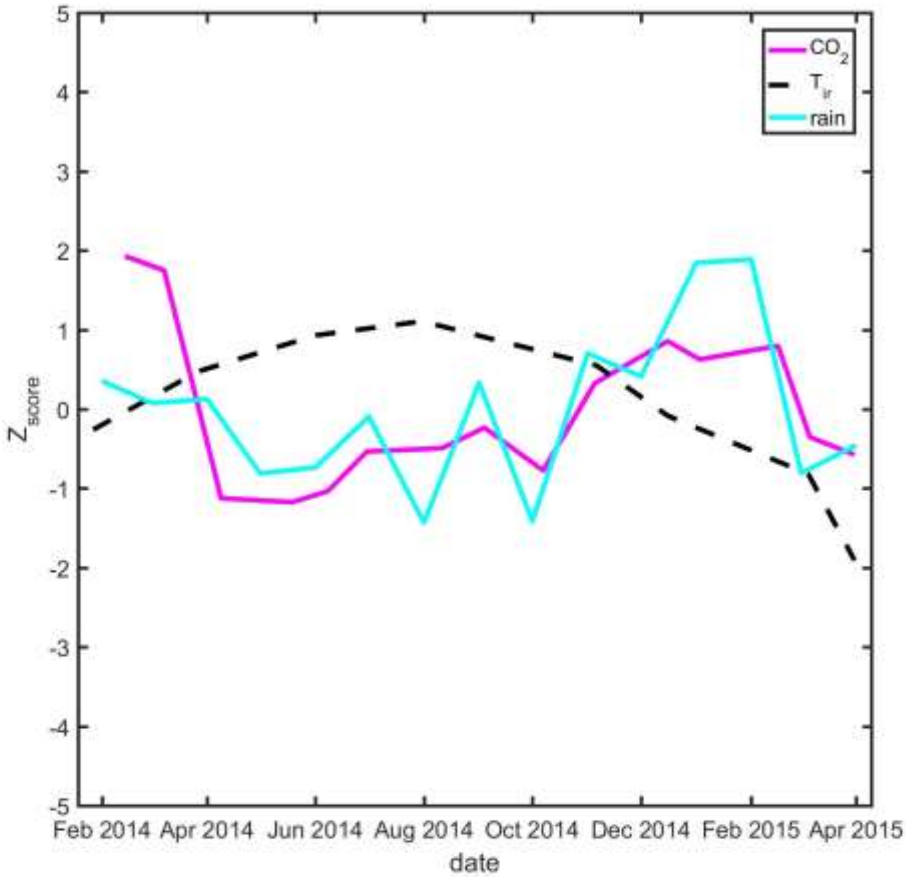
CO2
Tir
rain
Zscore
5
4
3
2
1
0
-1
-2
-3
-4
-5
Feb 2014 Apr 2014 Jun 2014 Aug 2014 Oct 2014 Dec 2014 Feb 2015 Apr 2015
date

Figure 8d.

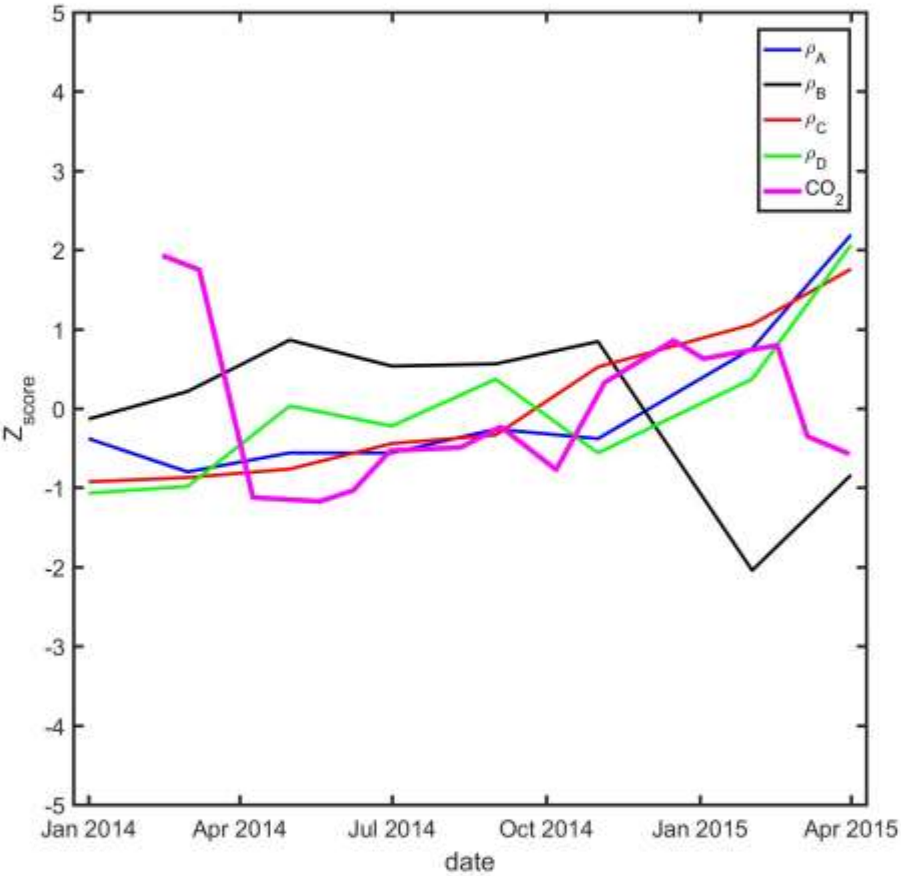
ρ_A
ρ_B
ρ_C
ρ_D
CO_2
5
4
3
2
1
0
-1
-2
-3
-4
-5
Z_{score}
Jan 2014
Apr 2014
Jul 2014
Oct 2014
Jan 2015
Apr 2015
date

Figure 8e.

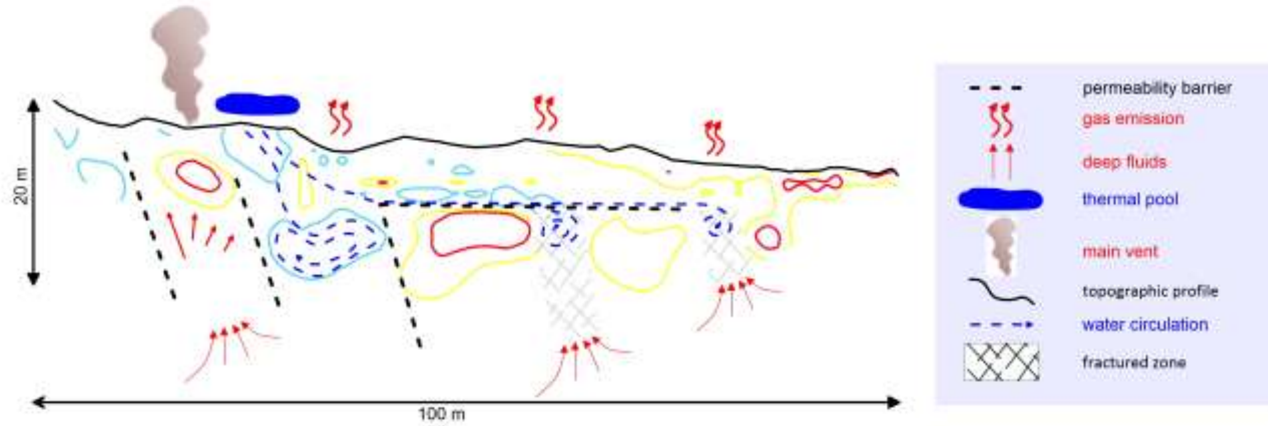
20 m
100 m
permeability barrier
gas emission
deep fluids
thermal pool
main vent
topographic profile
water circulation
fractured zone

Figure 9.

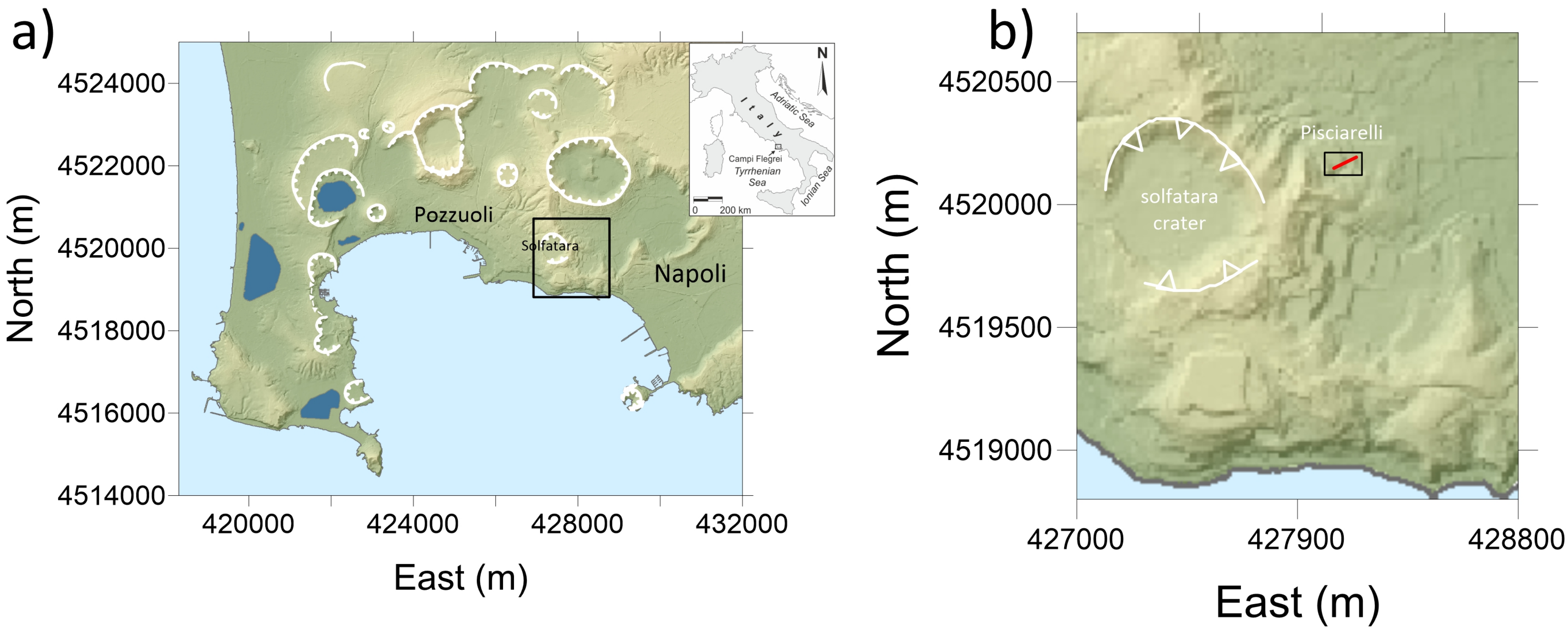
a)
4524000
4522000
4520000
4518000
4516000
4514000
North (m)
420000
424000
428000
432000
East (m)
Pozzuoli
Solfatara
Napoli
N
Italy
Adriatic Sea
Campi Flegrei
Tyrrhenian Sea
Ionian Sea
0
200 km
b)
4520500
4520000
4519500
4519000
North (m)
427000
427900
428800
East (m)
Pisciarelli
solfatara crater

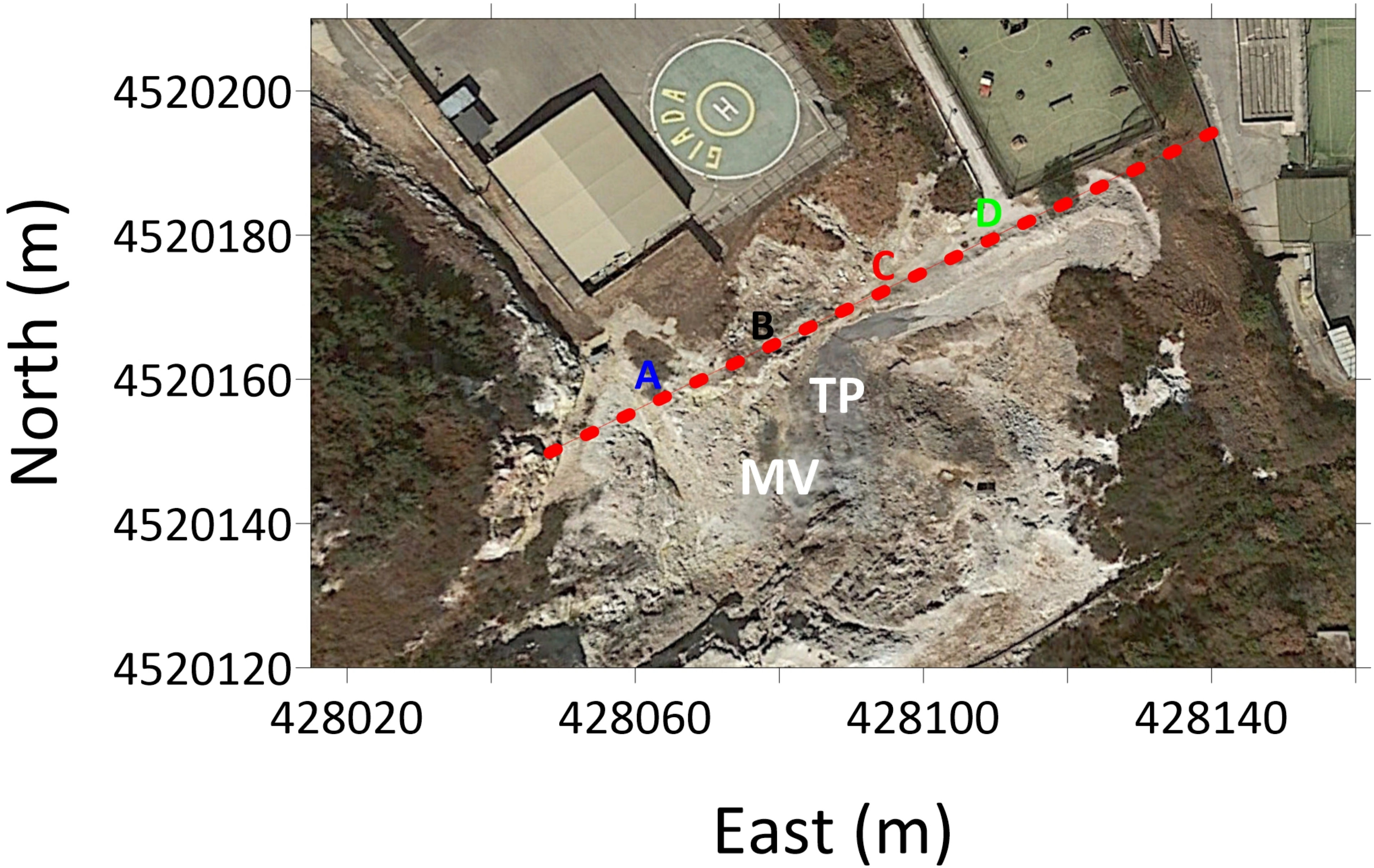

North (m)
4520200
4520180
4520160
4520140
4520120
East (m)
428020
428060
428100
428140
A
B
C
D
TP
MV
GIADA
H

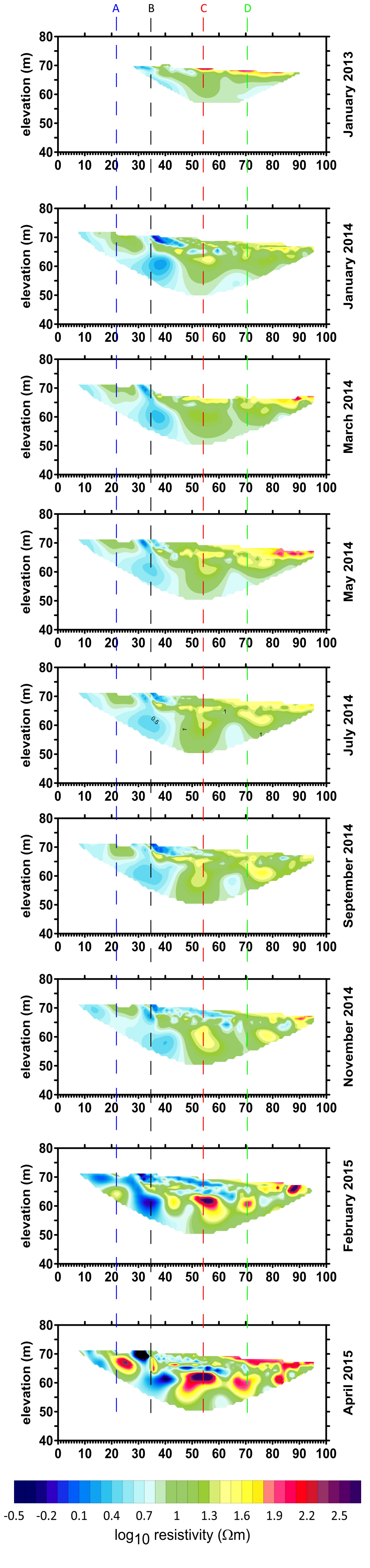

A
B
C
D
elevation (m)
January 2013
January 2014
March 2014
May 2014
July 2014
September 2014
November 2014
February 2015
April 2015
-0.5 -0.2 0.1 0.4 0.7 1 1.3 1.6 1.9 2.2 2.5
log10 resistivity (Ωm)

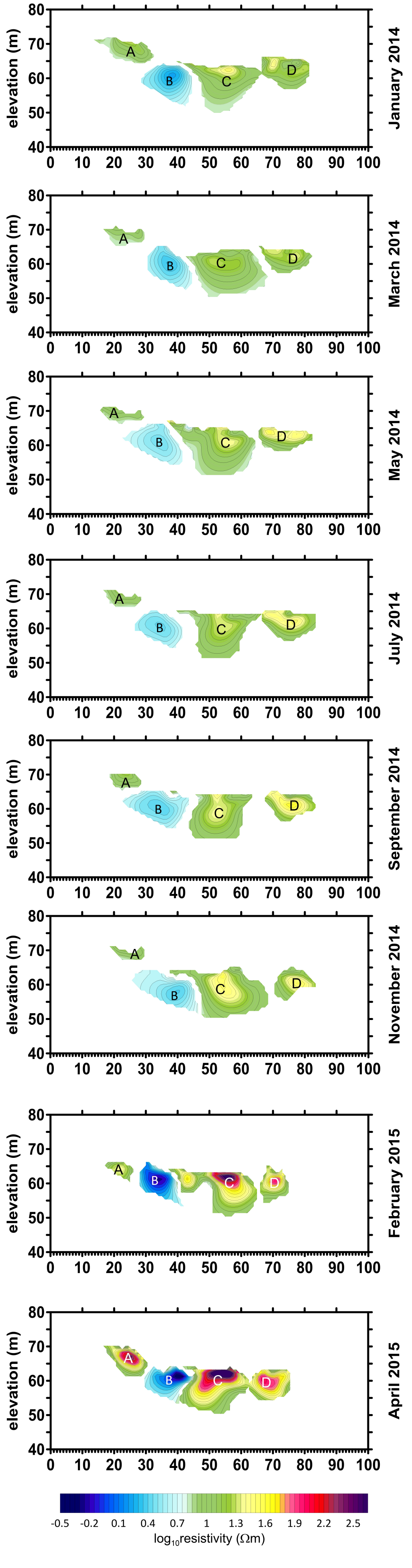
January 2014
March 2014
May 2014
July 2014
September 2014
November 2014
February 2015
April 2015
elevation (m)
A
B
C
D
-0.5 -0.2 0.1 0.4 0.7 1 1.3 1.6 1.9 2.2 2.5
log10resistivity (Ωm)

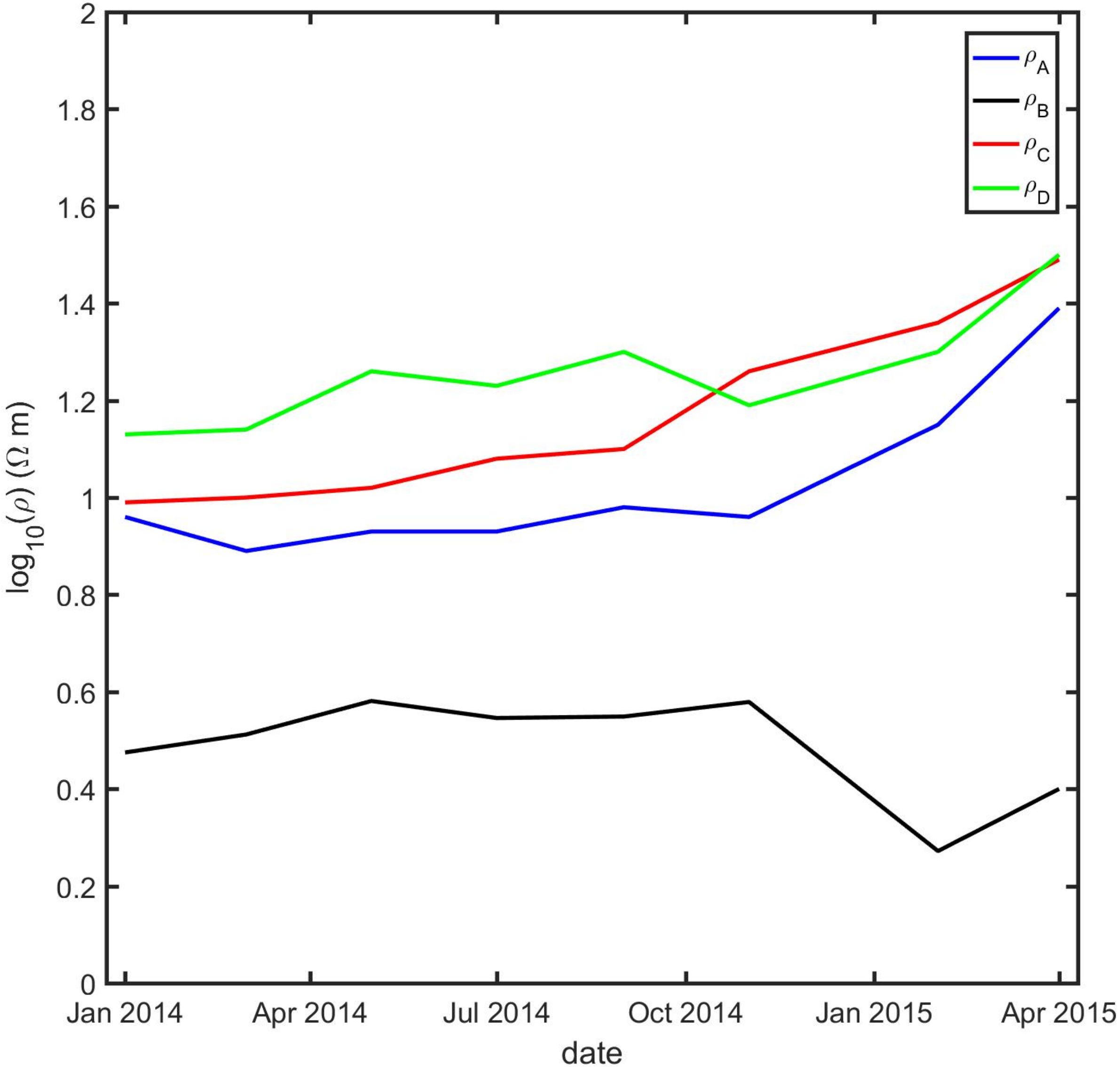

2
1.8
1.6
1.4
1.2
1
0.8
0.6
0.4
0.2
0
$\log_{10}(\rho)$ (Ω m)
Jan 2014
Apr 2014
Jul 2014
Oct 2014
Jan 2015
Apr 2015
date
ρ_A
ρ_B
ρ_C
ρ_D

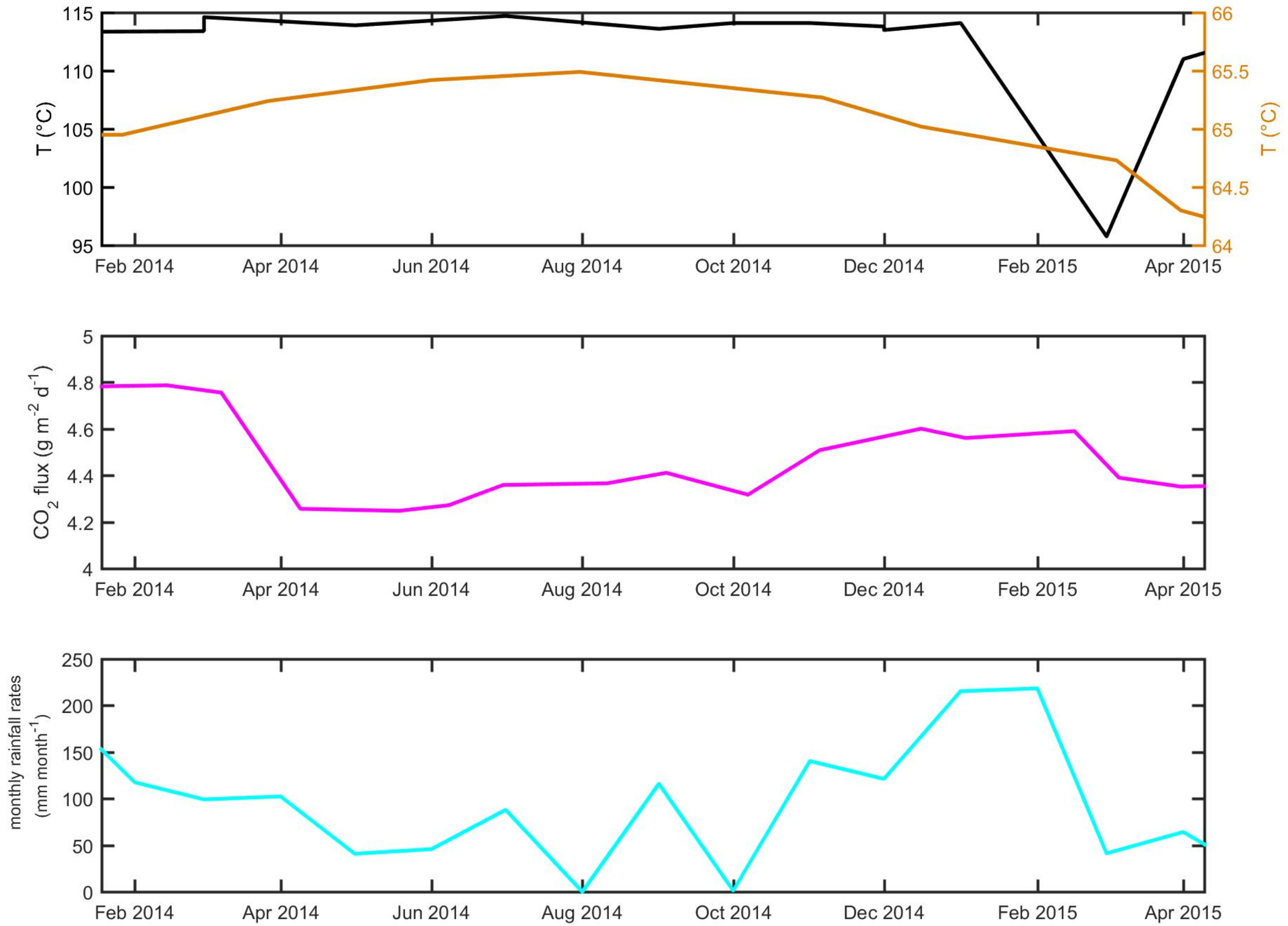

T (°C)
T (°C)
115
110
105
100
95
66
65.5
65
64.5
64
Feb 2014
Apr 2014
Jun 2014
Aug 2014
Oct 2014
Dec 2014
Feb 2015
Apr 2015
CO_2 flux (g m^{-2} d^{-1})
5
4.8
4.6
4.4
4.2
4
monthly rainfall rates
(mm month^{-1})
250
200
150
100
50
0

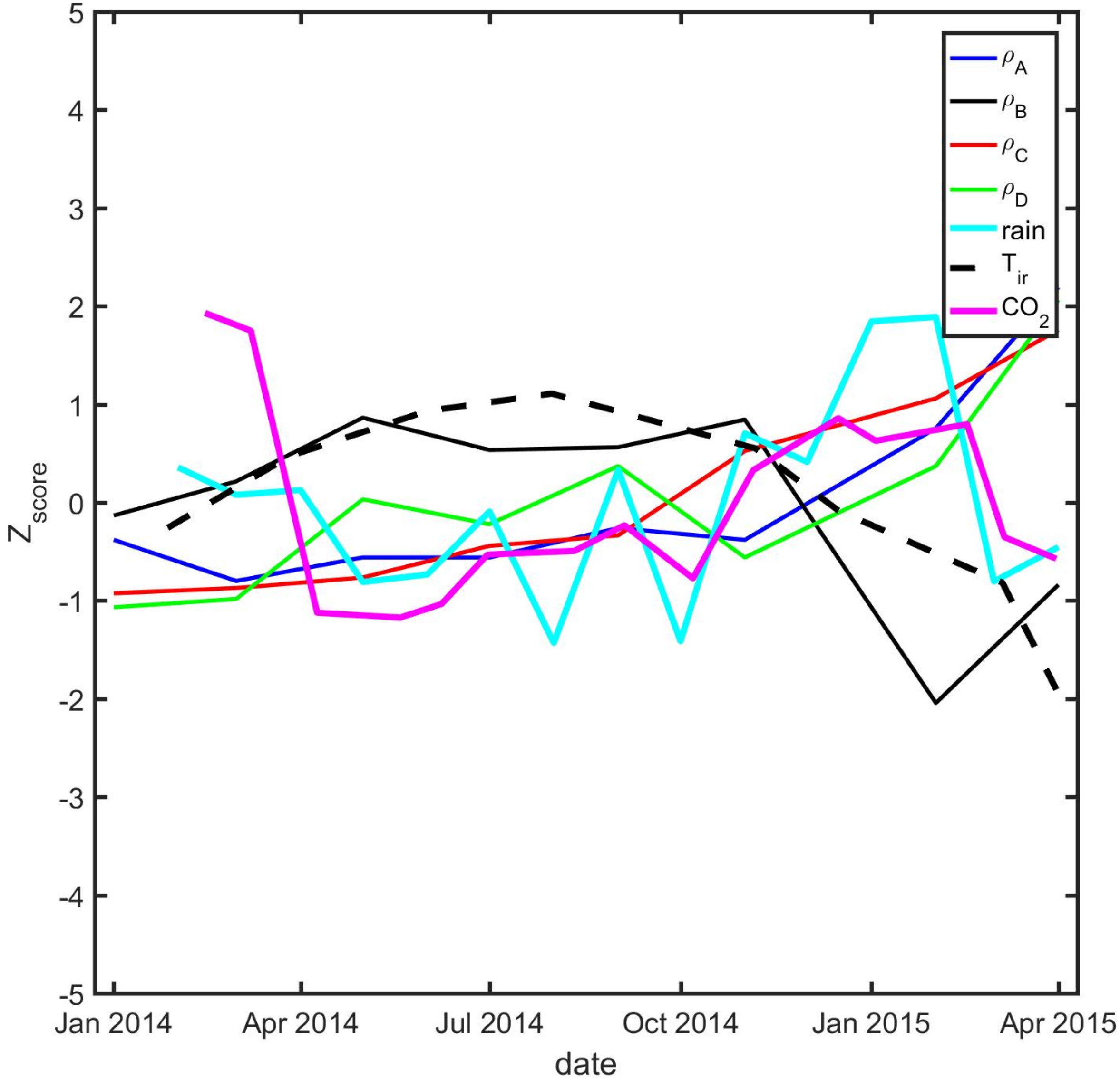

5
4
3
2
1
0
-1
-2
-3
-4
-5
Z_{score}
Jan 2014
Apr 2014
Jul 2014
Oct 2014
Jan 2015
Apr 2015
date
ρ_A
ρ_B
ρ_C
ρ_D
rain
T_{ir}
CO_2

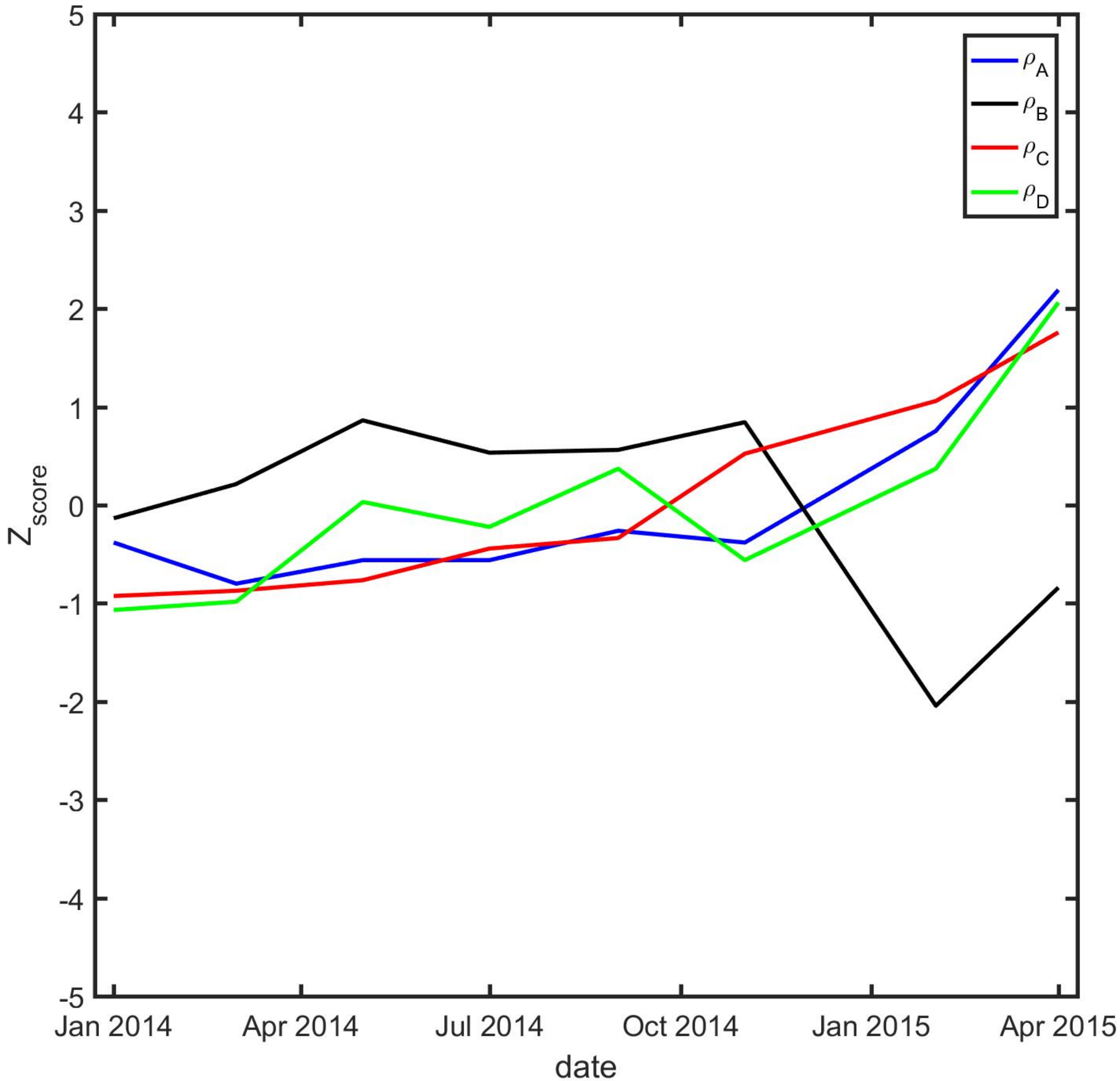

5
4
3
2
1
0
-1
-2
-3
-4
-5
Z_{score}
Jan 2014
Apr 2014
Jul 2014
Oct 2014
Jan 2015
Apr 2015
date
ρ_A
ρ_B
ρ_C
ρ_D

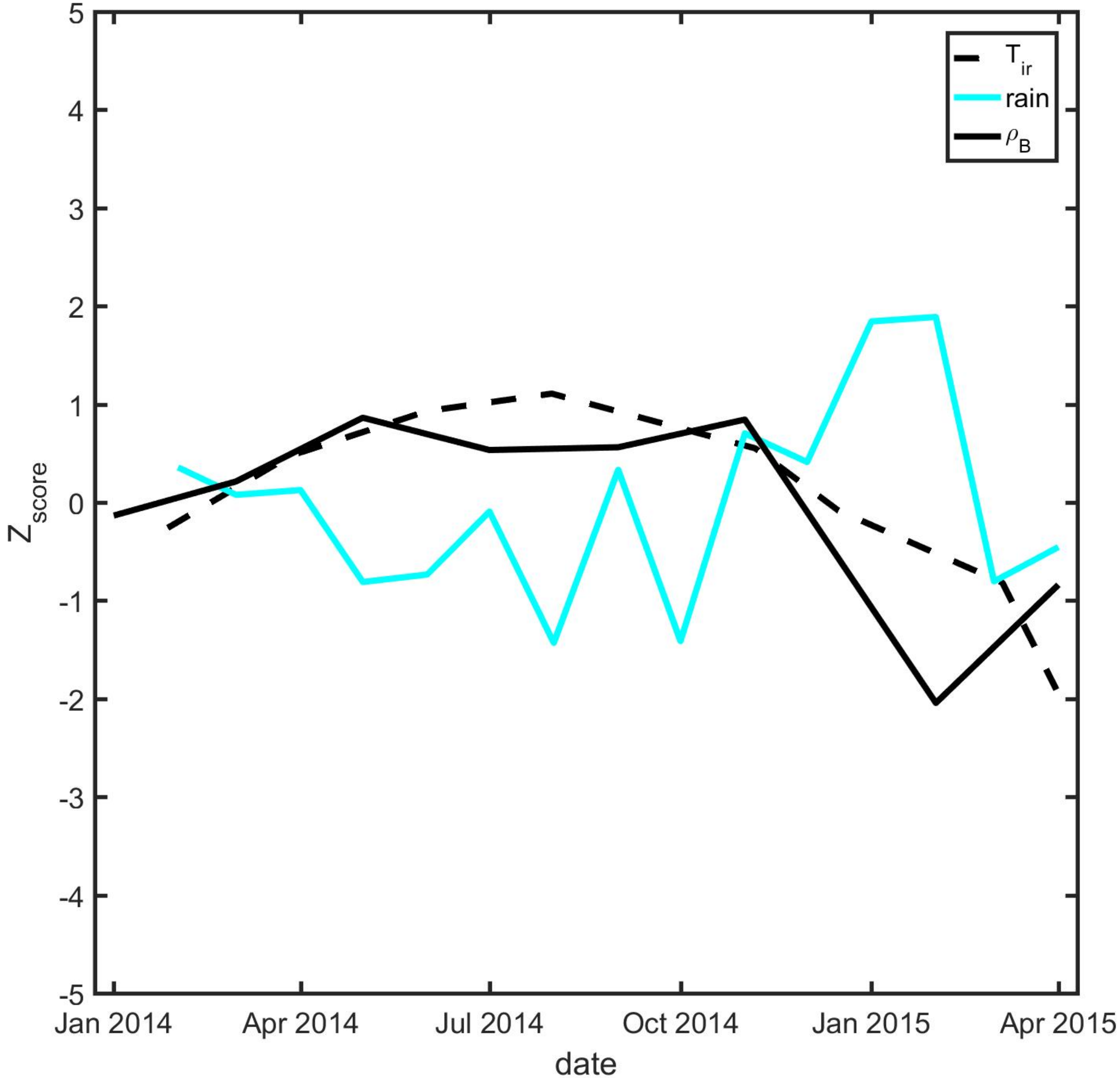

T_{ir}
rain
ρ_B
Z_{score}
5
4
3
2
1
0
-1
-2
-3
-4
-5
Jan 2014
Apr 2014
Jul 2014
Oct 2014
Jan 2015
Apr 2015
date

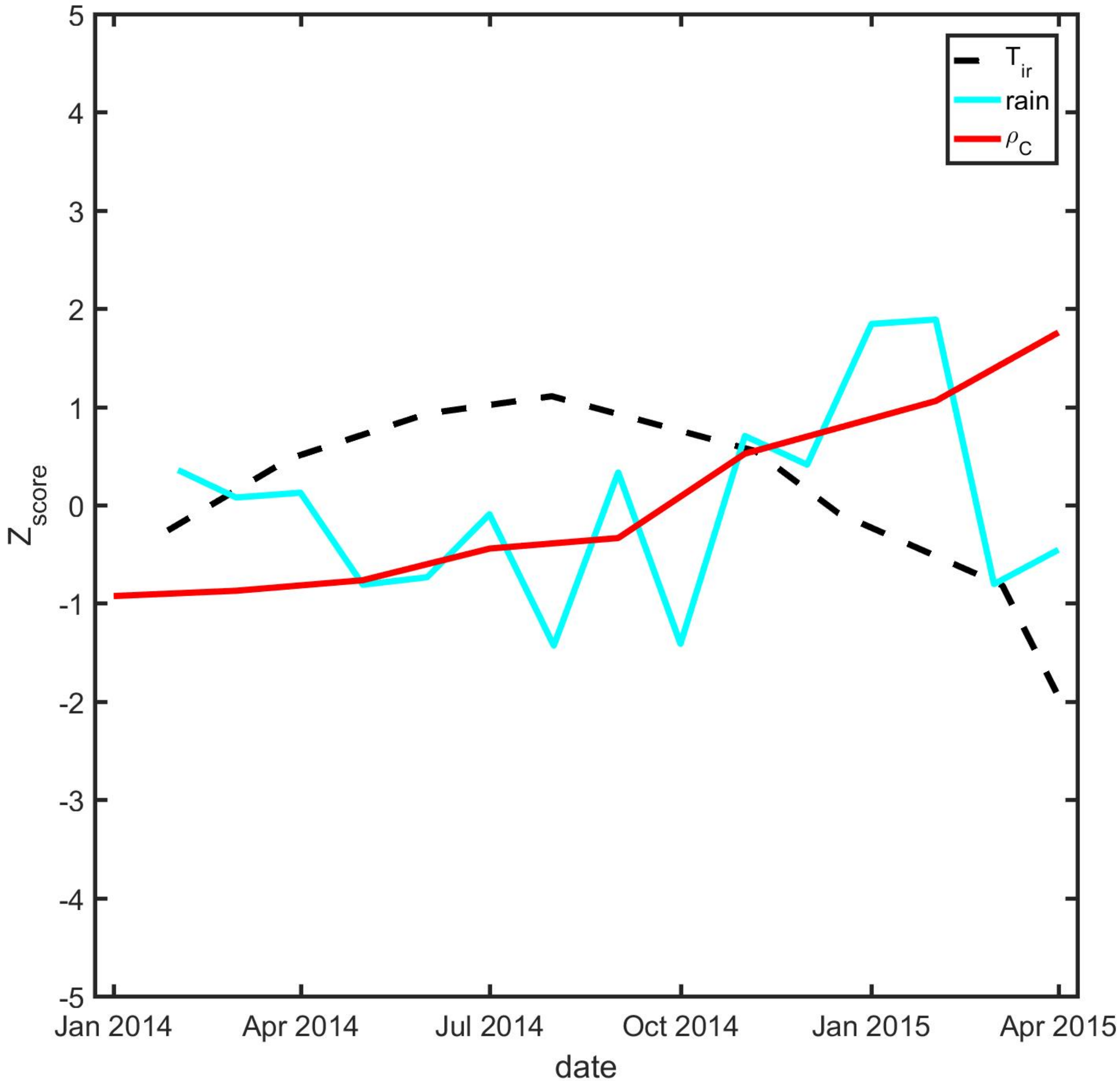

5
4
3
2
1
0
-1
-2
-3
-4
-5
Z_{score}
Jan 2014
Apr 2014
Jul 2014
Oct 2014
Jan 2015
Apr 2015
date
T_{ir}
rain
ρ_C

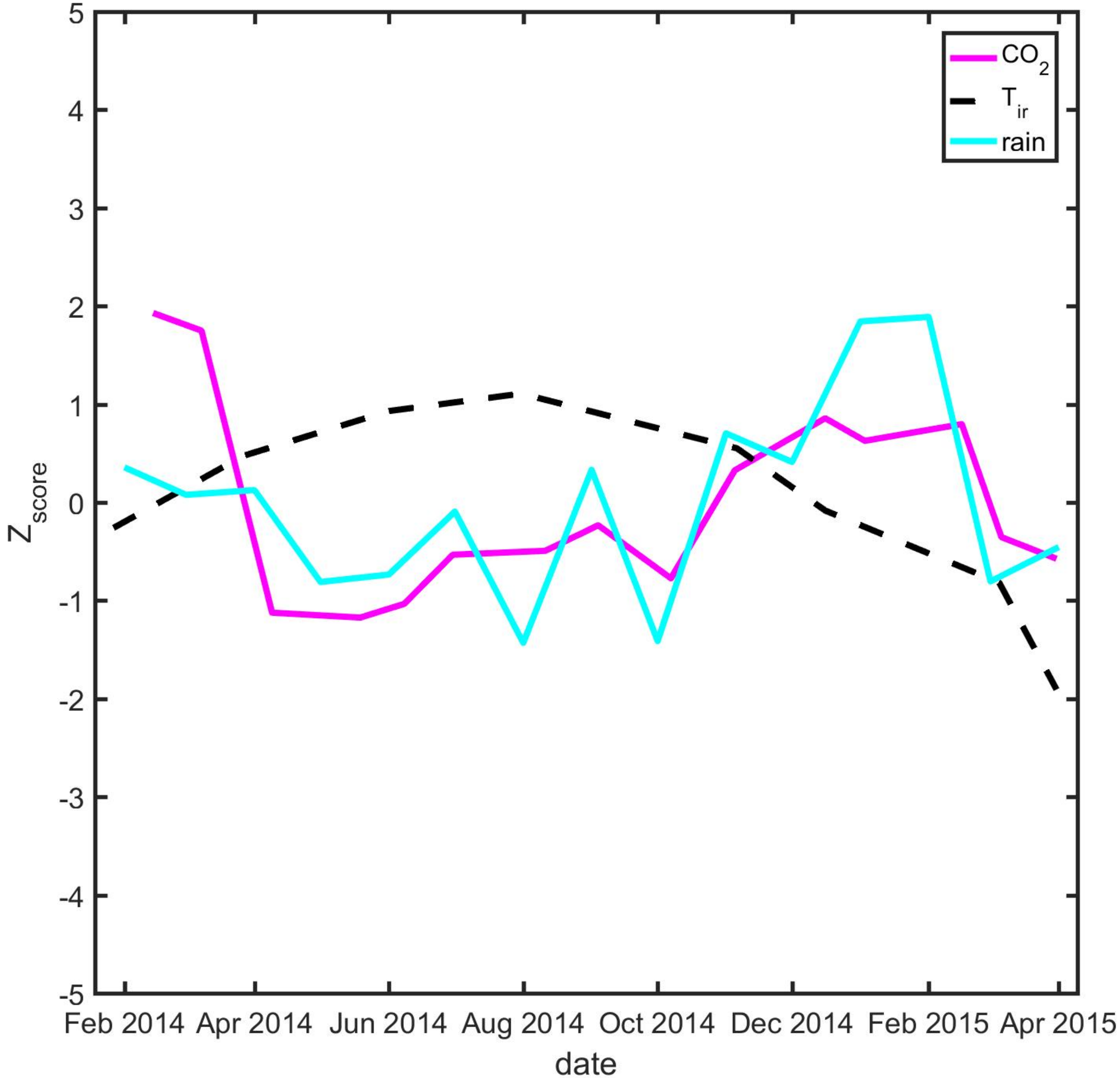

5
4
3
2
1
0
-1
-2
-3
-4
-5
Z_{score}
Feb 2014
Apr 2014
Jun 2014
Aug 2014
Oct 2014
Dec 2014
Feb 2015
Apr 2015
date
CO_2
T_{ir}
rain

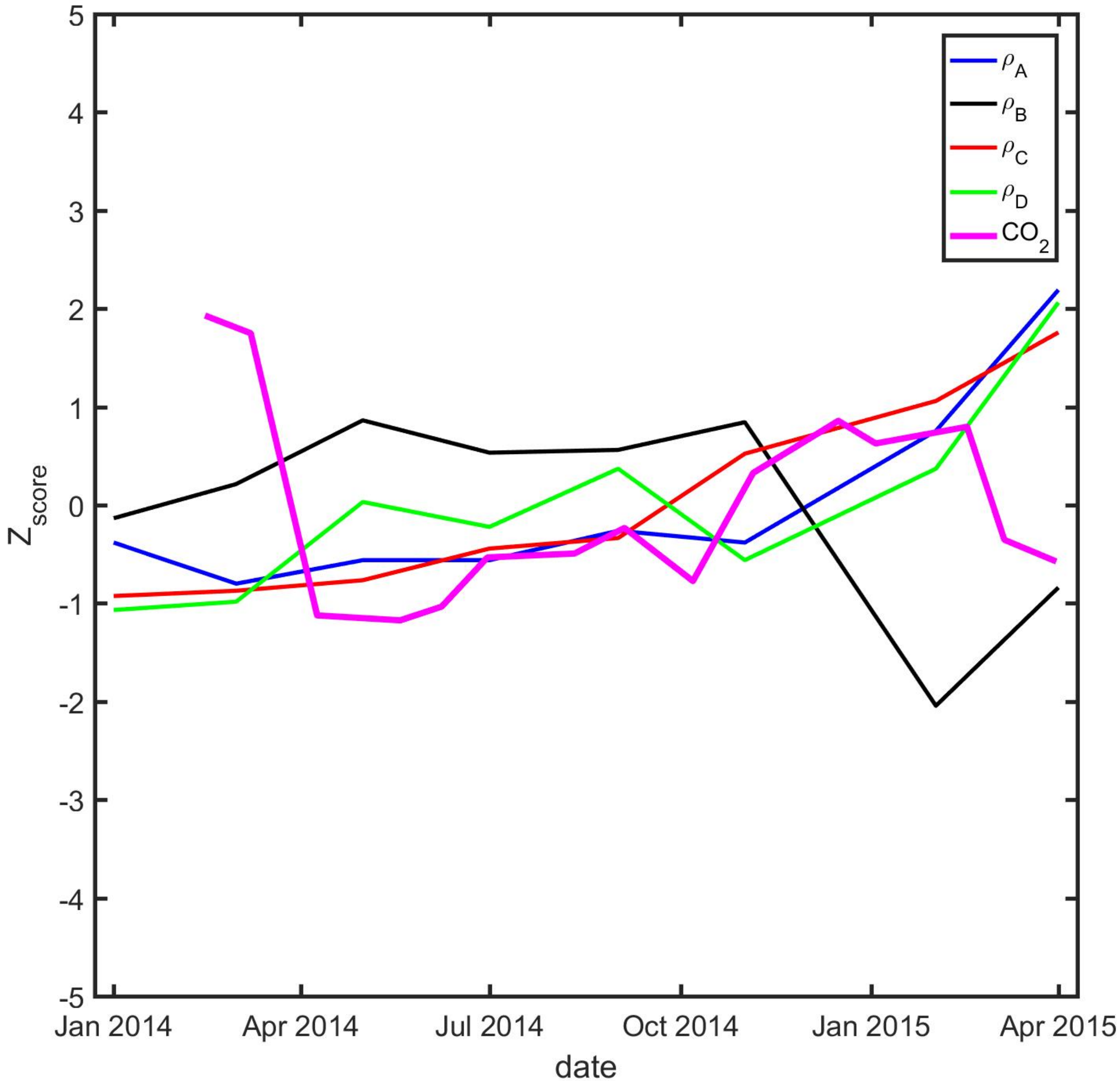

5
4
3
2
1
0
-1
-2
-3
-4
-5
Z_{score}
Jan 2014
Apr 2014
Jul 2014
Oct 2014
Jan 2015
Apr 2015
date
ρ_A
ρ_B
ρ_C
ρ_D
CO_2

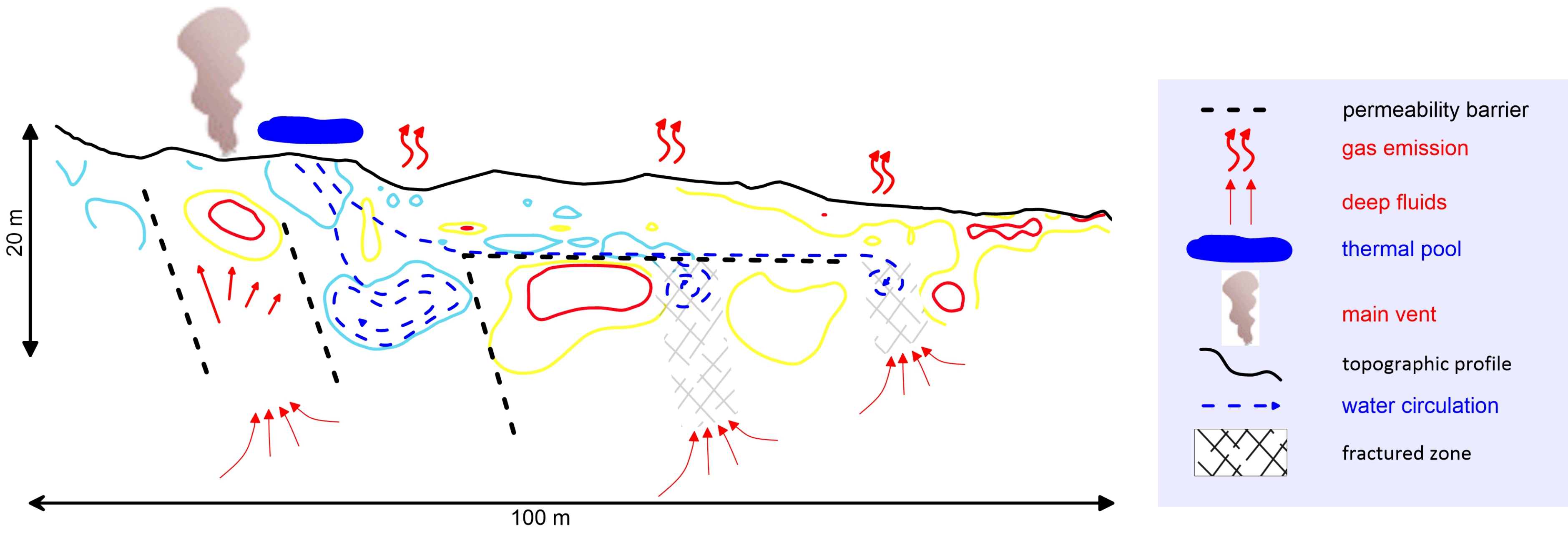

20 m
100 m
permeability barrier
gas emission
deep fluids
thermal pool
main vent
topographic profile
water circulation
fractured zone